UNIVERSIDADE DE COIMBRA
Faculdade de Ciências e Tecnologia
Departamento de Química

Double Many-Body Expansion Potential Energy Surfaces For NH_x (x=2, 3) Systems

Yong Qing Li

COIMBRA
2011

UNIVERSIDADE DE COIMBRA

Faculdade de Ciências e Tecnologia

Departamento de Química

Double Many-Body Expansion Potential Energy Surfaces For NH_x (x=2, 3) Systems

Dissertation presented for fulfillment of the requirements for the degree of "Doutor em Ciências, especialidade em Química Teórica"

Yong Qing Li

COIMBRA
2011

Dedicated to my family

Acknowledgments

First of all, I would like to give the most sincere thank to my adviser, Professor António Joaquim de Campos Varandas, for his inspirational instructions and patient guidance during the passed four years. His efforts lead me step by step to advance in my study and research, and finally make this dissertation possible.

Here I also thank Professor Sergio P. J. Rodrigues, giving very nice comments and suggestions. I would express my great appreciation to Dr. Pedro J. S. B. Caridade his valuable help and instructions. I acknowledge the members of Professor António Joaquim de Campos Varandass group, especially Dr. Y. Z. Song, Dr. Luís A. Poveda, Dr. Vinícius C. Mota, Dr. Luís P. Viegas, Dr. Breno R. L. Galvão and S. Joseph, for their friendship and valuable discussions.

I also acknowledge Professor K. L. Han in Dalian Institute of Chemical Physics, Chinese Academy of Sciences, China and Professor F. C. Ma in Department of Physics, Liaoning University, China, they recommended me to apply for the PhD position in Professor Varandas's group, thank their trust, encouragement and support.

Finally, in particular, I would like to thank my parents, my wife, my daughter and my son for their unlimited love, understanding, encouragement and countless support all these years.

This work has the financial support of Fundação para a Ciência e a Tecnologia (SFRH/BD/29336/2006), Portugal.

Contents

Foreword

Molecular systems involving nitrogen and hydrogen atoms play a significant role in many chemical processes as atmospheric chemistry [1], combustion of nitrogen containing fuel [2], atmospheric cycles of pollutants [3] and nitrogen fixation [4]. The availability of potential energy surfaces (PESs) for small molecules is key for reaction dynamics and kinetics studies.

Many important concepts that might appear to be mathematically challenging can be grasped intuitively with the insight provided by the idea of the PES. The molecular PES is the potential energy that determines the motion of the nuclei. In the Borm-Oppenheimer [5] approximation the electrons adjust their positions instantaneously to follow any movement of the nuclei, so that the PES can equally be thought of as the potential for the movement of atoms within a molecule or atoms in collision with one another. An analytical representation of the PES is obtained using different formalism, such as the double many-body expansion (DMBE) [6–9] method. Information about a PES can obtained both from the analysis of experimental data and from *ab initio* calculations. NH_2 and NH_3 are sufficiently small to allow the calculation of its electronic strcture with accurate *ab initio* methods and large basis sets, so it makes a possible to construct accurate and global *ab initio*-based PES. Amongst the tetratomic systems, the PES of NH_3 assumes special relevance because this species is a major constituent of some planetary atmospheres whose Boltzmann temperatures require for their determination an accurate knowledge of the ro-vibrational transition energies, and hence of its PES.

The main goal of the present doctoral thesis is the construction of DMBE PES for NH_x (x=2, 3) systems, which may used later in dynamics and kinetic studies of gas-phase reactions. PESs for the first excited state of NH_2 ($1\,^2A'$) and the

ground state NH_3 ($^1A_1$) were constructed, which can therefore be recommended as a building block for construction of DMBE forms for larger N_xH_y species.

This thesis is divided in two parts. The first concern with the theory and methods, while the case studies presented in second part. Chapter 1 presents the concept of PES. Chapter 2 gives a survey of the *ab initio* methods and the formalisms to obtain analytical representations. Chapter 3 deals with methods here employed to calculate spectroscopic and dynamics properties using these PESs. Some conclusions and outlook are given in Chapter 7.

In Chapter 4, both accurate DMBE/SEC and DMBE/CBS PESs for the $1\,^2A'$ state of NH_2 are presented [10], the various topographical features of both DMBE/SEC and DMBE/CBS PESs have been carefully examined, and compared with previous results. Both PESs have been built such as to become degenerate at linear geometries with the ground-state PES of $1^2A''$ [11] symmetry reported by our group, where both form a Renner-Teller pair [12–14].

In Chapter 5, we report a single-sheeted global DMBE PES for the ground electronic state of NH_3 [15], the DMBE PES shows the proper atom permutational symmetry. To warrant that the PES dissociates to the correct asymptotes, a generalization of the switching function proposed elsewhere [11] has been extended to the present four-atom species. The PES so obtained shows the correct long-range behavior at all dissociation channels while providing a realistic representation at all interatomic separations.

In Chapter 6, The single-sheeted DMBE PES for the ground-state of NH_2 is refined to attain near spectroscopic accuracy from a multiproperty fit to accurate *ab initio* energies and experimental vibrational levels, including the Renner-Teller effect for total angular momentum (excluding spin) of $N = 0$. Quasiclassical trajectory calculations on both the original and newly reported potential energy surfaces suggest that the dynamical properties of the original form remain essentially unaltered as aimed.

Bibliography

[1] A. N. Wright and C. A. Winkler, *Active Nitrogen* (Academic, New York, 1968).

[2] J. A. Miller and C. G. Bowman, Prog. Energy Combust. Sci. **15**, 287 (1989).

[3] R. P. Wayne, *Chemistry of Atmospheres* (Oxford University Press, Oxford, 2002).

[4] A. Hellman, E. J. Baerends, M. Biczysko, T. Bligaard, C. H. Christensen, D. C. Clary, S. Dahl, R. van Harrevelt, K. Honkala, H. Jonsson, G. J. Kroes, M. Luppi, U. Manthe, J. K. Nrskov, R. A. Olsen, J. Rossmeisl, E. Sklason, C. S. Tautermann, A. J. C. Varandas, and J. K. Vincent, J. Phys. Chem. B **110**, 17719 (2006).

[5] M. Born and J. R. Oppenheimer, Ann. Phys. **84**, 457 (1927).

[6] A. J. C. Varandas, Mol. Phys. **53**, 1303 (1984).

[7] A. J. C. Varandas, Adv. Chem. Phys. **74**, 255 (1988).

[8] A. J. C. Varandas, in *Lecture Notes in Chemistry*, edited by A. Laganá and A. Riganelli (Springer, Berlin, 2000), vol. 75, p. 33.

[9] A. J. C. Varandas, *Conical Intersections: Electronic Structure, Spectroscopy and Dynamics* (World Scientific Publishing, 2004), chap. 5, p. 91, Advanced Series in Physical Chemistry.

[10] Y. Q. Li and A. J. C. Varandas, J. Phys. Chem. A **114**, 9644 (2010).

[11] A. J. C. Varandas and L. A. Poveda, Theor. Chem. Acc. **116**, 404 (2006).

[12] R. Renner, Z. Phys. **92**, 172 (1934).

[13] A. Messiah, *Quantum Mechanics* (Wiley, New York, 1966).

[14] G. Herzberg, *Molecular Spectra and Molecular Structure Vol. III, Reprint Edition* (Krieger, Malabar, 1991).

[15] Y. Q. Li and A. J. C. Varandas, J. Phys. Chem. A **114**, 6669 (2010).

Part I

Theory and methods

Chapter 1

The concept of potential energy surface

The potential energy surface (PES) is related to the Born-Oppenheimer approximation [1] in molecular quantum mechanics. The Born-Oppenheimer approximation demonstrates that the simple picture of nuclei moving in a PES determined by electrons is justified due to the small mass ratio of electronic and nuclear. The validity of the separation between electronic and nuclear motion is also due to the small mass ratio between electronic and nuclear, the time scales with which the electrons and nuclei move are generally quite different. In particular, the heavy nuclei move more slowly than do the lighter electrons. Thus, we expect the electrons to be able to "adjust" their motions to the much more slowly moving nuclei. This observation motivates us to solve the Schrödinger equation for the movement of the electrons in the presence of fixed nuclei as a way to represent the fully-adjusted state of the electrons at any fixed positions of the nuclei[1]. This implies that the total molecular wavefunction is written as a product of an electronic wavefunction and a nuclear wavefunction. In this way, the resolution of the molecular problem is attained within the so called *adiabatic approximation*, in which an electronic Schrödinger equation is solved for a set of fixed nuclear arrangements, yielding the PES for the nuclei motion through a specific electronic state.

[1] This is why we say we "freeze the nuclei" in making the Born-Oppenheimer approximation. We don't really freeze them, we just solve first for the motions of the electrons at some specified (i.e., frozen set of nuclear positions) $\mathbf{R}$ values

1.1 The adiabatic and Born-Oppenheimer approximation

One of the most important approximations relating to applying quantum mechanics to molecules is known as the Born-Oppenheimer approximation [1]. For a general molecular system consisting of electrons and nuclei, let us consider a system comprising M nuclei and N electrons. By including only electrostatic interactions, the Hamiltonian of the system is given by

$$\hat{H}_{tot}(\mathbf{r},\mathbf{R}) = -\sum_{\alpha=1}^{M}\frac{\hbar^2\nabla_\alpha^2}{2M_\alpha} - \sum_{i=1}^{N}\frac{\hbar^2\nabla_i^2}{2m_e} + \hat{V}(\mathbf{r},\mathbf{R}) \tag{1.1}$$

where $\mathbf{r}$ and $\mathbf{R}$ are used as shorthand notation for the electronic $(r_1, r_2 \ldots, r_N)$ and nuclear coordinates $(R_1, R_2 \ldots, R_M)$, respectively. $\boldsymbol{\nabla}_\alpha$ is the nuclear gradient operator in coordinates of α-th nucleus, $\boldsymbol{\nabla}_i$ is the electronic gradient operator in coordinates of i-th nucleus. All electrostatic interactions, i.e. electron-electron, electron-nuclear, nuclear-nuclear, are included in $\hat{V}(\mathbf{r},\mathbf{R})$.

The Hamiltonian operator is first transformed to center of mass system where it is written as

$$\hat{H}_{tot} = \hat{T}_n + \hat{H}_e + \hat{H}_{mp} \tag{1.2}$$

where

$$\hat{H}_e = \hat{T}_e + \hat{V}_{ee} + \hat{V}_{ne} + \hat{V}_{nn} \tag{1.3}$$

and

$$\hat{H}_{mp} = -\frac{1}{2M_{tot}}\left(\sum_{i=1}^{N}\nabla_i\right)^2 \tag{1.4}$$

here $\hat{H}_e$ is the electronic Hamiltonian operator and $\hat{H}_{mp}$ is called the mass-polarization, which arises because it is not possible to rigorously separate center of mass motion from the internal motion for system with more than two particles.

The time-independent Schrödinger equation is the starting point:

$$H_{tot}\left|\Psi\left(\mathbf{r},\mathbf{R}\right)\right\rangle = E_{tot}\left|\Psi\left(\mathbf{r},\mathbf{R}\right)\right\rangle \tag{1.5}$$

where $\left|\Psi\left(\mathbf{r},\mathbf{R}\right)\right\rangle$ is the total (exact) wave function without any approximations, it can be written as an expansion in complete set of electronic functions, with the

expansion coefficients being functions of the nuclear coordinates.

$$|\Psi(\mathbf{r},\mathbf{R})\rangle = \sum_{i=1}^{\infty} \Psi_{ni}(\mathbf{R})\,|\Psi_i(\mathbf{r},\mathbf{R})\rangle \tag{1.6}$$

where $|\Psi_i(\mathbf{r},\mathbf{R})\rangle$ is electronic wave function defining by

$$\hat{H}_e(\mathbf{R})\,|\Psi_i(\mathbf{r},\mathbf{R})\rangle = E_i(\mathbf{R})\,|\Psi_i(\mathbf{r},\mathbf{R})\rangle\,;\ i = 1,2,...,\infty \tag{1.7}$$

the $|\Psi_i(\mathbf{r},\mathbf{R})\rangle$ can be chosen to be orthonormal

$$\langle\Psi_i(\mathbf{r},\mathbf{R})\,|\Psi_j(\mathbf{r},\mathbf{R})\rangle = \delta_{ij} \tag{1.8}$$

Introducing Eq. (1.2) and Eq. (1.6) into the The time-independent Schrödinger equation (1.5), we get

$$\sum_{i=1}^{\infty}(\hat{T}_n + \hat{H}_e + \hat{H}_{mp})\Psi_{ni}(\mathbf{R})\,|\Psi_i(\mathbf{r},\mathbf{R})\rangle = E_{tot}\sum_{i=1}^{\infty}\Psi_{ni}(\mathbf{R})\,|\Psi_i(\mathbf{r},\mathbf{R})\rangle \tag{1.9}$$

where the nuclear kinetic energy $\hat{T}_n$ is written as

$$\hat{T}_n = \sum_{a=1}^{M} -\frac{1}{2M_a}\nabla_a^2 = \nabla_n^2 \tag{1.10}$$

then, introducing Eq. (1.10) into Eq. (1.9)

$$\sum_{i=1}^{\infty}(\nabla_n^2 + \hat{H}_e + \hat{H}_{mp})\Psi_{ni}(\mathbf{R})\,|\Psi_i(\mathbf{r},\mathbf{R})\rangle = E_{tot}\sum_{i=1}^{\infty}\Psi_{ni}(\mathbf{R})\,|\Psi_i(\mathbf{r},\mathbf{R})\rangle \tag{1.11}$$

$$\begin{aligned}&\sum_{i=1}^{\infty}\big\{\nabla_n^2\Psi_{ni}(\mathbf{R})\,|\Psi_i(\mathbf{r},\mathbf{R})\rangle + \hat{H}_e\Psi_{ni}(\mathbf{R})\,|\Psi_i(\mathbf{r},\mathbf{R})\rangle\\ &+\hat{H}_{mp}\Psi_{ni}(\mathbf{R})\,|\Psi_i(\mathbf{r},\mathbf{R})\rangle\big\} = E_{tot}\sum_{i=1}^{\infty}\Psi_{ni}(\mathbf{R})\,|\Psi_i(\mathbf{r},\mathbf{R})\rangle\end{aligned} \tag{1.12}$$

noted the fact that $\hat{H}_e$ and $\hat{H}_{mp}$ only act on the electronic wave function $|\Psi_i(\mathbf{r},\mathbf{R})\rangle$, then introducing electronic Schrödinger equation Eq. (1.7) into Eq. (1.12)

$$\begin{aligned}&\sum_{i=1}^{\infty}\big\{\,|\Psi_i(\mathbf{r},\mathbf{R})\rangle\,\nabla_n^2\Psi_{ni}(\mathbf{R}) + 2[\nabla_n\,|\Psi_i(\mathbf{r},\mathbf{R})\rangle][\nabla_n\Psi_{ni}(\mathbf{R})]\\ &+\Psi_{ni}(\mathbf{R})\,\nabla_n^2\,|\Psi_i(\mathbf{r},\mathbf{R})\rangle + \Psi_{ni}(\mathbf{R})\,E_i(\mathbf{R})\,|\Psi_i(\mathbf{r},\mathbf{R})\rangle\\ &+\Psi_{ni}(\mathbf{R})\,\hat{H}_{mp}\,|\Psi_i(\mathbf{r},\mathbf{R})\rangle\big\} = E_{tot}\sum_{i=1}^{\infty}\Psi_{ni}(\mathbf{R})\,|\Psi_i(\mathbf{r},\mathbf{R})\rangle\end{aligned} \tag{1.13}$$

using the orthonormality of the $|\Psi_i(\mathbf{r},\mathbf{R})\rangle$ by multiplying from left by a specific electronic wave function $\langle\Psi_j(\mathbf{r},\mathbf{R})|$ and integrate the electron coordinates.

$$\begin{aligned}
&\nabla_n^2\Psi_{nj}(\mathbf{R}) + E_j(\mathbf{R})\Psi_{nj}(\mathbf{R}) \\
&+\sum_{i=1}^{\infty}\big\{2\langle\Psi_j(\mathbf{r},\mathbf{R})|\nabla_n|\Psi_i(\mathbf{r},\mathbf{R})\rangle\,\nabla_n\Psi_{ni}(\mathbf{R}) \\
&+\langle\Psi_j(\mathbf{r},\mathbf{R})|\nabla_n^2|\Psi_i(\mathbf{r},\mathbf{R})\rangle\,\Psi_{ni}(\mathbf{R}) \\
&+\langle\Psi_j(\mathbf{r},\mathbf{R})|\hat{H}_{mp}|\Psi_i(\mathbf{r},\mathbf{R})\rangle\,\Psi_{ni}(\mathbf{R})\big\} = E_{tot}\Psi_{nj}(\mathbf{R})
\end{aligned} \tag{1.14}$$

the electronic wave function has been removed from the first two terms, the first two terms in the curly bracket are the first- and second-order non-adiabatic coupling elements, respectively, while the last is the mass-polarization.

In the adiabatic approximation [2–7] the form of total wave function is restricted to one electronic surface, i.e., all coupling elements in Eq. (1.14) are neglected, only the terms with $i = j$ survive. Except for spatially degenerate wave functions, the diagonal first-order non-adiabatic coupling elements are zero.

$$\begin{aligned}
&\big\{\nabla_n^2 + E_j(\mathbf{R}) + \langle\Psi_j(\mathbf{r},\mathbf{R})|\nabla_n^2|\Psi_j(\mathbf{r},\mathbf{R})\rangle \\
&+\langle\Psi_j(\mathbf{r},\mathbf{R})|\hat{H}_{mp}|\Psi_j(\mathbf{r},\mathbf{R})\rangle\big\}\Psi_{nj}(\mathbf{R}) = E_{tot}\Psi_{nj}(\mathbf{R})
\end{aligned} \tag{1.15}$$

neglecting the mass-polarization and reintroducing the nuclear kinetic energy operator Eq. (1.10) into above equation

$$[\hat{T}_n + E_j(\mathbf{R}) + U(\mathbf{R})]\Psi_{nj}(\mathbf{R}) = E_{tot}\Psi_{nj}(\mathbf{R}) \tag{1.16}$$

where $U(\mathbf{R}) = \langle\Psi_j(\mathbf{r},\mathbf{R})|\nabla_n^2|\Psi_j(\mathbf{r},\mathbf{R})\rangle$ is the diagonal correction, is smaller than $E_j(\mathbf{R})$ by a factor roughly equal the ratio of the electronic and nuclear masses. It is usually varying function of $\mathbf{R}$, and the shape of the energy surface is therefore determined almost exclusively by $E_j(\mathbf{R})$ [7].

In the Born-Oppenheimer approximation, the diagonal correction is also neglected, the Eq. (1.16) become

$$[\hat{T}_n + E_j(\mathbf{R})]\Psi_{nj}(\mathbf{R}) = E_{tot}\Psi_{nj}(\mathbf{R}) \tag{1.17}$$

since the potential depends on the nuclear coordinates[2], the electronic wave functions depends parametrically on $\mathbf{R}$ and the "eigenvalue" $E_i(\mathbf{R})$ is a function of

[2]As usual the nuclei repulsion operator is included in the electronic Hamiltonian.

the nuclear coordinates. One obtains $E_i(\mathbf{R})$ as a function of $\mathbf{R}$. This is the PES: $E_i(\mathbf{R})$. In the Born-Oppenheimer picture, the nuclei move on a PES which is a solution to the electronic Schrdinger equation. The PES is independent of nuclear masses, but this is not the case when working in the adiabatic approximation since the diagonal correction (and mass-polarization) depends on the nuclear masses.

Eq. (1.17) and its implied assumption of the separability of the electronic and nuclear motions is called the Born-Oppenheimer approximation. This step of the Born-Oppenheimer approximation involves separation of vibrational, translational, and rotational motions. The eigenvalue E_{tot} in Eq. (1.17) is the total energy of the molecule, including contributions from electrons, nuclear vibrations, and overall rotation and translation of the molecule. The Eq. (1.17) expresses that the nuclei move in an effective potential which is the electronic energy $E_i(\mathbf{R})$ as a function of the internuclear distances is constant with respect to a translation and/or rotation of a fixed nuclear configuration.

1.2 Molecular geometry

PESs are important because they aid us in visualizing and understanding the relationship between potential energy and molecular geometry, and in understanding how computational chemistry programs locate and characterize structures of interest. Among the main tasks of computational chemistry are to determine the structure and energy of molecules and of the transition states involved in chemical reactions.

The geometry of a molecule determines many of its physical and chemical properties. This is why it is very important that we understand the geometry of a molecule when running computations. Given a PES, a geometry is just a point on it, and there are many other points on the PES. Among all the points on a surface, there are some points distinct from others. They are as follows:

Local minima: that point on the PES that is the lowest value in a particular section or region of the PES.

Global minima: that point on the PES that is the lowest value in the entire PES.

Saddle point: a point on the PES that is a maximum in one direction and a minimum in the othe. Saddle points represent a transition structure connecting two equilibrium structures.

If all of the first derivative are zero and all the second order derivative are positive at some point, then that point is a minimum. If all the first derivatives are zero and second derivatives are negative at some point, then it is a maxima. Saddle point is a point that is maximum in some directions and minimum in the other directions. For a saddle point in n-dimension space, if there are only one negative second order derivative, and all the others are positive, then it is called first order saddle point. If there are k negative second order derivative, then it is called k-th order saddle point. In the study of chemical reaction, only first order saddle point may of interest.

There are possibly many saddle points and local minima but only one global minimum. They are all called stationary points since their first order derivatives are all zero. The stationary points are very important to chemical reactions and also important in characterization PESs.

Stable molecules correspond to minima on the PES within the Born-Oppenheimer approximation and a chemical reaction can be described as nuclei moving from one minimum to another. The lowest energy pathway linking the two minima, the reaction coordinate or intrinsic reaction coordinate is the path that would be followed by a molecule in going from one minimum to another should it acquire just enough energy to overcome the activation barrier, pass through the transition state, and reach the other minimum.

In the lowest level of approximation, the motion is assumed to occur along the path of least energy, and this path forms the basis for transition state theory [8]. The transition state is the configuration that divides the reactant and product parts of the surface (i.e., a molecule that has reached the transition state will continue on to product), while the geometrical configuration of the energy maximum along the reaction path is called the transition structure. The transition structure a first-order saddle point on the PES is a maximum in the reaction coordinate direction and a minimum along all other coordinates.

1.3 The Renner-Teller effect

The Renner-Teller (RT) effect is one of the best characterized breakdowns of the the Born-Oppenheimer approximation in molecular spectroscopy. In its simplest manifestation, the RT effect occurs in linear triatomic molecules in orbitally degenerate electronic states, it is caused by a coupling between the electronic orbital angular momentum and the nuclear vibrational angular momentum associated with the bending vibration [9].

In 1933 G. Herzberg and E. Teller [10] recognized that the potential of a triatomic linear molecule in a degenerate electronic state splits into two when the molecule is bent. A year later this effect was worked out in detail by Rudolf Renner [11], who gave an explanation of this splitting and showed that the bending and electronic motion are coupled. He predicted that this coupling would give rise to anomalies in the vibrational side bands of electronic spectra. Herzberg refers to this as the "Renner-Teller" effect in one of his influential books [12] and consequently the effect is now generally called after Renner and Teller.

Let the electronic state $|\Lambda\rangle$ be an eigenstate of L_Z^{el}, the projection of the electronic angular momentum operator on the molecular axis, with eigenvalue $\hbar\Lambda$. The states $|\pm\Lambda\rangle$ are degenerate with energy $E_{|\Lambda|}^{el}$. Let $|v, l\rangle$ be a harmonic bending vibration function, which is an eigenfunction of L_Z^{vib} , the projection of the vibrational angular momentum operator on the molecular axis, with eigenvalue $\hbar l$. The v+1 states $|v, l\rangle$, $l = -v, -v + 2, \ldots, v$ are are degenerate with energy $h\nu(v + 1)$. The orthonormal product states

$$|1\rangle \equiv |\Lambda\rangle \otimes |v, K - \Lambda\rangle \tag{1.18}$$

and

$$|2\rangle \equiv |-\Lambda\rangle \otimes |v, K + \Lambda\rangle \tag{1.19}$$

are eigenfunctions of

$$L_Z^{\mathrm{tot}} \equiv L_Z^{\mathrm{el}} \otimes 1 + 1 \otimes L_Z^{\mathrm{vib}} \tag{1.20}$$

with eigenvalue $\hbar K$. In zeroth-order the product kets are degenerate with energy $E_{|\Lambda|}^{el} + h\nu(v + 1)$. The bending of the molecule generates a coupling between the electronic and vibrational motion (a so-called vibronic coupling) that acts as a

perturbation. Diagonalization of the 2×2 matrix of this perturbation on basis of $|1\rangle$ and $|2\rangle$ gives two new orthonormal zeroth-order eigenvectors

$$\Psi_{+}^{(0)} = \cos\alpha\,|1\rangle + \sin\alpha\,|2\rangle \tag{1.21}$$

and

$$\Psi_{-}^{(0)} = -\sin\alpha\,|1\rangle + \cos\alpha\,|2\rangle \tag{1.22}$$

with first order energies: $E_{\pm}^{(1)}$. Clearly, the functions $\Psi_{\pm}^{(0)}$ are no longer simple products; this breakdown of the Born-Oppenheimer approximation is the RT effect. Also belonging to the Renner-Teller effect is the observation that the functions $\Psi_{\pm}^{(0)}$ are not degenerate in first order. The linear combinations $\Psi_{\pm}^{(0)}$ are not eigenfunctions of $E_{|\Lambda|}^{el}$ and L_Z^{vib}. However, they are eigenfunctions of L_Z^{tot}.

The Renner-Teller effect was not observed until 1959, when K. Dressler and D. A. Ramsay [13] measured the electronic absorption spectrum of NH_2 and ND_2. They found that the first electronically excited states of these triatomic molecules have a linear geometry and observed in these excited states an unusual type of vibronic structure: the RennerTeller effect.

Bibliography

[1] M. Born and J. R. Oppenheimer, Ann. Phys. **84**, 457 (1927).

[2] M. Born and K. Huang, *Dynamical Theory of Crystal Lattices* (Clarendon Press, Oxford, 1954).

[3] A. S. Davidov, *Quantum Mechanics* (Pergamon, Oxford, 1965).

[4] A. Messiah, *Quantum Mechanics* (Wiley, New York, 1966).

[5] P. G. Wilkinson and H. O. Pritchard, Can. J. Phys. **47**, 2493 (1969).

[6] N. F. Stepanow, J. Structural. Chemistry **24**, 20 (1983).

[7] N. C. Handy and A. M. Lee, Chem. Phys. Lett. **252**, 425 (1996).

[8] H. Eyring, J. Chem. Phys. **37**, 107 (1935).

[9] H. L. Dai and R. W. Field, *Molecular Dynamics and Spectroscopy by Stimulated Emission Pumping* (World Scientific, Singapore, 1995).

[10] G. Herzberg and E. Teller, Z. Phys. Chem. **B21**, 410 (1933).

[11] R. Renner, Z. Phys. **92**, 172 (1934).

[12] G. Herzberg, *Molecular Spectra and Molecular Structure Vol. III, Reprint Edition* (Krieger, Malabar, 1991).

[13] K. Dressler and D. A. Ramsay, Phil. Trans. Roy. Soc. **251A**, 553 (1959).

Chapter 2

Ab initio-based potential energy surface

The modeling of potential energy surface (PES) can be obtained using different data, such as the *ab initio* electronic structure calculations. In this method one performs a large number of *ab initio* electronic structure calculations which may be very expensive and then fit the results using a least squares procedure. The reliability of the PES depends on the basis set completeness and how well electron correlation is accounted for.

The *ab initio* electronic structure methods are based upon quantum mechanics and therefore provide the most accurate and consistent predictions for chemical systems, it aim at solving Schrödinger equation for the chemical system using a "basis set" of functions that satisfy a series of rigorous mathematical approximations. The term *ab initio* implies that the computations are based solely on the laws of quantum mechanics. However *ab initio* methods are extremely computer intensive and capable of high accuracy predictions over a wide range of systems. Rapid advances in computer technology are making *ab initio* methods increasingly more practical for use with realistic chemical systems.

A large number of *ab initio* electronic structure methods are available in package programs to perform quantum chemistry calculations. One of the most commonly used, for high accuracy electronic structure calculation, is the Molpro package [1]. In the following sections a brief discussion of the standard models, adopted for the present calculations, is presented.

2.1 *Ab initio* calculations

All *ab initio* wave function methods commonly used in electronic structure theory in some way involve the orbital approximation, wherein antisymmetrized products (Slater determinants) of one-electron functions are used to represent many-electron (fermion) wave functions of chemical systems

$$|\mathbf{\Phi}\rangle = |\phi_1, \phi_2, \ldots, \phi_i, \ldots, \phi_n| \tag{2.1}$$

where i identifies electronic states and $\left\{ |\phi_i\rangle \right\}$ is an orthogonal basis set of one-electron molecular wave functions (molecular orbitals), each molecular orbital[1] $|\phi_i\rangle$ is expanded in terms of the basis function $|\chi_\alpha\rangle$, conventionally called atomic orbitals

$$|\phi_i\rangle = \sum_\alpha C_{\alpha i} |\chi_\alpha\rangle \tag{2.2}$$

the $C_{\alpha i}$ coefficients may be determined numerically by substitution of this equation into the Schrödinger equation and application of the variational principle. This method is called the linear combination of atomic orbitals approximation.

A variational solution of the Schrödinger equation (1.7) with trials Eq. (2.1) and Eq. (2.2), these are the Hartree-Fock equations in the atomic orbital basis, and all the equations may be collected in a matrix notation, is obtained by solving the Roothaan-Hall Hartree-Fock [2–4] equations

$$\mathbf{FC} = \mathbf{SC}\varepsilon \tag{2.3}$$

where ε is a diagonal matrix of the orbital energies, $\mathbf{C}$ is a matrix of coefficients, the $\mathbf{F}$ and $\mathbf{S}$ are the Fock and overlap matrices. The matrix elements of the overlap matrix are defined as

$$S_{\alpha\beta} = \langle \alpha | \beta \rangle = \langle \chi_\alpha | \chi_\beta \rangle \tag{2.4}$$

in general, the basis functions cannot be chosen in such a way that $\mathbf{S}$ is the unit matrix, the $\mathbf{S}$ matrix contains the overlap elements between basis functions. The Fock matrix is constructed from one- and two-electron integrals [5]

$$F_{\alpha\beta} = \langle \alpha | h | \beta \rangle + \sum_j \sum_{\rho,\sigma} C_{j\rho} C_{j\sigma} (2\langle \rho\sigma | \alpha\beta \rangle + \langle \rho\beta | \alpha\sigma \rangle) \tag{2.5}$$

[1] MO, molecular orbital = LCAO, Linear Combination of Atomic Orbitals

the matrix elements of the one-electron Hamiltonian (one-electron integrals) are given by

$$\langle \alpha | h | \beta \rangle = \langle \chi_\alpha | h | \chi_\beta \rangle = \int \chi_\alpha^* h \chi_\beta dr \tag{2.6}$$

and the two-electron integrals are given by

$$\langle \rho\sigma | \alpha\beta \rangle = \langle \chi_\rho \chi_\sigma | \chi_\alpha \chi_\beta \rangle = \int \chi_\rho^*(1) \chi_\sigma(1) \frac{1}{r_{12}} \chi_\alpha^*(2) \chi_\beta(2) dr_1 dr_2 \tag{2.7}$$

The Roothaan-Hall Eq. (2.3) is a determination of the eigenvalues of the Fock matrix. To determine the unknown coefficients $\mathbf{C}_{\alpha i}$, the Fock matrix must be diagonalized. However, the Fock matrix, Eq. (2.5), is only known if all the MO coefficients are known. The procedure therefore starts off by some guess of the coefficients, forms the $\mathbf{F}$ matrix, and diagonalizes it. The new set of coefficients is then used for calculating a new Fock matrix, etc. This is continued until the set of coefficients used for constructing the Fock matrix is equal to those resulting from the diagonalization. This set of coefficients determines a *self-consistent field* (SCF) solution.

2.1.1 CI method

The Hartree-Fock (HF) method generates solutions to the Schrödinger equation where the real electronelectron interaction is replaced by an average interaction. The difference in energy between the HF and the lowest possible energy in the given basis set is called the *Electron correlation* energy within the non-relativistic realm

$$E_{\text{corr}} = E_{\text{exact}} - E_{\text{HF}} \tag{2.8}$$

in contrast to the HF method, in order to account for electron correlation, the configuration interaction (CI) method uses a variational wave function that is a linear combination of configuration state functions (CSFs). In order to keep track of all the possible HF orbitals, we often write the ground-state Hartree-Fock wave function as $\mathbf{\Phi}_{\text{HF}}$, the Slater determinant with an electron "excited" from the ith occupied orbital to the ath unoccupied (virtual) orbital as $|\mathbf{\Phi}_i^a, \rangle$, the two electrons "doubly excited" from the ith and jth occupied orbital to the ath and bth unoccupied orbital as $\left|\mathbf{\Phi}_{ij}^{ab}, \right\rangle$, etc.. With this notation, we can write the CI

wave function as

$$|\Psi_{\mathrm{CI}}\rangle = C_0 |\Phi_{\mathrm{HF}}\rangle + \sum_{i,a} C_i^a |\Phi_i^a\rangle + \sum_{\substack{i>j \\ a>b}} C_{ij}^{ab} |\Phi_{ij}^{ab}\rangle + \sum_{\substack{i>j>k \\ a>b>c}} C_{ijk}^{abc} |\Phi_{ijk}^{abc}\rangle + \dots \quad (2.9)$$

for the determination of the expansion CI coefficients the variation principle is invoked. Of course, we need to truncate the expansion in Eq. (2.9) , and not consider any excitations above some order. When we truncate at zeroth-order, we have the Hartree-Fock method. At first order, we have *Configuration-Interaction with Single excitations* (CIS), at second order we have *Configuration Interaction with Single and Double excitations* (CISD), and so on: CISDT (third order), CISDTQ (fourth order), ... When we do not truncate the expansion (so that we include N-electron excitations) we say we are doing a *Full-Configuration-Interaction calculations*, which is called Full-CI (FCI). Full configuration interaction calculations are costly, and their cost is related to the binomial coefficient

$$\binom{K}{N} = \frac{K!}{(K-N)!N!} \quad (2.10)$$

where K is the total number of Hartree-Fock orbitals that were solved for and N is the number of electrons. For sufficiently large K, FCI calculations are essentially exact.

2.1.2 MCSCF method

In the sense that Hartree-Fock is a good zero-order approximation, and under such circumstances, single-reference methods provide an efficient and accurate way to getting correlation energies and correlated wave functions. However, wherever bonds are being broken, and for many excited states, the Hartree-Fock determinant does not dominate the wave function, and may sometimes be just one of a number of important electronic configurations. If this is the case, single-reference methods, which often depend formally on perturbation arguments for their validity, are inappropriate, and one must seek from the outset to have a first description of the system that is better than Hartree-Fock. Only then can one go on to attempt to recover the remaining dynamic correlation effects [6].

In contrast to the relationship between virtual and occupied orbitals, natural orbitals are localized in the same regions of physical space. The strong coupling

thus produced by the overlap of ground state and excited orbitals effectively lowers the energy of the system. Another method which achieves the same purpose and therefore improves the convergence of a CI expansion is the multiconfiguration self-consistent field (MCSCF) method. The method can be described as one which ensures that both the CI coefficients [C_i^a, C_{ij}^{ab}, C_{ijk}^{abc}, ... ,in Eq. (2.9)] and the molecular orbital coefficients [$C_{\alpha i}$ in Eq. (2.2)] have been varied to minimize the energy [7]. The general form of a MCSCF wavefunction is [8]

$$|\mathbf{\Psi}_{\mathrm{MCSCF}}\rangle = \sum_K C_k \, |\mathbf{\Phi}_k\rangle \tag{2.11}$$

which is a linear combination of several configurations [referred to as CSFs, $|\mathbf{\Phi}_k\rangle$]. Each CSF differs in how the electrons are placed in the MOs, $|\phi_i\rangle$. The MOs are usually expanded in a basis of AOs as shows in Eq. (2.2). A doubly iterative process is used which, upon convergence, yields the optimum orbitals and the optimum configurational mixing coefficients for the basis sets used. The optimization of the orbitals ensures that the virtual orbitals are in the same physical space as the occupied orbitals. Since the number of MCSCF iterations required for achieving convergence tends to increase with the number of configurations included, the size of MCSCF wave functions that can be treated is somewhat smaller than for CI methods.

The major problem with MCSCF methods is selecting which configurations are necessary to include for the property of interest. One of the most popular approaches is the Complete Active Space SCF (CASSCF) [9, 10] method [also called Full Optimized Reaction Space (FORS [11–16])]. Here the selection of configurations is done by partitioning the MOs into active and inactive spaces. The active MOs will typically be some of the highest occupied and some of the lowest unoccupied MOs. The inactive MOs have either 2 or 0 electrons, i.e., always either doubly occupied or empty [4].

2.1.3 MRCI method

The *multireference configuration interaction* (MRCI) wavefunction is obtained by taking as the reference not a Single Slater determinant like in Eq. (2.9), but a set as *reference configuration* optimized at the MCSCF level. In general, the MRCI

wavefunction can be written as,

$$|\Psi_{\mathrm{MRCI}}\rangle = \sum_I C^I \left|\Phi^I\right\rangle + \sum_S \sum_a C_a^S \left|\Phi_S^a\right\rangle + \sum_P \sum_a C_{ab}^p \left|\Phi_P^{ab}\right\rangle + \ldots \tag{2.12}$$

where a, b denote external orbitals (not occupied in the reference configurations) ans S and P denote internal $N-1$ and $N-2$ electron hole state. $\left|\Phi^I\right\rangle$, $|\Phi_S^a\rangle$ and $\left|\Phi_P^{ab}\right\rangle$ are internal, singly external, and doubly external configurations, respectively, and the set of configurations is the union of the sets of CSFs obtained by making all possible single and double excitations on each reference configuration in turn.

The main bottleneck of the MRCI method is the fact that the size of the configuration expansion and the computational effort rapidly increases with the number of reference configurations. This handicap become dramatic when studying PESs, where an reasonable number of configurations is needed to describe all the configuration space in a balanced way.

In order to reduce the number of variational parameters in MRCI wave functions different contraction schemes have been proposed. In the "externally" contracted CI of Siegbahn [17, 18] the singly and doubly external configurations are contracted as

$$|\Phi_S\rangle = \sum_a \alpha_a^S \left|\Phi_S^a\right\rangle \tag{2.13}$$

$$|\Phi_P\rangle = \sum_{ab} \alpha_{ab}^P \left|\Phi_P^{ab}\right\rangle \tag{2.14}$$

where the contraction coefficients α are obtained by first order perturbation theory. The number of variational parameters is then equal to the number of internal states.

Another contraction scheme was first discussed Meyer [19] and Siegbahn [20]. In this method the configurations are generated by applying pair excitation operators to the reference wave function as a whole. This effectively generates liner combinations of the configurations $\left|\Phi_P^{ab}\right\rangle$ with different internal states P and is therefore called "internally contracted CI" [20, 21]. The internally contracted doubly external configurations are defined as

$$\left|\Phi_{ij,\nu}^{ab}\right\rangle = \frac{1}{2}\left(\hat{E}_{ai,bj} + \nu \hat{E}_{bi,aj}\right)|\Phi_0\rangle \tag{2.15}$$

where $\nu = 1$ for external singlet pairs and $\nu = -1$ for triplet pairs, and $|\mathbf{\Phi}_0\rangle$ is the reference wave function, which may be composed of many configurations $|\mathbf{\Phi}_R\rangle$

$$|\mathbf{\Phi}_0\rangle = \sum_R \alpha^R |\mathbf{\Phi}_R\rangle \tag{2.16}$$

the $\hat{E}_{ai,bj}$ in Eq. (2.15) is the two-particle excitation operators in the form

$$\hat{E}_{ai,bj} = \sum_{\rho\sigma} \eta^\dagger_{b\rho}\eta^\dagger_{a\sigma}\eta_{i\rho}\eta_{j\sigma} = \hat{E}_{ai}\hat{E}_{bj} - \delta_{ib}\hat{E}_{aj} \tag{2.17}$$

where $\eta^\dagger_{a\sigma}$, $\eta_{i\rho}$ are creation and annihilation operators, ρ, σ denote the electron spin ($\rho, \sigma = \{\alpha, \beta\}$) and $\hat{E}_{ai}$ are one-particle excitation operators.

The contracted configurations $\left|\mathbf{\Phi}^{ab}_{ij,\nu}\right\rangle$ can be expanded in terms of the set of standard uncontracted doubly external CSFs $\left|\mathbf{\Phi}^{ab}_{P}\right\rangle$ according to

$$\left|\mathbf{\Phi}^{ab}_{ij,\nu}\right\rangle = \sum_P \langle\mathbf{\Phi}^{ab}_P \left|\mathbf{\Phi}^{ab}_{ij,\nu}\right\rangle \left|\mathbf{\Phi}^{ab}_P\right\rangle \tag{2.18}$$

Introducing Eqs. (2.15) and (2.16) into Eq. (2.18), the contracted configuration can be written as

$$\langle\mathbf{\Phi}^{ab}_P \left|\mathbf{\Phi}^{ab}_{ij,\nu}\right\rangle = \frac{1}{2}\sum_R \alpha^R \langle\mathbf{\Phi}^{ab}_P|\hat{E}_{ai,bj} + \nu\hat{E}_{bi,aj}\,|\mathbf{\Phi}_R\rangle \tag{2.19}$$

this shows that these configurations are obtained contracting different *internal* states.

The internally contracted configurations $\left|\mathbf{\Phi}^{ab}_{ij,\nu}\right\rangle$ defined in Eq. (2.15) are, in general, not orthonormal, The overlap matrix is given by

$$\langle\mathbf{\Phi}^{ab}_{ij,\nu} \left|\mathbf{\Phi}^{cd}_{kl,\mu}\right\rangle = \frac{1}{2}\delta_{\nu\mu}(\delta_{ac}\delta_{bd} + \nu\delta_{ad}\delta_{bc})\boldsymbol{S}^{(\nu)}_{ij,kl} \tag{2.20}$$

where the matrix $\boldsymbol{S}^{(\nu)}$ is determined by the second order density matrix of the reference wave function $|\mathbf{\Phi}_0\rangle$

$$\boldsymbol{S}^{(\nu)}_{ij,kl} = \langle\mathbf{\Phi}_0|\hat{E}_{ik,jl} + \nu\hat{E}_{il,jk}\,|\mathbf{\Phi}_0\rangle \tag{2.21}$$

the configurations can be orthogonalized by the symmetric orthogonalization

$$\left|\mathbf{\Phi}^{ab}_{D,\nu}\right\rangle = \sum_{i\geq j} (\boldsymbol{T}^{(\nu)}_{D,ij})^{-1/2} \left|\mathbf{\Phi}^{ab}_{ij,\nu}\right\rangle \tag{2.22}$$

$$\mathbf{T}^{(\nu)} = \mathbf{S}^{(\nu)} \tag{2.23}$$

In the orthogonal configuration basis, the residual vectors can be expressed as

$$\langle \mathbf{\Phi}^{ab}_{D,\nu} | \hat{H} - E \, | \mathbf{\Phi} \rangle = \left\{ \frac{1}{2} \left[\mathbf{G}^{D,\nu} + \nu (\mathbf{G}^{D,\nu})^{\dagger} \right] - E \mathbf{C}^{D,\nu} \right\}_{ab} \tag{2.24}$$

$$\langle \mathbf{\Phi}^{a}_{S} | \hat{H} - E \, | \mathbf{\Phi} \rangle = (\mathbf{g}^{S} - E \mathbf{C}^{S})_{a} \tag{2.25}$$

$$\langle \mathbf{\Phi}_{I} | \hat{H} - E \, | \mathbf{\Phi} \rangle = g^{I} - E C^{I} \tag{2.26}$$

where the index D denotes orthogonalized internally contracted $N-2$ electron states, the explicit formulas for the quantities $\mathbf{G}^{D,\nu}$, $\mathbf{g}^{S}$ and g^{I} are obtained as functions of the coupling coefficients [17, 18], which are calculated using an efficient direct CI method [22, 23], in which the coupling coefficients are obtained from a relatively small number of quantities by factorizing the high order density matrices into lower order density matrices.

2.1.4 Atomic basis sets

Ab initio electronic structure computations are almost always carried out numerically using a basis set of orbitals. A basis set is a combination of mathematical functions used to represent atomic orbitals, the employed mathematical functions describe the radial and angular distributions of electron density. It is important to choose a basis set large enough to give a good description of the molecular wave function [Eq. (2.2)]. Typically, the basis functions are centered on the atoms, and so sometimes they are called *atomic orbitals*.

There are two types of basis functions (also called Atomic Orbitals) commonly used in electronic structure calculations: Slater Type Orbitals (STOs) and Gaussian Type Orbitals (GTOs). The STOs [24] have the functional form

$$\chi^{\mathrm{STO}}_{nlm}(r, \theta, \varphi) = N Y_{lm}(\theta, \varphi) r^{n-1} e^{-\zeta r} \tag{2.27}$$

here N is a normalization constant and $Y_{l,m}(\theta, \varphi)$ are spherical harmonic functions for angular distribution, $r^{n-1}e^{-\zeta r}$ are exponential functions for radial distribution, the exponential dependence on the distance between the nucleus and electron mirrors the exact orbitals for the hydrogen atom.

The GTOs [25] can be written in terms of polar or Cartesian coordinates as

$$\chi_{nlm}^{\mathrm{GTO}}(r,\theta,\varphi) = NY_{lm}(\theta,\varphi)r^{2n-2-l}e^{-\zeta r^2} \tag{2.28}$$

the r^2 dependence in the exponential of Eq. (2.28) makes the GTOs inferior to the STOs in two respects. At the nucleus a GTO has a zero slope, in contrast to a STO which has a "cusp" (discontinuous derivative), and GTOs consequently have problems representing the proper behaviour near the nucleus. The other problem is that the GTO falls off too rapidly far from the nucleus compared with an STO. However, the GTOs are practically well suited since they are separable in the three Cartesian directions and since the product of two or more Cartesian GTOs on different centers may be written as a simple linear combination of Cartesian GTOs [26]. GTO is easy to handle because integrations can be calculated analytically, so it is used very commonly. Both STOs and GTOs can be chosen to form a complete basis, but the above considerations indicate that more GTOs are necessary for achieving a certain accuracy compared with STOs. A rough guideline says that three times as many GTOs as STOs are required for reaching a given level of accuracy.

Combining the full set of basis functions, known as the *primitive* GTOs (PGTO), into a smaller set of functions by forming fixed linear combinations is known as basis set contraction, and the resulting functions are called contracted GTOs (CGTOs).

$$\chi_{nlm}^{\mathrm{CGTO}} = \sum_i a_i \chi_{nlm,i}^{\mathrm{PGTO}}(r,\theta,\varphi) \tag{2.29}$$

where a_i is the expansion coefficients, which can be determined by least-square fits to accurate atomic orbitals or by a variational optimization of the atomic HF energy. To construct Gaussian basis sets different contraction scheme have been propose [27, 28], for example, *segmented* and *general* contraction. Usually a segmented contracted scheme is used, where each primitive functions is allowed to contribute to only one contracted orbital, simplifying the evaluation of molecular integrals [29, 30]. In a general contraction all primitives (on a given atom) enter all the contracted functions, but with different contraction coefficients.

STO-nG basis sets are Slater type orbitals consisting of n PGTOs [31]. This is a minimum type basis where the exponents of the PGTO are determined by fitting

to the STO, rather than optimizing them by a variational procedure. Although basis sets with n =2-6 have been derived, it has been found that using more than three PGTOs for representing the STO gives little improvement, and the STO-3G basis is a widely used minimum basis. This type of basis set has been determined for many elements of the periodic table.

An example particularly popular are the *split-valence* basis set of Pople and coworkers [32, 33], in which a single-zeta[2] representation of the core shell and a n-zeta representation of the valence shell is done. k-nlmG basis sets are the split valence type, with the k in front of the dash indicating how many PGTOs are used for representing the core orbitals. The nlm after the dash indicate both how many functions the valence orbitals are split into, and how many PGTOs are used for their representation. Two values (nl) indicate a split valence, while three values (nlm) indicate a triple split valence. In the 3-21G, This is a split valence basis, where the core orbitals are a contraction of three PGTOs, the inner part of the valence orbitals is a contraction of two PGTOs and the outer part of the valence is represented by one PGTO [32]. In the 6-31G basis [33], This is also a split valence basis, where the core orbitals are a contraction of six PGTOs, the inner part of the valence orbitals is a contraction of three PGTOs and the outer part of the valence is represented by one PGTO. 6-311G basis set is a triple split valence basis, where the core orbitals are a contraction of six PGTOs and the valence split into three functions, represented by three, one and one PGTOs [34].

To each of these basis sets can be added *polarization* [35] and/or *diffuse* [36] functions. When basis function of angular momentum higher than that of the occupied AOs are involved in the expansion, we have a polarized basis. The polarized functions are suited to describe the lower symmetry of molecular compared with that of their constitutes atoms and some properties due to physical perturbations. For example, in the 6-31G** basis, which is identical to 6-31G(d,p), the first asterisk indicate the addition of a set of d function on the first-row atoms and the second asterisk the addition of a p set on hydrogen [37]. The diffuse function can be added to the basis for a good description of diffuse electron distributions characteristic of anionic systems, excited states and some properties as dipole

[2]The term zeta stems from the fact that the exponent of basis functions is often denoted by the Greek letter ζ.

moments and polarizabilities. Diffuse functions are normally s- and p-functions and consequently go before the G. They are denoted by "+" or "++", with the first + indicating one set of diffuse s- and p-functions on heavy atoms, and the second + indicating that a diffuse s-function is added also to hydrogen.

When two contracted functions per valence orbital is called a valence *double zeta* (DZ)[3] basis set; three contracted functions per valence atomic orbital is called a valence *triple zeta* (TZ)[4] basis set; four contracted functions per valence valence orbital is called a valence *quadruple zeta* (QZ) basis set and so on.

For correlated calculations, the basis set requirements are different and more demanding since we must then describe the polarization of the change distribution and also provide an orbital space suitable for recovering correlation effects. For this purpose are very suited the *correlation-consistent basis set*, where each correlating orbital is represented by a single primitive Gaussian chosen so as to maximize its contribution to the correlation energy, and where all correlating orbitals that make similar contributions to the correlation energy are added simultaneously [38, 39]. The *correlation-consistent polarized valence basis set* is denoted by cc-pVXZ, where VXZ means *valence-X-zeta*. $X = D, T, Q$ or 5 indicate double-zeta, triple-zeta, quadruple-zeta or quintuple-zeta correlation consistent basis sets respectively. By adding diffuse functions so as to improve the flexibility in the outer valence region we get the *augmented correlation-consistent polarized valence basis set*, which is denoted by aug-cc-pVXZ [39] or AVXZ, where one set of diffuse functions is added for each angular momentum present in the cc-pVXZ basis.

The *basis set superposition error* (BSSE) is a spurious contribution to the interaction energy arising form the improved description of each fragment in the total basis as compared to the fragment basis alone. It is ultimately a consequence of the one-electron basis set incompleteness. Evidently, the BSSE error will vanish asymptotically as the complete one-electron basis is approached. BSSE appears whenever the molecular geometry is changed and is particularly important for the computation of interaction energies. Without correction an artificial increased binding energy is obtained. In particular when using modest basis sets, BSSE

[3]Examples of valence double zeta basis sets are the 3-21G basis set or the 6-31G basis set.
[4]An example of a valence triple zeta basis set is the 6-311G basis set.

can result in substantial distortions of the PES. A conceptually simple method to account for BSSE is the *counterpoise correction* method [40] in which the energies of the fragments are computed in the full basis of the entire complex and subtracted from the energy of the entire system. Although there is some debate about its accuracy it is the procedure of choice to account for BSSE [41].

BSSE, can be corrected by using an approach, as discussed in section 2.1.6, to scale the *ab initio* energy to the complete basis set limit. However, as discussed in the section 2.1.7, accurate extrapolation to the complete basis set limit must correct for BSSE prior to extrapolation.

2.1.5 Size-consistency and size-extensivity

Two important concepts in electronic structure theory are *size-consistency* and *size-extensivity* [42]. There are very important distinctions to be made between them.

A method is called size consistent if it gives an energy of two noninteracting systems equal the sum of the individual components.

$$E_{\mathrm{AB}}(R_{\mathrm{AB}} \to \infty) = E_{\mathrm{A}} + E_{\mathrm{B}} \tag{2.30}$$

there are two primary definitions of size-consistency in use. The first was employed by Pople [43] as one criterion for a well-constructed quantum chemical method. If we imagine two H_2 molecules, separated by a large distance (large enough that we may consider them to be non-interacting) then the energy calculated for both molecules simultaneously should be exactly twice that calculated for only one, isolated molecule of H_2, just like the exact energy. This "non-interacting limit" description is the original concept of size-consistency. From this perspective, size-consistency describes what has been referred to as the "additive separability" of the wavefunction. However, a recently imposed definition [44] requires that the method not only correctly describe the fragmentation limit, but the entire process (in a qualitative sense). That is, the entire potential energy curve mapped out when we bring our two non-interacting H_2 molecules close together must be correctly described as well.

Size extensivity is the most well-defined. A method is said to be size extensive if the energy calculated thereby scales linearly with the number of electrons. The

term was introduced to electronic structure theory by Bartlett [45], and is based on analogous "extensive" thermodynamic properties.

While the definition of size extensivity applies at any geometry, the original concept of size consistency applies only in the limiting case of infinite separation. So, size consistency usually also implies correct dissociation into fragments; this is the source of much of the confusion arising from this term. For example, restricted Hartree-Fock is size extensive, but it is not necessarily size consistent, since it cannot properly describe dissociation into open-shell fragments.

2.1.6 Semiempirical correction of *ab initio* energies

As all limited CI approaches, it is not size extensive [42], many corrections to account for the size-extensivity errors in CI calculations have been proposed in the literature [46]. Simple corrections to CISD have been suggested to account for the effects of higher excitations, Davidson [47] was the first to use such a correction:

$$E^Q = E_{\mathrm{SD}}(1 - C_0^2) \tag{2.31}$$

where E_{SD} is the correlation energy obtained from CISD calculations and C_0 is the coefficient of the reference configuration.

The superscript Q in Eq. (2.31) indicate that *Davidson correction* (DC) may be considered to correct for the lack of quadruple excitations effects. This correction, was justified by perturbation theory [46], although the final justification for the use DC is a empirical one, based on a large number of calculations. Essentially the same corrections as in the single reference case are usually applied in the multireference case. One has to replace C_0^2 with a sum of the squares of coefficients over the reference space, i.e.,

$$C_0^2 \rightarrow \sum_{i \in \mathrm{Ref}} |C_i|^2 \tag{2.32}$$

and taken as E_{SD} the *dynamical correlation* energy obtained by the difference between MRCISD and MCSCF energies.

The lack of Size-extensivity is linked to the fact that the truncate CI wave function do not include *dynamical* or *external* electron correlation effects. A

method to incorporated semiempirically the *external valence*[5] correlation energy was proposed by Brown and Truhlar [48]. In such approach the *non-dynamical* (*static*) or *internal* correlation energy is obtained by an MCSCF calculation and the part of external valence correlation energy by an MRCISD calculation based on the MCSCF wave function as references. Then, is assume that the MRCISD include a constant (geometry independent) fraction F of the external valence correlation energy, accordingly, the total energy has been written as [48]

$$E_{\mathrm{SEC}}(\mathbf{R}) = E_{\mathrm{MCSCF}}(\mathbf{R}) + \frac{E_{\mathrm{MRCISD}}(\mathbf{R}) - E_{\mathrm{MCSCF}}(\mathbf{R})}{F} \tag{2.33}$$

where $E_{\mathrm{SEC}}(\mathbf{R})$ denotes the scaled external correlation (SEC) energy, and The empiricism therefore enters in the calculation of the scaling factor F, which has been chosen for diatomics to reproduce a bond energy and for systems with three or more atoms to reproduce more than one bond energy but in an average sense.

An important element of the physical basis of the SEC method is that the MCSCF calculation must be large enough to include most of the nondynamical effects that are sensitive to optimization of the reference space, and that the one-electron basis sets are large enough to include an appreciable fraction of the external valence correlation.

Varandas [49] suggested a generalization of the SEC method by noticing the conceptual relationship between it and the double many-body expansion (DMBE) method [50]. In fact, in the DMBE scheme each n-body potential energy term is partitionaed into extended-Hartree-Fock (internal) and dynamic correlation (external correlation) parts. In his proposal, denoted as DMBE-SEC [49]. This author write the total interaction energy, relative to infinitely separated atoms in the appropriate electronic states, in the form

$$V(\mathbf{R}) = V_{\mathrm{MCSCF}}(\mathbf{R}) + V_{\mathrm{SEC}}(\mathbf{R}) \tag{2.34}$$

where

$$V_{\mathrm{MCSCF}}(\mathbf{R}) = \sum V^{(2)}_{\mathrm{AB,MCSCF}}(R_{AB}) + \sum V^{(3)}_{\mathrm{ABC,MCSCF}}(R_{AB}, R_{BC}, R_{AC}) + \ldots \tag{2.35}$$

[5]The external or dynamical correlation has a core contribution which may be as large as the valence contribution, but it can often be neglected since it is nearly constant across the potential energy surface.

$$V_{\mathrm{SEC}}(\mathbf{R}) = \sum V^{(2)}_{\mathrm{AB,SEC}}(R_{AB}) + \sum V^{(3)}_{\mathrm{ABC,SEC}}(R_{AB}, R_{BC}, R_{AC}) + \dots \qquad (2.36)$$

and the summations runs over the subcluster of atoms which compose the molecule.

The scaled external correlation energy for the n-th terms is given by

$$V^{(n)}_{\mathrm{AB...,SEC}}(R_{AB}, \dots) = \frac{V^{(n)}_{\mathrm{AB...,MRCISD}}(R_{AB}, \dots) - V^{(n)}_{\mathrm{AB...,MCSCF}}(R_{AB}, \dots)}{F^{(n)}_{\mathrm{AB...}}} \qquad (2.37)$$

where $F^{(n)}_{\mathrm{AB...}}$ is n-body geometry independent acsling factor, as in the original SEC method, optimal values for two-body factors $F^{(2)}_{AB}$ are chosen such as to reproduce the experimental dissociation energy of the corresponding AB diatomic, a criterion which may be adopted for higher-order terms if accurate dissociation energies exist for the relevance subsystems. For the triatomic case a good quess for $F^{(3)}_{\mathrm{ABC}}$ can be the average of the three two-body factors.

Improves agreement with experiment and best theoretical estimates, are obtained when *ab initio* energies are corrected with the DMBE-SEC method. Particularly important, for dynamics calculations, is the correct exothermicities for all arrangement channels, exhibit by the DMBE-SEC potential surfaces [49].

2.1.7 Extrapolation to CBS limit

One-electron basis sets are finite in solving the electronic Schrödinger equation, This makes method for extrapolating to a one-electron complete basis set (CBS) limit for a given level of electron correlation [51–56] most useful if we want to got accurate interaction energy.

Built in a systematic manner that is intended to relate the correlation energy to the cardinal number X, Dunning's correlation consistent basis sets allow the extrapolation of the raw energies to the CBS limit. To perform the extrapolation, the MRCI(Q) energy is treated as usual in split form by writing [57]

$$E_X(\mathbf{R}) = E_X^{\mathrm{CAS}}(\mathbf{R}) + E_X^{\mathrm{dc}}(\mathbf{R}) \qquad (2.38)$$

where the subscript X indicates that the energy has been calculated in the AVXZ basis, and the superscript dc stands for the dynamical correlation energy. Note

that all extrapolations are carried pointwise, and hence the vector **R** of the nuclear geometrical coordinates will be omitted for simplicity.

By carrying out calculations for several values of X, one may then exploit the X dependence of the calculated energy E_X to obtain its value E_∞ at the CBS limit. Several formulas have been proposed for extrapolating the CAS finite basis set results to the CBS limit. A proposed [57] generalization of the protocol adopted by Karton and Martin [58] to extrapolate single-reference self-consistent-field energies is utilized:

$$E_X^{\mathrm{CAS}} = E_\infty^{\mathrm{CAS}} + B/X^\alpha \tag{2.39}$$

where α is a predefined constant. Being a two-parameter protocol $(E_\infty^{\mathrm{CAS}}, B)$, a minimum of two raw energies will be required for the extrapolation.

For the dynamical correlation, a popular two-parameter CBS protocol is [59]

$$E_X^{\mathrm{dc}} = E_\infty^{\mathrm{dc}} + \frac{A_3}{(X+\alpha)^3} \tag{2.40}$$

where E_X^{dc} is the dynamic correlation energy obtained with the X-tuple basis set. Although Eq. (2.40) is known to perform accurately when extrapolating from energies based on large cardinal number pairs, its performance is significantly less satisfactory when using the (T, Q) pair. A more reliable scheme is the recently suggested USTE [57] model (see also Ref. 60), this has its basis on the three-parameter protocol

$$E_X^{\mathrm{dc}} = E_\infty^{\mathrm{dc}} + \frac{A_3}{(X+\alpha)^3} + \frac{A_5}{(X+\alpha)^5} \tag{2.41}$$

with A_5 being determined from the auxiliary relation

$$A_5 = A_5(0) + cA_3^m \tag{2.42}$$

where E_∞, $A_5(0)$, A_3, c, m, and α are parameters. By fixing α, $A_5(0)$, c and m from other criteria, Eq. (2.41) can then be transformed into an (E_∞, A_3) two-parameter rule [57]. In particular, for the dynamical correlation of 24 systems studied [57] using the MRCI(Q) method, the optimum values of the "universal-like" parameters were found to be $A_5(0) = 0.0037685459$, $c = -1.17847713\, E_h^{-5/4}$ and $m = 5/4$, with $\alpha = -3/8$. The method has since been successfully utilized

for a variety of other systems [61–67], either in its original version (USTE) or a slightly generalized variant (GUSTE [68]).

Since electronic degeneracies are often present in global PESs, it is appropriate to note that this may pose a subtle issue on extrapolation schemes. In fact, not only the location of the CI may differ in the two chosen bases but also a given basis set may prove to have somewhat different qualities when utilized for different electronic states [65]. Since this may cause small distortions on the data to be fitted, it is advocated by placing the raw *ab initio* points slightly away from such topological features and interpolating the CBS extrapolated data subsequently using the chosen functional form.

2.2 Analytical representation of potential energy surface

There have been dramatic improvements in both the accuracy and efficiency of high-level electronic structure calculations [69, 70]. Many uses of this vast supply of data require that it be expressed with a suitable local or global representation as a PES. Since the inception of quantum mechanics, considerable effort has been devoted to finding better ways of utilizing *ab initio* data or/and experimental data to construct PESs. The earliest and most common methods involve least-squares fitting to empirical or semiempirical functional forms [71, 72]. Another solution is to skip the surface construction step entirely and to use the *ab initio* results directly in dynamical studies [73]. However, the highest-accuracy *ab initio* calculations can take hours or more of computer time, even for small systems. Thus, the construction of accurate analytic representations of PES is a necessary step in full quantum spectroscopic and dynamics studies that adequately model results of state-of-the-art experiments.

Once collected and scaled an extensive data set of *ab initio* energies to map the PES, the major problem is the development of a realistic global representation of such potential. A function that match the *ab initio* data within the "chemical accuracy" provide a visualization of topographical surface features, that may not be evident from a coarse-grained *ab initio* study. Moreover, smooth and well behaved potential function can be used in dynamical studies, as theoretical

counterpart of experimental reaction dynamics.

PESs play an important role in the application of electronic structure methods to the study of molecular structures, properties and reactivities [71]. A good representations of the PES should smoothly connect the asymptotic and interaction regions of the configuration space, it should represent the true potential energy accurately in regions for which experimental or theoretical data are available, sometimes it even need to predict those parts of the interaction region for which no experimental or theoretical data are available, it should preserve any necessary permutation symmetry and it shouldn't introduce arbitrary features. Many other criteria that a successful representation of a PES must satisfy, can be found in the literature [74–76].

Methods to construct analytical PES have been developed for many years. Among the most popular approaches can be mentioned the semiempirical London-Eyring-Polanyi-Sato (LEPS) [77–79] based on a simple quantum mechanical description of the electronic wave function; the diatom-in-molecule (DIM) [80–82] methods, which use theoretical and experimental information to fit a functional form derived from simple molecular orbital theory; the modified Shepard (MS) method of Ischtwan and Collins [83–90], which uses the energy, gradient, and Hessian from *ab initio* data; The reproducing kernel Hilbert space (RKHS) method proposed by Ho and Rabitz [91–95] which provides a general approach to interpolation from grid of *ab initio* points. A general approach due to Murrell and co-workers [71, 96, 97] propose to represent the PES of a molecular as an expansion in energy terms of subclusters of atoms. This many-body expansion (MBE) function is an useful analytical representation even when the convergence of series is poor [71]. A practical advantage of the MBE approach is that relatively simple polynomial forms, in the internal coordinates of molecule, need to be fitted, in the least-squared sense, to gain chemical accuracy. The PES discussed in the present thesis are represented using an improved version of MBE due to Varandas [50]: the double many-body expansion (DMBE) method, which consists in partitioning each n-body contribution in short-range and long-range parts.

2.2.1 MBE method

In the MBE [71, 96, 97] method the single-valued PES of N-nucleus molecular is represented as a cluster expansion in the form

$$V(\mathbf{R}^N) = \sum_{n=1}^{N} \sum_{i=1}^{K} V_i^{(n)}(\mathbf{R}^n) \tag{2.43}$$

where $K = N!/n!(N-n)!$ is the number of n-body terms in N-atom system and $\mathbf{R}^n$ is the sit of $n(n-1)/2$ interatomic distances referring to n-atoms, $\mathbf{R}^n \subset \mathbf{R}^N$, $\mathbf{R}^N$ denotes the full set of $N(N-1)/2$ interatomic coordinates.

A n-body term tends asymptotically to zero if one atom in the cluster is removed to infinity. This requirement is satisfied by writing the term as

$$V^{(n)}(\mathbf{R}^n) = P^{(n)}(\mathbf{R}^n) T^{(n)}(\mathbf{R}^n) \tag{2.44}$$

where $P^{(n)}(\mathbf{R}^n)$ is a n-body polynomial in the internuclear distances and $T^{(n)}(\mathbf{R}^n)$ is a n-body range function which tends to zero when one of the internuclear coordinates in the n-body species tends to infinity [71].

The potential written in MBE form is guaranteed to satisfy all dissociation limits, an essential requirement for molecular dynamics studies. The MBE suggests a strategy for building up a polyatomic potential by studying the potential of all the fragments. Thus, a first estimate of the MBE-PES for a molecular can be made from the potential for the relevance states of the fragments. Also significant is the fact that the MBE becomes most suited for implementation as a data bank of PESs of small polyatomics [71].

2.2.2 DMBE method

Varandas [50] proposed an extension of the MBE approach by further partitioning each n-body term of Eq. (2.43), into extended Hartree-Fock (EHF) and dynamic correlation (dc) energy contributions, the single-sheeted PES is written as

$$V(\mathbf{R}^N) = \sum_{n=1}^{N} \sum_{i=1}^{K} [V_{i,\mathrm{EHF}}^{(n)}(\mathbf{R}^n) + V_{i,\mathrm{dc}}^{(n)}(\mathbf{R}^n)] \tag{2.45}$$

this DMBE method advocate for a reliable description of the potential surface from short to large interatomic separations, by including, through a semiem-

pirical potential, the dynamical correlation energy, in principle discarded in an uncorrelated electronic structure calculation.

At large interatomic separation, when charge overlap and electronic exchange effects can be neglected, the dynamic correlation energy term can be estimated using the Rayleight-Schrödinger perturbation theory combined with the multipolar expansion of the perturbation operator [98, 99].

In a series of papers Varandas and coworkers [100–105] proposed general expressions for the n-body dynamics correlation energy term, to reproduce the proper anisotropy and asymptotic behavior of the PES for the entire configuration space. An important result refers to the introduction of an universal charge-overlap damping function to account for the damping of the dispersion coefficients for intermediate and small interatomic separations [100].

General, in the DMBE formalism, the potential curves for the two-body fragments are based on the extended Hartree-Fock approximate correlation energy method for diatomic molecules including the united atom limit (EHFACE2U), which shows the correct behavior at the asymptotic limits when $R \to 0$ or $R \to \infty$. In turn, the three-body EHF energy potential has been modeled via the general form

$$V_{\rm EHF}^{(3)} = \sum_{j=1}^{m} \left\{ P^{(j)}(Q_1, Q_2, Q_3) \prod_{i=1}^{3} \left\{ 1 - \tanh[\gamma_i^{(j)}(R_i - R_i^{(j),ref})] \right\} \right\} \qquad (2.46)$$

where the polynomials $P^{(j)}(Q_1, Q_2, Q_3)$ are written in terms of symmetry coordinates, being all of order three. In turn, $R_i^{(j),ref}$ is a reference geometry, and $\gamma_i^{(j)}$ nonlinear range-determining parameters that have been optimized via a trial-and-error procedure that minimizes the root-mean-squared deviation (rmsd) while warranting the proper asymptotic behavior on dissociation.

As usual in the DMBE formalism, the EHF contributions are calibrated by fitting *ab initio* data to a suitable, physically motivated, functional form. In turn, the dc energies are modeled to a function that uses *ab initio* long-range dispersion energy coefficients, eventually estimated at the same level of *ab initio* theory. When judged relevant, *ab initio* induction and electrostatic long range coefficients are also taken into consideration in modeling the long range parts of the PES. Thus, no empirical information is required for the construction of the

final PES using DMBE theory, although the method affords sufficient physical content to be usable semi-empirically when judged convenient.

Bibliography

[1] H. J. Werner, P. J. Knowles, R. Lindh, F. R. Manby, M. Schütz, P. Celani, T. Korona, A. Mitrushenkov, G. Rauhut, T. B. Adler, R. D. Amos, A. Bernhardsson, A. Berning, D. L. Cooper, M. J. O. Deegan, A. J. Dobbyn, F. Eckert, E. Goll, C. Hampel, G. Hetzer, T. Hrenar, G. Knizia, C. Köppl, Y. Liu, A. W. Lloyd, R. A. Mata, A. J. May, S. J. McNicholas, W. Meyer, M. E. Mura, A. Nicklass, P. Palmieri, K. Pflüger, R. Pitzer, M. Reiher, U. Schumann, H. Stoll, A. J. Stone, R. Tarroni, T. Thorsteinsson, M. Wang, and A. Wolf, Molpro, version 2008.3, a package of *ab initio* programs. (2008).

[2] C. C. J. Roothaan, Rev. Mod. Phys. **23**, 69 (1951).

[3] G. G. Hall, Proc. R. Soc. **A205**, 541 (1951).

[4] F. Jensen, *Introduction to Computational Chemistry, Second Edition* (Wiley, New York, 2006).

[5] V. Staemmler, in *Computational Nanoscience: Do It Yourself!*, edited by D. M. J. Grotendorst, S. Blügel (John von Neumann Institute for Computing, Jülich, NIC Series, Vol. 31, ISBN 3-00-017350-1, New York, 2006), p. 1.

[6] P. Knowles, M. Schütz, and H. J. Werner, in *Computational Nanoscience: Do It Yourself!*, edited by J. Grotendorst (Modern Methods and Algorithms of Quantum Chemistry, Proceedings, Second Edition, John von Neumann Institute for Computing, Jülich, NIC Series, Vol. 3, 3-00-005834-6, New York, 2000), p. 97.

[7] R. F. W. Bader and R. A. Gangi, *Ab initio calculation of potential energy surfaces. In Theoretical Chemistry, A Specialist Periodical Report* (The Chemical Society, London, 1975).

[8] M. W. Schmidt and M. S. Gordon, Annu. Rev. Phys. Chem. **49**, 233 (1998).

[9] B. O. Roos, Adv. Chem. Phys. **69**, 399 (1987).

[10] B. O. Roos, in *Lecture Notes in Chemistry* (Springer-Verlag, Berlin, 2000), p. 177.

[11] L. M. Cheung, K. Sundberg, and K. Ruedenberg, J. Am. Chem. Soc. **100**, 8024 (1978).

[12] L. M. Cheung, K. Sundberg, and K. Ruedenberg, Int. J. Quantum. Chem. **16**, 1103 (1979).

[13] K. Ruedenberg, M. W. Schmidt, M. M. Gilbert, and S. T. Elbert, Chem. Phys. **71**, 41 (1982).

[14] K. Ruedenberg, M. W. Schmidt, and M. M. Gilbert, Chem. Phys. **71**, 51 (1982).

[15] K. Ruedenberg, M. W. Schmidt, M. M. Gilbert, and S. T. Elbert, Chem. Phys. **71**, 65 (1982).

[16] D. F. Feller, M. W. Schmidt, and K. Ruedenberg, J. Am. Chem. Soc. **104**, 960 (1982).

[17] P. E. M. Siegbahn, Chem. Phys. Lett. **25**, 197 (1977).

[18] P. E. M. Siegbahn, Int. J. Quantum Chem. **23**, 1869 (1983).

[19] W. Meyer, in *Modern Theoretical Chemistry*, edited by H. F. Schaefer III (Plenum Press, New York, 1977).

[20] P. E. M. Siegbahn, Int. J. Quantum Chem. **18**, 1229 (1980).

[21] H. Werner and E. A. Reinsch, J. Chem. Phys. **76**, 3144 (1982).

[22] H.-J. Werner and P. J. Knowles, J. Chem. Phys. **89**, 5803 (1988).

[23] B. O. Roos, Chem. Phys. Lett. **15**, 153 (1972).

[24] J. C. Slater, Phys. Rev. **36**, 57 (1930).

[25] S. F. Boys, Proc. R. Soc., London **A200**, 542 (1950).

[26] T. Helgaker, P. Jørgensen, and J. Olsen, *Molecular Electronic-Structure Theory* (Wiley, London, 2000).

[27] R. C. Raffenetti, J. Chem. Phys. **58**, 4452 (1973).

[28] J. A. P. R. Taylor, Chem. Phys. **87**, 4047 (1987).

[29] T. H. Dunning, J. Chem. Phys. **53**, 2823 (1970).

[30] T. H. Dunning, J. Chem. Phys. **55**, 716 (1971).

[31] W. J. Hehre, R. F. Stewart, and J. A. Pople, J. Chem. Phys. **51**, 2657 (1969).

[32] J. Binkley, J. Pople, and W. Hehre, J. Am. Chem. Soc. **102**, 939 (1980).

[33] W. J. Hehre, R. Ditchfield, and J. A. Pople, J. Chem. Phys. **56**, 2257 (1972).

[34] R. Krishnan, J. S. Binkley, and J. A. Pople, J. Chem. Phys. **72**, 650 (1980).

[35] M. M. Francl, W. J. Pietro, W. J. Hehre, J. S. Binkley, M. S. Gordon, D. J. DeFrees, and J. Pople, J. Chem. Phys. **77**, 3654 (1982).

[36] M. J. Frish, J. A. Pople, and J. S. Binkley, J. Chem. Phys. **50**, 3265 (1984).

[37] P. Hariharan and J. Pople, Theoret. Chim. Acta **28**, 213 (1973).

[38] T. H. Dunning, J. Chem. Phys. **90**, 1007 (1989).

[39] R. A. Kendall, T. H. Dunning, and R. J. Harrison, J. Chem. Phys. **96**, 6796 (1992).

[40] F. Boys and F. Bernardi, Mol. Phys. **19**, 553 (1970).

[41] F. B. van Duijneveldt, J. G. C. M. van Duijneveldt-van de Rijdt, and J. H. van Lenthe, Chem. Rev. **94**, 1873 (1994).

[42] W. Duch and G. H. F. Diercksen, J. Chem. Phys. **101**, 3018 (1994).

[43] J. A. Pople, J. S. Binkley, and R. Seeger, Int. J. Quant. Chem. Symp. **10**, 1 (1976).

[44] P. R. Taylor, in *Lecture Notes in Chemistry* (Springer-Verlag, Berlin, 1994), p. 125.

[45] R. J. Bartlett, Annu. Rev. Phys. Chem. **32**, 359 (1981).

[46] K. Jankowski, L. Meissner, and J. Wasilewski, Int. J. Quantum Chem. **28**, 931 (1985).

[47] S. R. Langhoff and E. R. Davidson, Int. J. Quant. Chem. **8**, 61 (1974).

[48] F. B. Brown and D. G. Truhlar, Chem. Phys. Lett. **117**, 307 (1985).

[49] A. J. C. Varandas, J. Chem. Phys. **90**, 4379 (1989).

[50] A. J. C. Varandas, Mol. Phys. **53**, 1303 (1984).

[51] D. Feller, J. Chem. Phys. **96**, 6104 (1992).

[52] K. A. Peterson and T. H. Dunning, J. Phys. Chem. **99**, 3898 (1995).

[53] J. M. L. Martin, Chem. Phys. Lett. **259**, 669 (1996).

[54] J. M. L. Martin and P. R. Taylor, J. Chem. Phys. **105**, 8620 (1997).

[55] A. Halkier, T. Helgaker, P. Jrgensen, W. Klopper, H. Koch, J. Olsen, and A. K. Wilson, Chem. Phys. Lett. **286**, 243 (1998).

[56] D. G. Truhlar, Chem. Phys. Lett. **294**, 45 (1998).

[57] A. J. C. Varandas, J. Chem. Phys. **126**, 244105 (2007).

[58] A. Karton and J. M. L. Martin, Theoret. Chim. Acta **115**, 330 (2006).

[59] T. Helgaker, W. Klopper, H. Koch, and J. Noga, J. Chem. Phys. **106**, 9639 (1997).

[60] A. J. C. Varandas, J. Chem. Phys. **113**, 8880 (2000).

[61] A. J. C. Varandas, Chem. Phys. Lett. **443**, 398 (2007).

[62] A. J. C. Varandas, J. Chem. Phys. **129**, 234103 (2008).

[63] A. J. C. Varandas, Chem. Phys. Lett. **463**, 225 (2008).

[64] A. J. C. Varandas, J. Comput. Chem. **30**, 379 (2009).

[65] A. J. C. Varandas, J. Chem. Phys. **131**, 124128 (2009).

[66] Y. Z. Song and A. J. C. Varandas, J. Chem. Phys. **130**, 134317 (2009).

[67] Y. Q. Li and A. J. C. Varandas, J. Phys. Chem. A **114**, 9644 (2010).

[68] A. J. C. Varandas, J. Phys. Chem. A **112**, 1841 (2008).

[69] Y. Yamaguchi, Y. Osamura, J. D. Goddard, and H. F. Schaeffer, *New Dimension to Quantum Chemistry: Analytic Derivativ Methods in* ab initio *Molecular Electronic Structure Theory* (Oxford University Press, Oxford, 1994).

[70] W. Kohn, A. D. Becke, and R. G. Parr, J. Phys. Chem. **100**, 12974 (1996).

[71] J. N. Murrell, S. Carter, S. C. Farantos, P. Huxley, and A. J. C. Varandas, *Molecular Potential Energy Functions* (Wiley, Chichester, 1984).

[72] D. G. Truhlar, R. Steckler, and M. S. Gordon, Chem. Rev. **87**, 215 (1987).

[73] T. Helgaker, E. Uggerud, and H. J. Jensen, Chem. Phys. Lett. **173**, 145 (1990).

[74] J. S. Wright and S. K. Gray, J. Chem. Phys. **69**, 67 (1978).

[75] J. N. L. Connor, Comp. Phys. Comm. **17**, 117 (1979).

[76] G. C. Schatz, Rev. Mod. Phys. **61**, 669 (1989).

[77] F. London, Z. Electrochem. **35**, 552 (1929).

[78] S. Sato, J. Chem. Phys. **23**, 2465 (1955).

[79] H. Eyring and M. Polanyi, Z. Phys. Chem. B **12**, 279 (1931).

[80] F. O. Ellison, J. Am. Chem. Soc. **85**, 3540 (1963).

[81] J. C. Tully, Adv. Chem. Phys. **42**, 63 (1980).

[82] P. J. Kuntz, in *Atom-Molecule Collision Theory*, edited by R. Bernstein (Plenum, New York, 1979), p. 79.

[83] M. A. Collins, Adv. Chem. Phys. **93**, 389 (1996).

[84] M. J. T. Jordan, K. C. Thompson, and M. A. Collins, J. Chem. Phys. **102**, 5647 (1995).

[85] M. J. T. Jordan, K. C. Thompson, and M. A. Collins, J. Chem. Phys. **103**, 9669 (1995).

[86] M. J. T. Jordan, K. C. Thompson, and M. A. Collins, J. Chem. Phys. **104**, 4600 (1996).

[87] K. C. Thompson and M. A. Collins, J. Chem. Soc. Faraday Trans. **93**, 871 (1997).

[88] K. C. Thompson, M. J. T. Jordan, and M. A. Collins, J. Chem. Phys. **108**, 564 (1998).

[89] K. C. Thompson, M. J. T. Jordan, and M. A. Collins, J. Chem. Phys. **108**, 8302 (1998).

[90] T. Ishida and G. C. Schatz, J. Chem. Phys. **107**, 3558 (1997).

[91] T.-S. Ho and H. Rabitz, J. Chem. Phys. **104**, 2584 (1996).

[92] T.-S. Ho, T. Hollebeek, and H. Rabitz, J. Chem. Phys. **105**, 10472 (1996).

[93] T. Hollebeek, T.-S. Ho, and H. Rabitz, J. Chem. Phys. **106**, 7223 (1997).

[94] T. Hollebeek, T.-S. Ho, and H. Rabitz, Annu. Rev. Phys. Chem. **46**, 169 (1999).

[95] T. S. Ho, T. Hollebeek, H. Rabitz, S. D. Chao, R. T. Skodje, A. S. Zyubin, and A. M. Mebel, J. Chem. Phys. **116**, 4124 (2002).

[96] K. S. Sorbie and J. N. Murrell, Mol. Phys. **29**, 1387 (1975).

[97] A. J. C. Varandas and J. N. Murrell, Faraday Discuss. Chem. Soc. **62**, 92 (1977).

[98] J. S. Dahler, J. Chem. Phys. **25**, 986 (1956).

[99] A. D. Buckingham, Adv. Chem. Phys. **12**, 107 (1967).

[100] A. J. C. Varandas and J. Brandão, Mol. Phys. **45**, 857 (1982).

[101] A. J. C. Varandas, J. Mol. Struct. Theochem. **120**, 401 (1985).

[102] A. J. C. Varandas and J. B. ao, Mol. Phys. **57**, 387 (1986).

[103] A. J. C. Varandas and J. D. Silva, J. Chem. Soc., Faraday Trans. 2 **82**, 593 (1986).

[104] A. J. C. Varandas, Adv. Chem. Phys. **74**, 255 (1988).

[105] A. J. C. Varandas, Chem. Phys. Lett. **194**, 333 (1992).

Chapter 3

Probing PESs via spectroscopic and dynamics calculations

The spectroscopic and dynamical quantities are very sensitive to the details of the potential energy surface (PES) and, such studies, besides their predictive purposes, prove the accuracy of the PES and provides additional information for further refinements. Being simple analytical forms, the DMBE-PESs here presented can be used in accurate and fast procedures to numerically evaluate the corresponding equations of motion. In the present chapter, methods to calculate resonance state and rate constants, will be addressed.

One of the most important results of quantum scattering theory is the phenomenon of resonance [1]. The resonance structure of atoms and molecules plays a central role in many interesting phenomena in physics and chemistry [2]. Formally these states are associated with complex poles of the resolvent operator and the corresponding eigenstates are nonnormalized solutions characterized by well defined boundary conditions [3, 4].

In the complex scaling method [5–7] the resonances eigenvalues can be directly obtained upon scaling the internal degree of freedom of the Hamiltonian by an complex phase factor $Exp\,(i\theta)$, which represent a 2θ rotation of the lower half complex energy plane. Such a transformation enables the resonances wavefunctions to be obtained in a square-integrable form, and use standard bound-state procedures to calculate resonance positions and widths. The complex absorbing potential (CAP) method [2, 8, 9], transform the Hamiltonian representing resonances to an L^2 non Hermitian effective Hamiltonian by introducing an op-

tical potential (OP) in the asymptotic potential region. In this field the CAP method was first used by Jolicard and Austin [8]. An alternative to an exact scattering calculation to characterize resonances is provided by a variety of essentially real bound-state, L^2 methods. These approaches are physically intuitive and also provide a more familiar method to solve the problem. Due to the nature of resonances which are embedded in the continuum of scattering states, real L^2 functions provide an excellent starting point for characterizing their behavior [10]. To overcome the difficulties of continually repeating the diagonalization of large matrices, various schemes combine a complex method with perturbative [11], coupled-channel [12] or finite difference [9] approaches. In the present work the CAP method is combined with the discrete variable representation (DVR) method [13], a very suited approach for study of large amplitude motion vibrations.

A rigorous treatment of the dynamics of molecular collisions require the use of quantum scattering methods, based on the resolution of the time-dependent Schrödinger equation [1]. In fact, Schrödinger equation constitute the basic concept to understand, at the atomic and molecular levels, the collision processes and correlated this with observable phenomena. However, if the process under study can be assumed as an adiabatic one, a more simple and useful treatment involves the use of a PES as an interparticle interaction potential in classical equations of motion. Indeed, when dealing with slow molecular collisions, a PES, as discussed in the present work, provide the interaction energy as a function of the configuration of the system throughout the rearrangement from reactants to products. A common approach to study the dynamics of chemical reactions is the quasiclassical trajectory (QCT) method [14–17], in which the time evolution of the system is obtained by numerical integration of the classical equations of motion and the prefix "quasi" indicate that initial conditions are chosen such that the energy in the various degrees of freedom approximately correspond to a quantum mechanical energy level. The QCT method assumes that each of the nuclei comprising a chemical system moves according to the laws of classical mechanics in the force field arising from the adiabatic electronic energy of the system. In the QCT method, molecules are prepared in discrete internal energy states corresponding to the quantum states of the molecular.

3.1 The CAP-DVR method

Imposing resonance boundary conditions [3], resonance states are obtained as discrete eigenstates of quantum system [18, 19]. A resonance wave function is exponentially divergent at large distances from the scattering center [20]. The complex absorbing potential method [8] is based in the main premise that the exact asymptotic form of the exact wavefunction is not required for derivation of the resonances eigenvalues. In this way, square integrable functions are derived from the asymptotically diverging resonance states by introducing an imaginary optical potential (OP) iV which absorbs the purely outgoing wave. Thus, an L^2 complex Hamiltonian determine the nth resonance state through the Schrödinger equation

$$\left(\hat{H} - iV\right)\psi_n = \left(E_n - i\frac{\Gamma_n}{2}\right)\psi_n \tag{3.1}$$

where $\hat{H}$ is the usual L^2 real Hamiltonian, the eigenenergy, $E_n - i\Gamma_n/2$, is complex. E_n is the resonance position and Γ_n the resonance width (inverse lifetime[1]). The approach is to represent the ψ_n in a basis of L^2 function, which are eigenfunctions of the real Hamiltonian $\hat{H}$.

The complex eigenfunctions of $\hat{H} - iV$ are obtained in a two-step procedure, as described previously [21]. First, the real Hamiltonian $\hat{H}$ is diagonalized in a large basis. It is essential that the basis in the dissociative degree of freedom extend into the noninteraction region, where the absorbing potential is nonnegligible. This condition is easy to satisfy by simply using a large, extended basis, e.g., particle-in-a-box functions, in that degree of freedom. However, for more than two-mode problems, a direct-product basis consisting of this extended basis plus internal basis functions would result in a prohibitively large basis size. Thus, we have a used a truncation/recoupling procedure [21, 22] to precondition the final basis.

The solutions of the equation (3.1) can be found by representing the complex Hamiltonian in a finite basis set of the real vibrational Hamiltonian $\hat{H}$. In order to minimize errors associated to basis set truncation and artificial perturbations induced by the absorbing potential, a variational parameter (λ) is included in the

[1]The corresponding lifetime of the resonance is $\hbar/\Gamma_n$

potential, which is then optimized respect to the complex eigenvalue of (3.1) [2, 8, 23]. The latter is carried out by diagonalizing the complex Hamiltonian for a set of λ values. Thus, the complex eigenvalue for the optimal λ is the best estimate to the exact resonance, $E_n - i\,(\Gamma_n/2)$.

A simple and fast numerical procedure to solve (3.1) is attained by using a discrete variable representation (DVR) method as suggested by Light and coworkers [13, 24–27], for the calculation of ro-vibrational states. The DVR, is isomorphic to an approximate *finite basis representation* (FBR) in which some matrix elements of the Hamiltonian are determined by numerical quadrature over the DVR points. Thus the definition of a DVR requires both the definition of an appropriate set of N basis functions $\{\phi_i; i = 1, \ldots, N\}$ and the definition of an appropriate quadrature over the DVR basis of points $\{x_\alpha; \alpha = 1, \ldots, N\}$. The standard DVRs are defined in terms of classical polynomials such as particle-in-a-box functions (Chebyshev polynomials), harmonic oscillator functions (Hermite polynomials), Legendre polynomials, Laguerre polynomials, etc., their related weight functions and Gaussian quadratures.

The Hamiltonian evaluation in the DVR relied in the fact that an "exact" representation of the Hamiltonian matrix in a *variational basis representation* (VBR), can be approximated by an FBR, in which some matrix elements of the Hamiltonian are determined by numerical quadrature over the DVR points [28]. In turn, for basis of N classical orthogonal polynomials exist an isomorphism between DVR and FBR defined by the orthogonal transformation [29, 30]

$$\mathbf{U}_{i\alpha} = \boldsymbol{\phi}_i\,(x_\alpha)\,\boldsymbol{\omega}_\alpha^{1/2} \tag{3.2}$$

where $\{x_\alpha; \alpha = 1, \ldots, N\}$ and $\{\omega_\alpha; \alpha = 1, \ldots, N\}$ are the quadrature points and weights for the classical polynomial basis sets $\{\phi_i; i = 1, \ldots, N\}$.

Thus, in the orthonormal DVR basis, obtained by direct diagonalization of the position operator [31] or from the polynomial themselves via

$$\varphi_\alpha\,(x) = \sum_{i=1}^{N} U_{i\alpha}^{\dagger}\phi_i\,(x) \tag{3.3}$$

and the DVR potential matrix is approximated by the simple diagonal form

$$\left(\mathbf{V}^{\mathrm{DVR}}\right)_{\alpha\beta} = V\,(x_\alpha)\,\delta_{\alpha\beta} = \left(\mathbf{U}^{\dagger}\mathbf{V}^{\mathrm{FBR}}\mathbf{U}\right)_{\alpha\beta} \tag{3.4}$$

In practice the appropriate Gaussian quadrature scheme is generated from (3.2), and for the multidimensional case the required composite transformation is written as a product of 1D transformations [27]. Hence, a sequential truncation/diagonalization procedure can be used, in which the structure sparseness of the DVR Hamiltonian is exploited to generate in a sequential fashion good contracted basis sets in an increasing number of dimension [31].

3.2 The QCT method

The QCT method assumes that each of nuclei comprising a chemical system moves according to the laws of classical mechanics in the force field arising from the adiabatic electronic energy of the system. The term "quasiclassical" is used to denote the manner in which molecular are prepare before collision (i.e., the initial conditions) [15].

In the QCT method the time evolution of the classical degrees of freedom of individual atoms are simulated by solving Hamilton's or Newton's equations of motion expressed in term of the coordinates $\mathbf{q}$ and momentum $\mathbf{p}$ of the system. In the Hamilton formulation [32] propagation is done by numerical integration of the first-order differential equations [33]

$$\frac{\partial H(\mathbf{q},\mathbf{p})}{\partial q_i} = \frac{-dp_i}{dt} \quad \text{and} \quad \frac{\partial H(\mathbf{q},\mathbf{p})}{\partial p_i} = \frac{dq_i}{dt} \tag{3.5}$$

where the H, the sum of the kinetic $T(\mathbf{q},\mathbf{p})$ and potential energies $V(\mathbf{q})$, is the system's Hamiltonian

$$H(\mathbf{q},\mathbf{p}) = T(\mathbf{q},\mathbf{p}) + V(\mathbf{q}) \tag{3.6}$$

for the most general case $T(\mathbf{q},\mathbf{p})$ depends on both the momenta $\mathbf{p}$ and the coordinate $\mathbf{q}$.

There are several components to quasiclassical trajectory simulation [14, 15, 34]. A potential energy function $V(\mathbf{q})$ must be formulated. Hamilton's equations of motion (3.5) are solved numerically and numerous algorithms have been developed and tested for doing this is an efficient and accurate manner [14, 15, 32, 34–39]. When the trajectory is completed, the final values for the momenta and coordinates are transformed into properties that may be used to make predictions

about the chemical system's molecular dynamics, and compared with experiment and/or theory, such as product vibrational, rotational, and relative translational energies.

3.2.1 Unimolecular decomposition

In a unimolecular reaction a reactant A is excited above its unimolecular threshold so that it may dissociate to product(s).

$$\mathrm{A}^* \rightarrow \text{product(s)} \tag{3.7}$$

where the A^* denotes vibrational-rotational state of the reactant A. Assuming that the system is initially excited with a microcanonical ensemble and its intramolecular dynamics is ergodic, such is called Rice-Ramsperger-Kassel-Marcus (RRKM) behavior [40–42], for which all the accessible states of the molecule are occupied in random order, the lifetime distribution $P(t)$, namely, the probability of decomposition per unit time will be

$$P(t) = k(E) \exp\left[-k(E)\, t\right] \tag{3.8}$$

given equal probability during any time interval for reaction to occur [40–42], where $k(E)$ is the classical microcanonical unimolecular rate constant. It may be expressed as [43]

$$k(E) = \frac{N^{\ddagger}(E)}{h\rho(E)} \tag{3.9}$$

where $N^{\ddagger}(E)$ is the sum of states at the transition state for decomposition and $\rho(E)$ is the density of state for A^*. However, for a large number of experiments the Eq. (3.8) does not hold, due to the not random character of the transition between states. Indeed, for a not sufficiently fast intramolecular vibrational-energy redistribution (IVR), the transition between some states will be more probable than others.

An important question is whether an unimolecular decomposition is random in the sense (3.8), or does not obey such equation [43–45]. In this way, different schemes have been developed, as the Monte Carlo sampling, for exciting A^* randomly with a microcanonical ensemble of states, and nonrandomly excitation procedures, involving specific state selection [17, 46].

3.2.2 Bimolecular reactions

In principle, the cross section for the reaction between A and B to form products

$$\mathrm{A} + \mathrm{B} \rightarrow \text{products} \tag{3.10}$$

may be measured as a function of the A + B relative velocity v_{rel} and the vibrational-rotational energy of A and B [47]. For bimolecular reactions the quantities of interest in such studies commonly included the reaction cross section and the thermal bimolecular rate constant. For the simple case of an atom B plus a symmetric top polyatomic molecule A, the reactive cross section may be expressed as $\sigma_r\left(v_{rel}, \nu_A, J_A, K_A\right)$, where v_{rel} is the A + B relative velocity, ν_A, J_A and K_A are the polyatomic's collections of vibrational and rotational quantum numbers.

Assuming Boltzmann distributions of vibrational-rotational levels specified by temperature T_A, the reactive Boltzmann-average cross section can be obtained as

$$\sigma_r\left(v_{rel}; T_A\right) = \sum_{\nu_A} \sum_{J_A, K_A} \sigma_r\left(v_{rel}, \nu_A, J_A, K_A\right) P\left(\nu_A; T_A\right) P\left(J_A, K_A; T_A\right) \tag{3.11}$$

where $P\left(\nu_A; T_A\right)$ and $P\left(J_A, K_A; T_A\right)$ are the normalized Boltzmann distribution for ν_A and J_A, K_A at temperature T_A.

Multiplying the above cross sections $\sigma_r\left(v_{rel}; T_A\right)$ by v_{rel} gives the bimolecular rate constant for a fixed relative velocity

$$k(v_{rel}; T_A) = v_{rel}\sigma_r\left(v_{rel}; T_A\right) \tag{3.12}$$

integrating the rate constant in Eq. (3.12) over the Boltzmann relative velocity distribution $P\left(v_{rel}; T\right)$ for temperature $T = T_A$ gives the thermal bimolecular rate constant as

$$k\left(T\right) = \int_0^\infty v_{rel}\sigma_r\left(v_{rel}; T\right) P\left(v_{rel}; T\right) dv_{rel} \tag{3.13}$$

the Maxwell-Boltzmann distribution for $P\left(v_{rel}; T\right)$ is given by

$$P\left(v_{rel}; T\right) = 4\pi \left(\frac{\mu}{2\pi kT}\right)^{3/2} e^{-\mu v_{rel}^2/2kT} v_{rel}^2 \tag{3.14}$$

inserting the Maxwell-Boltzmann distribution Eq. (3.14) into Eq (3.13) to give

$$k\left(T\right) = \left(\frac{\mu}{2\pi kT}\right)^{3/2} 4\pi \int_0^\infty \sigma_r\left(v_{rel}; T\right) v_{rel}^3 e^{-\mu v_{rel}^2/2kT} dv_{rel} \tag{3.15}$$

changing the integration variable to the translational energy by the relation $E_{tr} = \mu_{AB} v_{rel}^2/2$ gives

$$k\left(T\right) = \left(\frac{8kT}{\pi\mu}\right)^{1/2} \int_0^\infty \sigma_r(E_{tr}) \frac{E_{tr}}{(kT)^2} e^{-E_{tr}/kT} d_{E_{tr}} \tag{3.16}$$

thus, the thermal rate constant may be written as

$$k\left(T\right) = \left(\frac{8kT}{\pi\mu}\right)^{1/2} \left\langle \sigma_r\left(E_{tr}\right)\right\rangle \tag{3.17}$$

where the average cross section for temperature T will be

$$\left\langle \sigma_r\left(E_{tr}\right)\right\rangle = \int_0^\infty \sigma_r\left(E_{tr}\right) P(E_{tr}) dE_{tr} = \int_0^\infty \sigma_r\left(E_{tr}\right) \frac{E_{tr}}{\left(kT\right)^2} e^{-E_{tr}/kT} dE_{tr} \tag{3.18}$$

where $P(E_{tr})$, normalized to unity for E_{tr} of 0 to ∞, is

$$P(E_{tr}) = \frac{E_{tr}}{\left(kT\right)^2} e^{-E_{tr}/kT} \tag{3.19}$$

In turn, a simple expression for the reaction cross section can be derived from the classical mechanical expression for this quantity [48]

$$\sigma_r = \int_0^{b_{max}} P_r\left(b\right) 2\pi b db \tag{3.20}$$

where b is the collision impact parameter, b_{max} is the largest impact parameter that leads to reaction, and $P_r\left(b\right)$ is the so-called opacity function given the impact parameter distribution.

One may determine σ_r from Eq. (3.20) by integrating over $P_r\left(b\right)$ or from the average $P_r\left(b\right)$, which is given by

$$\left\langle P_r\left(b\right)\right\rangle = \frac{\int_0^{b_{max}} P_r\left(b\right) 2\pi b db}{\int_0^{b_{max}} 2\pi b db} = \frac{\int_0^{b_{max}} P_r\left(b\right) 2\pi b db}{\pi b_{max}^2} \tag{3.21}$$

comparison of Eqs. (3.20) and (3.21) gives that

$$\sigma_r = \left\langle P_r\left(b\right)\right\rangle \pi b_{max}^2 \tag{3.22}$$

the average reaction probability $\left\langle P_r\left(b\right)\right\rangle$ is evaluated from trajectories with b chosen randomly according to the distribution function

$$f\left(b\right) db = \frac{2\pi b\, db}{\pi b_{max}^2} \tag{3.23}$$

random values of b between 0 and b_{max} may be sampled with the cumulative distribution function (CDF)

$$\xi = \int_0^b f(b)\, db \tag{3.24}$$

introducing Eq. (3.23) into Eq.(3.24), one can obtain

$$\xi = \int_0^b \frac{2\pi b\, db}{\pi b_{max}^2} = \frac{b^2}{b_{max}^2} \tag{3.25}$$

to give

$$b = \xi^{1/2} b_{max} \tag{3.26}$$

with b chosen randomly between 0 and b_{max}. The average reaction probability is $\langle P_r(b)\rangle = N_r/N$, where N is the total number of trajectories and N_r the number which are reactives. By substituting in (3.22), the reaction cross section is [17]

$$\sigma_r = \frac{N_r}{N}\pi b_{max}^2 \tag{3.27}$$

inserting the reaction cross section Eq. (3.27) and the average cross section Eq. (3.18) into the thermal rate constant Eq. (3.17) to give

$$k(T) = \left(\frac{8kT}{\pi\mu}\right)^{1/2} \frac{N_r}{N}\pi b_{max}^2 \int_0^\infty P(E_{tr}) dE_{tr} \tag{3.28}$$

noted that the translational energy in Eq. (3.19) may be randomly sampled by the von Neumann rejection method, or by the CDF [14]

$$E_{tr} = -kT \ln\left(\xi_{tr}^{(1)} \xi_{tr}^{(2)}\right) \tag{3.29}$$

where $\xi_{tr}^{(1)}$ and $\xi_{tr}^{(2)}$ are two independent uniform random numbers. When choosing the relative translational energy in $P(E_{tr})$ of Eq. (3.19) randomly in accord with Eq. (3.29), in another word, neglecting the influence of electronic degeneracy, the Eq. (3.28) gives

$$k(T) = \left(\frac{8kT}{\pi\mu}\right)^{1/2} \frac{N_r}{N}\pi b_{max}^2 \tag{3.30}$$

when electronic degeneracy is included, the bimolecular rate constant Eq. (3.28) may be expressed as [17]

$$k(T) = g_e(T) \left(\frac{8kT}{\pi\mu}\right)^{1/2} \frac{N_r}{N}\pi b_{max}^2 \tag{3.31}$$

where $g_e(T)$ is the temperature dependent electronic degeneracy factor [49–53], which is equal to the product of the reactant electronic partition functions divided by the electronic partition function of the product [53], introduced to account for the probability of a collision occurring on a particular surface.

Complex bimolecular reactions [54] is a particular type of chemical activation system in which two chemical species react together to produce a short lived, highly vibrationally excited intermediate complex that can decompose to produce new products, or re-dissociate to regenerate the original reactants. In the latter case, there is no net reaction; in the former case, the reaction appears to be a simple bimolecular process. If the intermediate complex undergoes collisional relaxation, re-dissociation is reduced and production of the new products is enhanced or the intermediate is stabilized. Because collisional relaxation is involved, the overall process is pressure-dependent. At ordinary pressures, the intermediate complex often cannot be isolated.

3.2.3 Energy transfer and chaperon mechanism of recombination process

An exothermic radical + radical recombination reaction produces an excited product with enough energy to redissociate. In order to obtain a stable product, the energy must be removed [55]. In the limit of zero pressure, energy may be lost by spontaneous infrared emission, resulting in stabilized product molecules [56], but at higher pressures, interactions with the bath gas are dominant in producing a stabilized product [57]. In describing the pressure dependence of recombination process usually two mechanisms must be considered, for lager free radicals at low to moderate densities, the energy transfer mechanism (ETM), or Lindemann mechanism, is probably most important, for a process of the type [55–59]

$$\mathrm{A} + \mathrm{B} + \mathrm{M} \rightarrow \mathrm{AB} + \mathrm{M} \tag{3.32}$$

can be formulated symbolically in terms of the steps

$$\mathrm{A} + \mathrm{B} \rightarrow \mathrm{AB}^{*} \tag{3.33}$$

$$\mathrm{AB}^{\star} \rightarrow \mathrm{A} + \mathrm{B} \tag{3.34}$$

$$\mathrm{AB}^{\star} + \mathrm{M} \rightarrow \mathrm{AB} + \mathrm{M} \tag{3.35}$$

with steady-state concentrations of AB*, where A and B are reactants, AB is the product, the asterisk denotes internal excitation, and M is an energy transfer collider, this leads to a rate expression

$$\frac{\mathrm{d[AB]}}{\mathrm{d}t} = k_{\mathrm{ETM}}[A][B] \tag{3.36}$$

with a pseudo-second-order rate coefficient

$$k_{\mathrm{ETM}} = k_1 \left(\frac{k_2[M]}{k_{-1} + k_2[M]} \right) \tag{3.37}$$

where the brackets denote concentration, the k_1, k_{-1} and k_2 denote the rate coefficients of reaction (3.33), (3.34) and (3.35), respectively. Eq. (3.37) is easily interpreted by identifying the maximum value of k_{ETM} with the rate constant k_1 for formation of the highly excited unstable adduct AB* via reaction (3.33) and by identifying the parenthesis at the right-hand side of Eq. (3.37) with the fraction of which is collisionally stabilized by reaction (3.35) rather then being redissociated via reaction (3.34). Eq. (3.37) is the basis for the strong collision and master equation versions of the Rice-Ramsperger-Kassell-Marcus (RRKM) theory [60–62].

At higher densities, lower temperatures, and for smaller reactant species, a second mechanism may become important, the chaperon mechanism(CM), or radical complex [55–59].

$$\mathrm{A} + \mathrm{M} \rightarrow \mathrm{M...A} \tag{3.38}$$

$$\mathrm{M...A} \rightarrow \mathrm{A} + \mathrm{M} \tag{3.39}$$

$$\mathrm{M...A} + \mathrm{B} \rightarrow \mathrm{AB} + \mathrm{M} \tag{3.40}$$

where the dots emphasize, as usual, the weak nature of the van der Waals (VDW) bond, and the reaction rate constant is given by

$$k_{\mathrm{CM}} = k_4 \left(\frac{k_3[M]}{k_{-3} + k_3[M]} \right) = k_4 \left(\frac{K_3[M]}{1 + K_3[M]} \right) \tag{3.41}$$

where $K_3 = k_3/k_{-3}$ and the k_3, k_{-3} and k_4 denote the rate coefficients of reaction (3.38), (3.39) and (3.40), respectively. As pointed out elsewhere [55], the ETM is

used in the conventional analysis of recombination rate data. If the ETM analysis fails in some way, the CM is often implicated by default. Quantitative assessment of the ETM is relatively routine because widely available master equation codes are all based on the ETM [54]. The same is not true of the CM.

3.2.4 Products properties from QCT runs

The end point of a trajectory occurs when it enters a regions of phase space designated as reactants or products space. Once the product molecules have been determined by testing interatomic distances, using geometric and energetic criteria can be determined whether the molecules are in bound, quasi-bound or dissociative states.

Among the products properties in a QCT run are the relative translational energy of the formed molecules, the scattering angle between the initial and final relative velocity vectors and their vibrational and rotational energies. For diatomics, almost all of these quantities are straightforward from the coordinates and velocities of the product molecules [17]. For example, vibrational and rotational quantum numbers are determined for a diatomic from the Einstein-Brillouin-Keller (EBK) semiclassical quantization condition [63–65]. For polyatomics, no general algorithm have been established for finding their vibrational and rotational quantum numbers [17], mainly due to vibrational-rotational couplings, the multidimensionality of the problem, and possible resonances between the vibrational modes [17].

Bibliography

[1] J. Z. H. Zhang, *Theory and Applications of Quantum Molecular Dynamics* (World Scientific, Singapore, 1999).

[2] C. L. G. Jolicard and E. J. Austin, J. Chem. Phys. **88**, 1026 (1987).

[3] A. F. J. Siegert, Phys. Rev. **56**, 750 (1939).

[4] J. L. Jackson and R. E. Wyatt, Chem. Phys. Lett. **4**, 643 (1970).

[5] J. Aguilar and J. M. Combes, Commun. Math. Phys. **22**, 269 (1971).

[6] E. Baslev and J. M. Combes, Commun. Math. Phys. **22**, 280 (1971).

[7] B. Simon, Commun. Math. Phys. **27**, 1 (1972).

[8] G. Jolicard and E. J. Austin, Chem. Phys. Lett. **121**, 106 (1985).

[9] G. Jolicard and G. D. Billing, J. Chem. Phys. **97**, 997 (1992).

[10] R. C. Mayrhofer and J. M. Bowman, J. Chem. Phys. **100**, 7229 (1994).

[11] N. Moiseyev and P. R. Certain, Mol. Phys. **37**, 1621 (1979).

[12] O. Atabek and R. Lefebvre, Phys. Rev. **22**, 1817 (1980).

[13] J. V. Lill, G. A. Parker, and J. C. Light, Chem. Phys. Lett. **89**, 483 (1982).

[14] D. L. Bunker, Comp. Physics. **10**, 287 (1971).

[15] D. L. Bunker, Comp. Physics. **10**, 287 (1971).

[16] L. M. Raff and D. L. Thompson, *in* Theory of Chemical Reaction Dynamics*, edited by M. Baer* (Chemical Rubber, Boca Raton, 1985).

[17] W. L. Hase, Encyclopedia of Computational Chemistry,*edited by M. Baer* (Wiley, New York, 1998).

[18] W. L. Hase, Scattering Theory of Waves and Particles (Dover, Mineola,, 2002).

[19] R. M. More and E. Gerjuoy, Phys. Rev. A **7**, 1288 (1973).

[20] R. Santra, Phys. Rev. A **74**, 034701 (2006).

[21] D. Wang and J. M. Bowman, J. Chem. Phys. **100**, 1021 (1994).

[22] J. M. Bowman and B. Gazdy, J. Chem. Phys. **94**, 454 (1991).

[23] G. Jolicard and E. J. Austin, Chem. Phys. **103**, 295 (1986).

[24] R. W. Heather and J. C. Light, J. Chem. Phys. **79**, 147 (1983).

[25] Z. Bacic and J. C. Light, J. Chem. Phys. **85**, 4594 (1986).

[26] Z. Bacic and J. C. Light, J. Chem. Phys. **86**, 3065 (1987).

[27] Z. Bačić and J. C. Light, Annu. Rev. Phys. Chem. **40**, 469 (1989).

[28] D. O. Harris, G. G. Engerlhom, and W. D. Gwinn, J. Chem. Phys. **43**, 1515 (1965).

[29] A. S. Dickinson and P. R. Certain, J. Chem. Phys. **49**, 4209 (1968).

[30] J. C. Light, I. P. Hamilton, and J. V. Lillb, J. Chem. Phys. **82**, 1400 (1985).

[31] J. C. Light and T. Carrington Jr., Adv. Chem. Phys. **114**, 263 (2000).

[32] H. Goldstein, *Classical Mechanics* (Addison-Wesley, Reading, 1980).

[33] M. Karplus, R. N. Porter, and R. D. Siiarma, J. Chem. Phys. **43**, 3259 (1965).

[34] R. Porter and L. Raft, *in Modern Theoretical Chemistry* (Plenum Press, New York, 1976).

[35] F. Zhang, J. Chem. Phys. **99**, 53 (1996).

[36] V. L. Arnold, Mathematical Methods of Classical Mechanics (Springer-Verlag, New York, 1978).

[37] W. H. Press, S. A. Teukolski, W. T. Vetterling, and B. P. Flannery, *Numerical Recipes in Fortran: the Art of Scientific Computing* (Cambridge University Press, New York, 1992).

[38] K. Bolton and S. Nordholm, J. Comp. Chem. **113**, 320 (1994).

[39] J. D. Meiss, Rev. Mod. Phys. **64**, 795 (1992).

[40] R. A. Marcus and O. K. Rice, J. Phys. and Colloid Chem. **55**, 894 (1951).

[41] R. A. Marcus, J. Chem. Phys. **20**, 359 (1952).

[42] D. M. Wardlaw and R. A. Marcus, Adv. Chem. Phys. **70**, 231 (1988).

[43] T. Baer and W. L. Hase, Unimolecular Reaction Dynamics. Theory and Experiments (Oxford University Press, New York, 1996).

[44] D. L. Bunker, J. Chem. Phys. **40**, 1946 (1964).

[45] D. L. Bunker and W. L. Hase, J. Chem. Phys. **54**, 4621 (1973).

[46] G. H. Peslherbe, H. B. Wang, , and W. L. Hase, Adv. Chem. Phys. **105**, 171 (1999).

[47] R. D. Levine and R. B. Bernstein, *Molecular Reaction Dynamics and Chemical Reactivity* (Oxford University Press, New York, 1987).

[48] G. D. Billing, Introduction to Molecular Dynamics and Chemical Kinetics (Wiley, New York, 1996).

[49] J. Keck, J. Chem. Phys. **29**, 410 (1958).

[50] D. L. Bunker, J. Chem. Phys. **32**, 1001 (1960).

[51] D. G. Truhlar, J. Chem. Phys. **56**, 3189 (1972).

[52] J. T. Muckerman and M. D. Newton, J. Chem. Phys. **56**, 3191 (1972).

[53] Y. Liu, L. L. Lohr, and J. R. Barker, J. Phys. Chem. A **110**, 1267 (2006).

[54] J. R. Barker and D. M. Golden, Chem. Rev. **103**, 4577 (2003).

[55] J. Y. Liu and J. R. Barker, J. Phys. Chem. A **111**, 8689 (2007).

[56] J. R. Barker, J. Phys. Chem. **96**, 7361 (1992).

[57] F. A. Lindemann, Trans. Faraday Soc. **17**, 598 (1922).

[58] A. J. C. Varandas, A. A. C. C. Pais, J. M. C. Marques, and W. Wang, Chem. Phys. Lett. **249**, 264 (1996).

[59] J. Troe, Chem. Rev. **103**, 4565 (2003).

[60] W. Forst, *Theory of Unimolecular Reactions* (Academic Press, New York, 1973).

[61] R. G. Gilbert and S. C. Smith, *Theory of Unimolecular and Recombination Reactions* (Blackwell Scientific Publications: Oxford, 1990).

[62] K. A. Holbrook, M. J. Pilling, and S. H. Robertson, *Unimolecular Reactions* (Wiley, Chichester, 1996).

[63] A. Einstein, Verh. Dtsch. Phys. Ges. **19**, 82 (1917).

[64] L. Brillouin, J. Phys. Radium **7**, 353 (1926).

[65] J. B. Keller, Ann. Phys. **4**, 180 (1958).

Part II

Cases studies

Chapter 4

DMBE-PES for the first excited state of NH_2

J. Phys. Chem. A. **114**, 9644-9654 (2010).

Accurate potential energy surface for the $1\,^2A'$ state of NH_2: scaling of the external correlation versus extrapolation to complete-basis-set limit

Y. Q. Li and A.J.C. Varandas

Departamento de Química, Universidade de Coimbra
3004-535 Coimbra Codex, Portugal.

(Received: January 11, 2010; In final form: February 22, 2010)

Abstract

An accurate single-sheeted double many-body expansion potential energy surface is reported for the title system which is suitable for dynamics and kinetics studies of the reactions $N(^2D) + H_2(X^1\Sigma_g^+) \rightleftharpoons NH(a^1\Delta) + H(^2S)$ and their isotopomeric variants. It is obtained by fitting *ab initio* energies calculated at the multireference configuration interaction level with the aug-cc-pVQZ basis set, after slightly correcting semiempirically the dynamical correlation using the double many-body expansion-scaled external correlation method. The function so obtained is compared in detail with a potential energy surface of the same family obtained by extrapolating the calculated raw energies to the complete basis set limit. The topographical features of the novel global potential energy surface are examined in detail, and found to be in general good agreement with those calculated directly from the raw *ab initio* energies, as well as previous calculations available in the literature. The novel function has been built such as to become degenerate at linear geometries with the ground-state potential energy surface of A'' symmetry reported by our group, where both form a Renner-Teller pair.

1 Introduction

The reactivity of atomic nitrogen is of fundamental importance in various fields such as atmospheric chemistry and combustion processes.[1] In the first and second excited states [N(^2D) and N(^2P)], atomic nitrogen atoms are metastable with common wisdom attributing to N(^2P) a greater reactivity than ground state N(^4S), while N(^2D) is known to be highly reactive.[2] During the past decade, the reaction N(^2D) + H$_2$($X\,^1\Sigma_g^+$) $\rightarrow$ NH($X^3\Sigma^-$) + H(^2S) has been much studied both experimentally[3–6] and theoretically.[1, 2, 7–17] Most such studies have dealt with the ground electronic adiabatic state potential energy surface (PES), and the first excited state one (labeled $1\,^2A''$ and $1\,^2A'$ in C_s symmetry, respectively). In this case, such studies have often been oriented from the perspective that the two PESs form a Renner-Teller (RT) pair, a topic that has impact both in reaction dynamics and spectroscopy beyond the Born-Oppenheimer approximation. Amongst the theoretical studies, Pederson et al.[18, 19] reported accurate *ab initio* calculations and global PESs for the lowest ($1\,^2A''$) and second lowest ($1\,^2A'$) electronic states using an interpolation technique known as reproducing kernel Hilbert space (RKHS). They reveal the degeneracy at linear HNH geometries forming a RT coupled pair of $^2\Pi$ symmetry. In particular, their $1\,^2A'$ PES is based on multireference configuration interaction (MRCI) calculations with a triple-zeta basis set of the correlation consistent type (aug-cc-pVTZ; the popular notation is generically aug-cc-pVXZ or AVXZ, with $X = D, T, Q, 5, ...$ standing for the so-called cardinal number that identifies the basis set). It shows a barrier along the minimum energy path for the N(^2D) + H$_2$ reaction of 3.4 kcal mol^{-1}, before entering a well whose minimum lies about 93.5 kcal mol^{-1} deeper than the reactants and finally leading adiabatically to NH($a^1\Delta$) + H products with an endoergicity of 8.3 kcal mol^{-1}. This is to be compared with the PES for the ground electronic state of NH$_2$ ($1\,^2A''$) that connects N(^2D) + H$_2$ to ground state products [NH($X\,^3\Sigma^-$) + H(^2S)] via rather similar topographical attributes, but being exoergic by 29.4 kcal mol^{-1} according to their own MRCI/AVTZ calculations.

Despite connecting adiabatically reactants to NH($a^1\Delta$) + H products, there is a possibility that collisions occurring on the $1\,^2A'$ PES may lead to ground state products via the non-adiabatic RT interaction mentioned above. Thus, the

$1\,^2A'$ excited state PES of NH_2 may have an impact on the overall dynamics and kinetics of the $N(^2D) + H_2$ reaction, not to mention its well known role in the spectroscopy of the ground state molecule. Indeed, quasiclassical trajectory calculations[18, 19] and quantum mechanical reactive scattering studies[20] carried out on such PESs have shown satisfactory agreement with the experimental results.

Calculations of PESs for the above two electronic states of NH_2 have also been performed by Qu *et al.*[13] using the MRCI approach, mostly with the AV*Q*Z basis set and cubic-spline fits for the representation. Similar calculations have been reported for the ground-state ($1\,^2A''$) PES by Varandas and Poveda,[14] with the novelty being its representation via a switching function formalism within the double many-body expansion (DMBE) strategy for single-sheeted functions. Such a DMBE function has its global minimum 126.4 kcal mol^{-1} below the energy of the reactants, while the products lie 97.6 kcal mol^{-1} above the minimum. Thus, reaction occurs on the ground state DMBE form with an exoergicity of 28.8 kcal mol^{-1}. Of relevance is also the fact that the minimum of $D_{\infty h}$ symmetry (topographically a saddle point in 3D) occurs about 33.7 kcal mol^{-1} above the global minimum of the $1\,^2A''$ PES where it becomes degenerate with the corresponding $D_{\infty h}$ minimum of the $1\,^2A'$ PES forming a RT pair of states. Since the minimum of the $1\,^2A'$ PES is predicted in this work to lie 94.58 kcal mol^{-1} below reactants, it follows that the energy for optimized bending is 1.92 kcal mol^{-1} on this PES, in good agreement with other available estimates.[13, 21]

An aspect of the $N(^2D) + H_2(X^1\Sigma_g^+)$ reaction dynamics that has not been sufficiently studied is the role of excited electronic states. There are five doublet states that correlate to $N(^2D) + H_2(X^1\Sigma_g^+)$, and one of the excited states ($1\,^2A'$) may have important implications on such dynamics studies [for a recent publication that addresses this issue for the $N(^2D) + HD$ reaction, see Ref. 22] as suggested by the correlation rules:

$$NH_2(1^2A') \rightarrow N(^2D) + H_2(X^1\Sigma_g^+) \quad (1)$$

$$\rightarrow NH(a^1\Delta) + H(^2S) \quad (2)$$

$$\rightarrow N(^2D) + H(^2S) + H(^2S) \quad (3)$$

The major goal of the present work is therefore to report an accurate global PES for $NH_2(1\,^2A')$ based on DMBE theory.[23–26] Being a fragment of larger N_xH_y

species like those of relevance in studying the synthesis of ammonia, such a PES may then be of key importance also for constructing DMBE forms for such larger systems. Indeed, this has been a major motivation for modeling an accurate single-sheeted DMBE function for the title system. To calibrate such a function, a few thousand *ab initio* points have been calculated at the MRCI[27, 28] level using the full valence complete active space (FVCAS)[27] reference function with the AVQZ basis set. For improved accuracy, the raw *ab initio* energies are corrected semiempirically using the double many-body expansion-scaled external correlation (DMBE-SEC[29]) method such as to extrapolate to the limit of a one-electron complete basis set (CBS) and full CI expansion; this PES will be denoted hereafter as DMBE/SEC. The DMBE/SEC function so obtained will then be compared in detail with another of the same family but calibrated from energies obtained by extrapolating the calculated raw ones to the CBS limit.[30] For this, 2210 MRCI points have been calculated using both AVTZ and AVQZ basis,[31, 32] being the final PES denoted as DMBE/CBS. Suffice it to indicate at this point that the uniform singlet- and triplet-electron pair extrapolation (USTE) scheme[33, 34] has been utilized on this endeavor for the dynamical correlation energy, by far the most difficult contribution to obtain accurately via *ab initio* techniques. As usual in DMBE theory,[23–26] both the DMBE/SEC and DMBE/CBS PESs show the correct long-range behavior at all dissociation limits.

The paper is organized as follows. Section 2 describes the *ab initio* calculations, while the analytical representation of the PES is discussed in section 2. Specifically, section 3.1 focuses on the two-body energy terms, while section 3.2 is devoted to three-body ones. Section 3.3 discusses the Renner-Teller degeneracy. The main topographical features of the $NH_2(1\,^2A')$ PES will be examined in section 3, while some conclusions are gathered in section 4.

2 Computational details

2.1 *Ab initio* calculations and scaling of external correlation

To map the DMBE/SEC PES, a total of 2454 points has been calculated for $N - H_2$ regions defined by $1.2 \leq R_{H_2}/a_0 \leq 3.6$, $0.4 \leq r_{N-H_2}/a_0 \leq 10$, and

$0 \leq \gamma/\,\mathrm{deg} \leq 90$ while, for H − NH, they cover geometries defined by $1.8 \leq R_{\mathrm{NH}}/\mathrm{a_0} \leq 3.6$, $1.2 \leq r_{\mathrm{H-NH}}/\mathrm{a_0} \leq 10$, and $0 \leq \gamma/\,\mathrm{deg} \leq 180$; R, r, and γ are atom-diatom Jacobi coordinates. All *ab initio* energies have been obtained at the MRCI[27, 28]level with the Molpro[35] package for electronic structure calculations, using the FVCAS[27] wave function as reference. This involves 7 correlated electrons in 6 active orbitals ($5a' + 1a''$), amounts to a total of 82 configuration state functions. The AVQZ atomic basis sets[36] of Dunning have been employed. For simplicity, core effects have been neglected by freezing the core electrons. Despite being a seemingly unacceptable simplification when aiming at high-accuracy requirements, its impact will be clarified along the paper. Of course, such improved calculations should, for consistency, not be done with the standard basis sets described above but with correlation consistent core-valence ones. Along this line of reasoning, one should further recall that other effects, often of competitive magnitude, are altogether also neglected, namely, relativistic and nonadiabatic ones. A final pragmatic reason for improving cost-effectiveness of the calculations stems from the observation that the data are going to be modeled with an accuracy that probably falls close to or even exceeds the error that can be attributed to the neglect of such core correlation effects. This does not imply that a high-accuracy PES cannot be envisaged within our scheme. On the contrary, we generally advocate a dual-level approach, where the first step involves a relatively modest cost study such as the present one and a second step involves an independent study involving a direct fit to available spectroscopic data, as suggested elsewhere.[37, 38]

In addition to the reasons already mentioned in the previous paragraph, a major one for adopting the frozen core approximation lies on the fact that the raw *ab initio* energies are subsequently corrected semiempirically (although this involves only a correction of tiny magnitude, it can be of significant impact on dynamics attributes) with the DMBE-SEC method such as to account for electronic excitations beyond singles and doubles, (core effects) and most importantly for the incompleteness of the basis set. The total DMBE-SEC interaction energy assumes the form[29]

$$V(\mathbf{R}) = V_{\mathrm{CAS}}(\mathbf{R}) + V_{\mathrm{SEC}}(\mathbf{R}) \tag{4}$$

where

$$V_{\rm CAS}(\mathbf{R}) = \sum_{\rm AB} V^{(2)}_{\rm AB,CAS}(R_{AB}) + V^{(3)}_{\rm ABC,CAS}(\mathbf{R}) \tag{5}$$

$$V_{\rm SEC}(\mathbf{R}) = \sum_{\rm AB} V^{(2)}_{\rm AB,SEC}(R_{AB}) + V^{(3)}_{\rm ABC,SEC}(\mathbf{R}) \tag{6}$$

where CAS is a simplified notation for FVCAS and $\mathbf{R} = \left\{R_{AB}, R_{AC}, R_{BC}\right\}$ is a collective variable of all internuclear distances. Explicitly, the terms in Eq. (6) assume the form:

$$V^{(2)}_{\rm AB,SEC}(R_{AB}) = \frac{V^{(2)}_{\rm AB,CAS-CISD}(R_{AB}) - V^{(2)}_{\rm AB,CAS}(R_{AB})}{F^{(2)}_{AB}} \tag{7}$$

$$V^{(3)}_{\rm ABC,SEC}(\mathbf{R}) = \frac{V^{(3)}_{\rm ABC,CAS-CISD}(\mathbf{R}) - V^{(3)}_{\rm AB,CAS}(\mathbf{R})}{F^{(3)}_{AB}} \tag{8}$$

As usual, $F^{(2)}_{AB}$ in Eq. (7) is chosen such as to reproduce the bond dissociation energy of the corresponding AB diatomic, while $F^{(3)}_{AB}$ is estimated as the average of the three two-body F-factors. In this work, $F^{(2)}_{\rm HH} = 0.9050$, $F^{(2)}_{\rm NH}$ =0.9340, and $F^{(3)}_{\rm NHH} = 0.9243$.

2.2 Further *ab initio* calculations and extrapolation to CBS limit

A further consistency test to the reported DMBE/SEC PES will be made by producing another function of the same family but purely *ab initio* and based on the extrapolation of the correlation energy to the one-electron CBS limit. For this, a total of 2210 points (out of the 2454 considered before) has been utilized to map the DMBE/CBS function. Note that these calculations covered the same configuration space as in section 2.1 but only at the MRCI(Q)/AVTZ level such as to form the energy-pairs required by the CBS/(T, Q) approach here utilized. Thus, only a small fraction of additional computational time (typically an order of magnitude smaller) has been required.

Built in a systematic manner that is intended to relate the correlation energy to the cardinal number X, Dunning's correlation consistent basis sets allow the extrapolation of the raw energies to the CBS limit. To perform the extrapolation,

the MRCI(Q) energy is treated as usual in split form by writing[33]

$$E_X(\mathbf{R}) = E_X^{\mathrm{CAS}}(\mathbf{R}) + E_X^{\mathrm{dc}}(\mathbf{R}) \tag{9}$$

where the subscript X indicates that the energy has been calculated in the AVXZ basis, and the superscript dc stands for the dynamical correlation energy. Note that all extrapolations are carried pointwise, and hence the vector $\mathbf{R}$ of the nuclear geometrical coordinates will be omitted for simplicity.

To extrapolate the CAS energy (uncorrelated in the sense of lacking dynamical correlation), a proposed[33] generalization of the protocol adopted by Karton and Martin[39] (KM) to extrapolate single-reference self-consistent-field energies is utilized:

$$E_X^{\mathrm{CAS}} = E_\infty^{\mathrm{CAS}} + B/X^\alpha \tag{10}$$

where α is a predefined constant. Being a two-parameter protocol ($E_\infty^{\mathrm{CAS}}, B$), a minimum of two raw energies will be required for the extrapolation. Specifically, Eq. (10) will be calibrated from the CAS/AV(T,Q)Z energy pairs, using a value of $\alpha = 5.34$ which has been found optimal when extrapolating HF energies to the CBS limit.

For the dynamical correlation, a popular two-parameter CBS protocol is[40]

$$E_X^{\mathrm{dc}} = E_\infty^{\mathrm{dc}} + \frac{A_3}{(X+\alpha)^3} \tag{11}$$

where E_X^{dc} is the dynamic correlation energy obtained with the X-tuple basis set. Although Eq. (11) is known to perform accurately when extrapolating from energies based on large cardinal number pairs, its performance is significantly less satisfactory when using the (T,Q) pair. A more reliable scheme is the recently suggested USTE[33] model (see also Ref. 41). This has its basis on the three-parameter protocol

$$E_X^{\mathrm{dc}} = E_\infty^{\mathrm{dc}} + \frac{A_3}{(X+\alpha)^3} + \frac{A_5}{(X+\alpha)^5} \tag{12}$$

with A_5 being determined from the auxiliary relation

$$A_5 = A_5(0) + cA_3^m \tag{13}$$

where E_∞, $A_5(0)$, A_3, c, m, and α are parameters. By fixing α, $A_5(0)$, c and m from other criteria (none utilizing data alien to the employed *ab initio* theory), Eq. (12) can then be transformed into an (E_∞, A_3) two-parameter rule.[33] Using USTE, it has been shown in Ref. 33 that both the full correlation in systems studied by the popular single-reference Møller-Plesset (MP2) and coupled cluster [CCSD and CCSD(T)] methods as well as its dynamical part in MRCI(Q) calculations can be accurately extrapolated to the CBS limit. In particular, for the dynamical correlation of 24 systems studied[33] using the MRCI(Q) method, the optimum values of the "universal-like" parameters were found to be $A_5(0) = 0.0037685459$, $c = -1.17847713\, E_h^{-5/4}$ and $m = 5/4$, with $\alpha = -3/8$. In fact, the method has since been successfully utilized for a variety of other systems,[33, 42–47] either in its original version (USTE) or a slightly generalized variant (GUSTE[48]). The USTE/(T, Q) scheme will then be employed here to extrapolate the dynamical correlation in $NH_2(1\,^2A')$. Since electronic degeneracies are often present in global PESs, including the present one, it is appropriate to note that this may pose a subtle issue on extrapolation schemes. In fact, not only the location of the CI may differ in the two chosen bases but also a given basis set may prove to have somewhat different qualities when utilized for different electronic states.[46] Since this may cause small distortions on the data to be fitted, it is advocated by placing the raw ab initio points slightly away from such topological features and interpolating the CBS extrapolated data subsequently using the chosen functional form, here DMBE.

3 Single-sheeted DMBE potential energy surface

Within the framework of DMBE theory,[14, 49] the single-sheeted PES is written as

$$V(\mathbf{R}) = \sum_{x=\mathrm{EHF,dc}} \left[\sum_{i=1}^{3} V_x^{(2)}(R_i) + V_x^{(3)}(\mathbf{R}) \right] \tag{14}$$

where $V^{(2)}$ and $V^{(3)}$ are the two- and three-body terms in the cluster expansion of the CAS (this will be denoted as extended-Hartree-Fock, EHF) and dynamical correlation energies.

As usual in the DMBE formalism, the EHF contributions are calibrated by

fitting *ab initio* data to a suitable, physically motivated, functional form. In turn, the dc energies are modeled to a function that uses *ab initio* long-range dispersion energy coefficients, eventually estimated at the same level of *ab initio* theory. When judged relevant, *ab initio* induction and electrostatic long range coefficients are also taken into consideration in modeling the long range parts of the PES. Thus, no empirical information is required for the construction of the final PES using DMBE theory, although the method affords sufficient physical content to be usable semi-empirically when judged convenient. The following sections give the details of the specific forms that are employed in Eq. (14).

3.1 Two-body energy terms

The potential curves for the two-body fragments are based on the extended Hartree-Fock approximate correlation energy method for diatomic molecules including the united atom limit[50] (EHFACE2U), and hence show the correct behavior at the asymptotic limits when $R \to 0$ or $R \to \infty$. They are given by the sum of $V_{\rm EHF}^{(2)}$ and $V_{\rm dc}^{(2)}$ contributions for each pair. Specifically, the two-body EHF term is written as

$$V_{\rm EHF}^{(2)}(R) = -\frac{D}{R}\left(1 + \sum_{i=1}^{n} \alpha_i r^i\right) \exp(-\gamma r) + \chi_{\rm exc}(R) V_{\rm exc}^{\rm asym}(R) \tag{15}$$

where

$$\gamma = \gamma_0[1 + \gamma_1 \tanh(\gamma_2 r)]\,. \tag{16}$$

and

$$V_{\rm exc}^{\rm asym}(R) = -\widetilde{A} R^{\widetilde{\alpha}}(1 + \widetilde{\alpha}_1 R + \widetilde{\alpha}_2 R^2)\exp(-\widetilde{\gamma} R) \tag{17}$$

is the asymptotic exchange energy, $\chi_{\rm exc}(R)$ a convenient damping function that accounts for charge overlap effects, and $r = R - R_e$ the displacement coordinate relative to equilibrium geometry. In turn, the two-body dynamical correlation $V_{\rm dc}^{(2)}$ assumes the form

$$V_{\rm dc}^{(2)}(R) = -\sum_{i=6,8,10} C_n \chi_n(R) R^{-n} \tag{18}$$

where

$$\chi_n(R) = \left[1 - \exp\left(-A_n \frac{R}{\rho} - B_n \frac{R^2}{\rho^2}\right)\right]^n \tag{19}$$

is a charge-overlap dispersion damping function. Moreover, $A_n = \alpha_0 n^{-\alpha_1}$ and $B_n = \beta_0 \exp(-\beta_1 n)$ are auxiliary functions;[23, 51] $\alpha_0 = 16.36606$, $\alpha_1 = 0.70172$, $\beta_0 = 17.19338$, and $\beta_1 = 0.09574$. In turn, for the atom-pair JK, the scaling parameter is defined by $\rho = 5.5 + 1.25(\langle r_{\rm J}^2\rangle^{1/2} + \langle r_{\rm K}^2\rangle^{1/2})$. Finally, the coefficients in Eqs. (3)-(7) are chosen to reproduce available theoretical data for the diatomic as described elsewhere.[23, 50] For a slightly improved accuracy, the EHFACE2U potential energy curve for the ground state $H_2(X^1\Sigma_g^+)$ reported in Ref. 52 has been adopted in the present work. For imidogen, $NH(a^1\Delta)$, the potential curve has been chosen to mimic the SEC/MRCI *ab initio* energies here reported. All parameters are gathered in Table 1 of the Supplementary Information (SI). As seen, the value of the diatomic equilibrium geometry ($R_e = 1.974\,a_0$) is in very good agreement with the experimental value of $1.973\,a_0$[53] and the recent theoretical values of $1.975\,a_0$[54] and $1.976\,a_0$.[13]

3.2 Three-body energy terms

The three-body dynamical correlation is written as[52]

$$V_{\rm dc}^{(3)} = -\sum_i \sum_n f_i({\rm R}) C_n^{(i)}(R_i,\theta_i)\chi_n(r_i) r_i^{-n} \tag{20}$$

where r_i, θ_i and R_i are the Jacobi coordinates corresponding to a specific geometry of the triatomic and $f_i = \frac{1}{2}\{1 - \tanh[\xi(\eta R_i - R_j - R_k)]\}$ is a switching function. Following recent work on $NH_2(1^2A'')$,[14] the parameters have been fixed at $\eta = 6$, $\xi = 1.0 a_0^{-1}$, and $\rho = 16.125 a_0$. Regarding $\chi_n(r_i)$, Eq. (7) is still adopted but R is replaced as usual by the center-of-mass separation for the relevant atom-diatom channel. In turn, the atom-diatom dispersion coefficients in Eq. (20) assume their typical form

$$C_n^{(i)}(R_i) = \sum_L C_n^L(R) P_L(cos\theta_i) \tag{21}$$

where $P_L(\cos\theta_i)$ denotes the L-th Legendre polynomial. The expansion in Eq. (21) has been truncated by considering only the coefficients C_6^0, C_6^2, C_8^0, C_8^2, C_8^4 and C_{10}^0; all other coefficients are assumed to make a negligible contribution, and hence neglected. Furthermore, the atom-diatom dispersion coefficients assume

Table 1. Accumulated (acc.) and stratum (strat.) root-mean-square deviations (in kcal mol^{-1}) of DMBE/SEC PES.

Energy		N^a		max. dev.^{b}		rmsd		$N^c>$ rmsd	
Acc.	Strat.	Acc.	Strat.	Acc.	Strat.	Acc.	Strat.	Acc.	Strat.
10	0-10	235	235	0.053	0.053	0.005	0.005	26	26
20	10-20	290	55	0.372	0.372	0.028	0.065	8	2
30	20-30	310	20	0.982	0.982	0.076	0.280	7	3
40	30-40	332	22	1.659	1.659	0.212	0.774	15	7
50	40-50	353	21	1.659	1.383	0.234	0.454	23	6
60	50-60	374	21	2.984	2.984	0.343	1.085	31	5
70	60-70	394	20	2.984	2.554	0.418	1.113	41	4
75	70-75	407	13	2.984	2.253	0.442	0.904	45	3
80	75-80	436	29	3.729	3.729	0.564	1.428	52	8
90	80-90	491	55	3.729	2.939	0.650	1.121	77	17
100	90-100	703	212	3.729	3.151	0.668	0.706	121	44
125	100-125	1529	826	3.729	3.564	0.689	0.707	279	156
150	125-150	1889	360	3.729	2.906	0.717	0.825	391	101
175	150-175	2231	342	3.965	3.965	0.772	1.022	474	93
200	175-200	2450	219	3.965	3.929	0.806	1.095	528	51

[a] Number of calculated MRCI/SEC points up to the indicated energy range. [b] Maximum deviation up to the indicated energy range. [c] Number of calculated MRCI/SEC points with an energy deviation larger than the root-mean-square deviation.

the usual form

$$C_n^{L,A-BC}(R) = C_n^{L,AB} + C_n^{L,AC} + D_M \left(1 + \sum_{l=1}^{3} a_i r^i\right) \exp\left(\sum_{l=1}^{3} b_i r^i\right) \qquad (22)$$

Since Eq. (21) is known to cause an overestimation of the dynamical correlation energy at the atom-diatom dissociation channels,[52] the two-body dynamical correlation energy for the ith pair has been multiplied by $\Pi_{j\neq i}(1-f_j)$. This ensures[37, 52] that the only two-body contribution at the i-th channel will be the jk one. The parameters in Eqs. (20)-(22) have been taken from Ref. 14 for ground state NH_2, with the notation and numerical values kept unchanged to prevent any confusion.

By removing, for a given triatomic geometry, the sum of the two-body energy terms from the corresponding interaction energies, one obtains the total three-body energy. By then subtracting the three-body dynamical correlation contri-

bution in Eq. (20) from the total three-body energy, the three-body EHF energy contribution is obtained. This has been modeled via the three-body distributed-polynomial[14, 55] form

$$V_{\rm EHF}^{(3)} = \sum_{j=1}^{3} \left\{ P^{(j)}(Q_1, Q_2, Q_3) \prod_{i=1}^{3} \left\{ 1 - \tanh[\gamma_i^{(j)}(R_i - R_i^{(j),ref})] \right\} \right\} \qquad (23)$$

where the polynomials $P^{(j)}(Q_1, Q_2, Q_3)$ are written in terms of symmetry coordinates, being all of order three. In turn, $R_i^{(j),ref}$ is a reference geometry, and $\gamma_i^{(j)}$ nonlinear range-determining parameters that have been optimized via a trial-and-error procedure that minimizes the root-mean-squared deviation (rmsd) while warranting the proper asymptotic behavior on dissociation. The complete set of parameters totals 150 linear coefficients, 9 nonlinear ones, and 9 reference bond distances. For the DMBE/SEC PES, a total of 2454 points covering an energy range of over 210 kcal mol^{-1} above the NH_2 global minimum has been utilized in the least-squares fit, with special weights having been attributed to the points close to stationary points. Table 2 gathers the reference geometries and nonlinear range-determining parameters, while Table 3 collects the linear ones, both given as SI. The partial and accumulated stratified rmsd of the final DMBE/SEC PES with respect to all fitted energies are given in Table 2. As shown, the DMBE/SEC form fits regions up to the linear and C_{2v} barriers (100 kcal mol^{-1} above the global minimum) with a rmsd smaller than 0.67 kcal mol^{-1} and a maximum unsigned deviation smaller than 3.8 kcal mol^{-1}. Only 17.2% of the fitted points deviate by more than the rmsd value.

As already noted, the DMBE/CBS PES has employed a total of 2210 points for the fit covering an energy range of over 210 kcal mol^{-1} above the NH_2 global minimum. Special fitting weights have been also attributed to the points close to stationary points. Table 4 of the SI gathers the reference geometries and nonlinear range-determining parameters, while Table 5 of the SI collects the linear ones. The rmsd of the final DMBE/CBS PES with respect to all fitted *ab initio* energies are given in Table 2. As shown, the fit up to the linear and C_{2v} barriers shows a rmsd smaller than 0.34 kcal mol^{-1} and a maximum unsigned deviation smaller than 2.4 kcal mol^{-1}. Of the fitted points, only 13.5% show a deviation larger than the corresponding rmsd value. Thus, both DMBE PESs fit the data with a

Table 2. Accumulated (acc.) and stratum (strat.) root-mean-square deviations (in kcal mol^{-1}) of DMBE/CBS PES.

Energy		N^a		max. dev.^{b}		rmsd		$N^c>$ rmsd	
Acc.	Strat.	Acc.	Strat.	Acc.	Strat.	Acc.	Strat.	Acc.	Strat.
10	0-10	237	237	0.034	0.034	0.003	0.003	19	19
20	10-20	290	53	0.081	0.081	0.009	0.020	18	7
30	20-30	308	18	0.179	0.179	0.024	0.093	17	7
40	30-40	326	18	0.485	0.485	0.050	0.186	27	6
50	40-50	344	18	0.677	0.677	0.088	0.323	33	5
60	50-60	360	16	1.111	1.111	0.149	0.575	38	5
70	60-70	376	16	1.360	1.360	0.200	0.665	43	5
75	70-75	385	9	1.360	1.024	0.224	0.684	45	4
80	75-80	406	21	2.307	2.307	0.286	0.817	44	5
90	80-90	445	39	2.307	1.805	0.343	0.700	60	11
100	90-100	697	252	2.307	1.700	0.333	0.316	94	33
125	100-125	1434	737	2.307	2.125	0.380	0.420	234	137
150	125-150	1735	301	3.118	3.118	0.452	0.699	342	80
175	150-175	2020	285	3.118	2.345	0.470	0.569	431	82
200	175-200	2207	187	3.118	1.996	0.469	0.460	468	37

[a] Number of calculated MRCI/CBS points up to the indicated energy range. [b] Maximum deviation up to the indicated energy range. [c] Number of calculated MRCI/CBS points with an energy deviation larger than the root-mean-square deviation.

stratified rmsd $\ll 1\%$ of the stratum energy.

3.3 Treatment of the Renner-Teller degeneracy

The interaction between the various electronic states of NH_2 is intricate,[2, 13] especially at the NH + H channel. As noted elsewhere,[13, 56] stretching of a N − H bond in linear H − N − H makes the $^2\Pi$ ground-state conically intersect the $^2\Sigma^-$, $^2\Delta$, and $^2\Sigma^+$ ones, which correlate with different states of the NH + H products. As a result, the ground state $1\,^2A''$ PES (which correlates with the $X\,^3\Sigma^-$ state of NH), can also yield $^2\Pi$ product NH diatomics. Similarly, the $1\,^2A'$ excited state [which correlates with NH($a\,^1\Delta$)] may form either $^2\Pi$ or $^2\Delta$ states of NH. This may be explained from the fact that the ground ($1\,^2A''$) and first-excited ($1\,^2A'$) states become degenerate at small HN − H bond distances for linear geometries.

To study the RT coupling, it is critical that the $1\,^2A'$ and $1\,^2A''$ PESs show

Table 3. Stationary points at the valence region of $NH_2(1\,^2A')$ PES.

Feature	R_1/a_0	R_2/a_0	R_3/a_0	V/E_h[a]	ΔV[b]/kcal mol^{-1}	$\omega_{\rm sym}$	$\omega_{\rm asym}$	$\omega_{\rm sym}$
				Global minimun				
DMBE-SEC[c]	3.5914	1.8819	1.8819	−0.3252	−94.58	3639	3953	978
DMBE/SEC[d]	3.5899	1.8807	1.8807	−0.3252	−94.58	3641	3956	985
DMBE-CBS[e]	3.5943	1.8836	1.8836	−0.3272	−95.85	3638	3952	979
DMBE/CBS[f]	3.5927	1.8824	1.8824	−0.3272	−95.85	3631	3944	982
RKRS[g]	3.5555	1.8763	1.8763		−93.5	3615	3912	1056
				C_{2v}barrier				
DMBE/SEC[d]	1.4190	3.8150	3.8150	−0.1692	3.29	4359	583i	253
DMBE/CBS[f]	1.4195	3.8150	3.8150	−0.1703	2.64	4291	496i	399
RKRS[g]	1.42	3.768	3.768		3.39	4218	558i	446
				$C_{\infty v}$barrier				
DMBE/SEC[d]	1.4135	3.0458	4.4592	−0.1650	5.96	4454	671i	597i
DMBE/CBS[f]	1.4087	2.6656	4.0742	−0.1647	6.13	4254	882i	532i
RKRS[g]	1.48	2.95	4.43		4.61	1612	2184i	914i
				$D_{\infty h}$barrier				
DMBE/SEC[d]	3.7418	1.8709	1.8709	−0.3221	−92.66	3676	7029	1166i
DMBE/CBS[f]	3.7389	1.8695	1.8695	−0.3241	−93.92	3676	7030	1201i

[a] Relative to the $N(^2D)+H+H$ asymptote. [b] Relative to the $N(^2D)+H_2$ asymptote . [c] Fitted to a dense grid of MRCI/AVQZ points, which is then scaled using the DMBE-SEC method. [d] From global DMBE/SEC PES. [e] Fitted to a dense grid of extrapolated CBS/MRCI(Q) /AV(T,Q)Z points. [f] From global DMBE/CBS PES. [g] RKHS PES (Ref.19).

Table 4. Attributes of $N(^2D) - H_2$ van der Waals stationary points.

	DMBE/SEC[a]			DMBE/CBS[b]		
Feature	C_{2v} min.[c]	$C_{\infty v}$ min.[c]	C_s s.p.[d]	C_{2v} min.[c]	$C_{\infty v}$ min.[c]	C_s s.p.[d]
R_1/a_0	1.4012	1.4024	1.4017	1.4019	1.4014	1.4009
R_2/a_0	6.1625	5.9056	5.9793	5.8288	5.7287	5.8088
R_3/a_0	6.1625	7.3080	6.9162	5.8288	7.1301	6.7053
V^e	−0.17475	−0.17475	−0.17473	−0.17499	−0.17498	−0.17492
ΔV^f	−0.1739	−0.1735	−0.1583	−0.3232	−0.3170	−0.2820
ω_1(intra)/cm^{-1}	4417	4395	4406	4390	4390	4397
ω_2(inter)/cm^{-1}	80	72	73	146	111	111
ω_3(bend)/cm^{-1}	79	66	65i	104	95	94i

[a] From global DMBE/SEC PES. [b] From global DMBE/CBS PES. [c] Van der Waals minimum. [d] Saddle point connecting the two van der Waals minima. [e] Relative to the $N(^2D) + H + H$ asymptote (in E_h). [f] Relative to the $N(^2D) + H_2$ asymptote (in kcal mol^{-1}).

the correct topology at the linear degeneracy locus where both form a RT pair. Because the $1\,^2A''$ state PES previously reported is of DMBE/SEC type, we refer explicitly in this work to the excited state $1\,^2A'$ DMBE/SEC PES. In fact, due to their similar accuracies, the RT degeneracy can simply be imposed (when using DMBE/SEC) by appropriate weighting of the dense grid of raw energies which has been calculated to model the degeneracy locus. Since there might still occur some tiny difference due to its least-squares nature, we adopted in the SEC case too the procedure described next for further accuracy. For the $1\,^2A'$ DMBE/CBS PES, a somewhat different procedure has been envisaged to ensure a smooth degeneracy behavior. Specifically, the excited state $1\,^2A'$ PES has been written as

$$V'(\mathbf{R}) = V(\mathbf{R})(1 - f(\mathbf{R})) + V''(\mathbf{R})f(\mathbf{R}) \tag{24}$$

where $V(\mathbf{R})$ is the excited state $1\,^2A'$ DMBE/CBS PES as defined in Eq. (14), and $V''(\mathbf{R})$ is the ground state $1\,^2A''$ PES reported in Ref. 14. In turn, $f(\mathbf{R})$ is a three-dimensional switching function which has been conveniently written as

$$f(\mathbf{R}) = f_{\mathrm{HH}}(R_1)f_{\mathrm{NH}}(R_2)f_{\mathrm{NH}}(R_3)f_\theta(\theta) \tag{25}$$

where

$$f_{\rm HH}(R_1) = \frac{1}{2}\left\{1 - \tanh[\alpha(R_1 - R_1^0)]\right\} \tag{26}$$

$$f_{\rm NH}(R_2) = \frac{1}{2}\left\{1 - \tanh[\alpha(R_2 - R_2^0)]\right\} \tag{27}$$

$$f_\theta(\theta) = \exp\left\{-[\beta(\mathrm{Cos}(\theta) - 1)]^\gamma\right\} \tag{28}$$

with θ being the $\mathrm{H-N-H}$ bending angle, and the remaining symbols having the meaning previously assigned. The parameters in Eq. (25) have been calculated using a trial-and-error procedure ensuring that the $1\,^2A''$ and $1\,^2A'$ PESs become degenerate at HNH linear geometries with small NH bond lengths. Such a procedure led to $\alpha = 7.0\,a_0^{-1}$, $\beta = 10^4$, $\gamma = 1.5$, $R_1^0 = 5.2\,a_0$ and $R_2^0 = 3.0\,a_0$. Needless to say, the above procedure warrants the RT degeneracy but not the degeneracy at the $\mathrm{N(^2D) + H_2}$ asymptote [due to the small difference between the CBS and SEC values of the $\mathrm{N(^2D)}$ energy]. However, one may approximately cope with this too in two steps, first by applying the procedure described in eq 24 to warrant the RT degeneracy and then using a procedure similar to this to impose degeneracy at the asymptote. This second step has not been carried out in the SI material.

4 Features of the $\mathbf{NH_2(1\,^2A')}$ potential energy surface

The optimized C_{2v} bending curve of the $\mathrm{NH_2}(1\,^2A')$ DMBE/SEC PES is displayed in Figure 1 as a function of the bending angle, with the bond distance of NH optimized at each angle. Also shown for comparison in this figure is the bending curve of the accurate DMBE/CBS PES. Note that the barrier to linearity calculated from the DMBE/SEC PES is $673\,\mathrm{cm^{-1}}$, This compares well with the one of $674\,\mathrm{cm^{-1}}$ obtained from the DMBE/CBS PES, which is predicted to be only $1\,\mathrm{cm^{-1}}$ smaller. The near parallel behavior of the DMBE/SEC and DMBE/CBS PESs is highlighted in the bottom panel of Figure 1, with DMBE/CBS predicting a slightly deeper well depth. This may largely be due to the fact that the DMBE-SEC method employs a single constant scaling factor for all points calculated with the AVQZ basis set. It may also be due to the fact that the MRCI energies utilized to calibrate the DMBE/CBS form include the Davidson correction. This

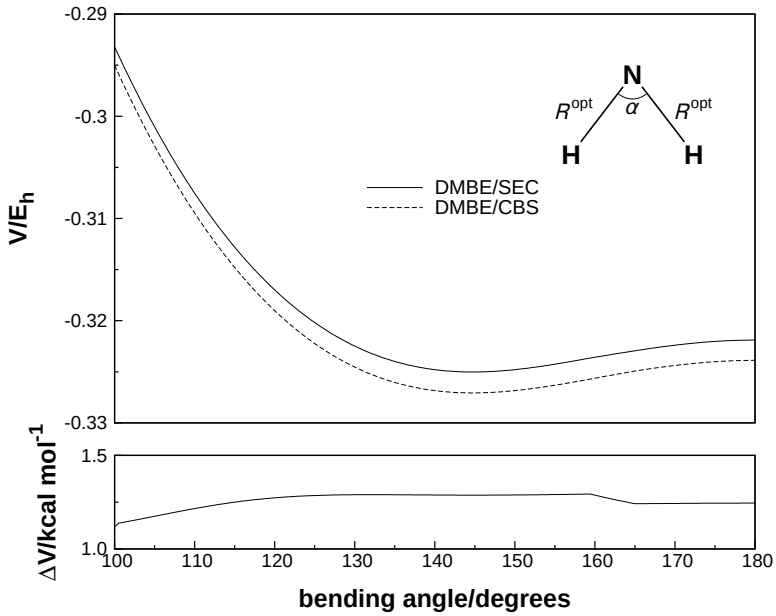

Figure 1. Optimized C_{2v} bending curve of $NH_2(1\,^2A')$ as a function of the bending angle, with the bond distance of NH optimized at each bending angle.

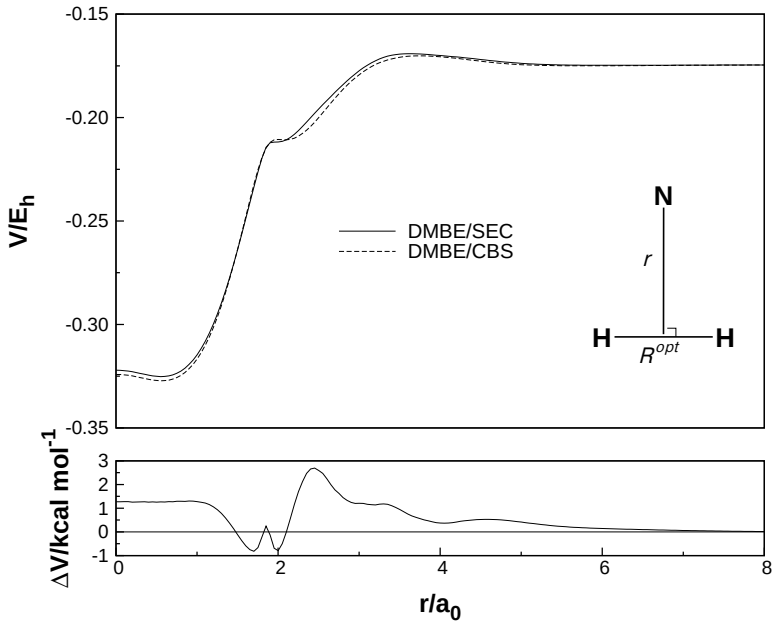

Figure 2. Approximate minimum energy path as a function of r (distance between the N atom and the center of the HH diatom), with the HH bond length optimized at each value of r .

suggests that the DMBE-SEC scheme slightly underestimates such a popular correction, a finding also supported from our recent work on the ground state NH_2[14] and SH_2[47] systems. Quantitatively, the energy difference at the global minimum in Figure 1 amounts to $\sim 1.25\,\mathrm{kcal\,mol^{-1}}$, with the well depths calculated relative to the three-atom dissociation limit being $-0.3252\,\mathrm{E_h}$ and $-0.3272\,\mathrm{E_h}$ for the DMBE/SEC and DMBE/CBS PESs, respectively. Thus, the well depth at equilibrium $NH_2(1\,^2A')$ is enhanced by $\sim 0.0036\,\mathrm{E_h}$ ($2.25\,\mathrm{kcal\,mol^{-1}}$) by the Davidson correction. In fact, if this is not included for the AVTZ and AVQZ energies, the CBS well depth would be $0.3272 - 0.0036 = 0.3236\,\mathrm{E_h}$, thus only $\sim 1.0\,\mathrm{kcal\,mol^{-1}}$ smaller than the well depth of the DMBE/SEC PES. Not surprisingly, as seen from Figure 2, the parallelism noted above largely disappears when one considers the optimized path for insertion of $N(^2D)$ into H_2. This is likely attributable to the very nature of the least-squares fit as the deviations fall on average close to the values given above. The above results then corroborate the high reliability and consistency of the CBS and DMBE-SEC methods. Needless to say, it cannot be discarded that the above differences may partly be attributable also to the fact that core correlation effects are absent in the CBS energies while they are effectively taken into account in the empirical SEC correction.

Table 3 compares the attributes of the stationary points of the DMBE/SEC and DMBE/CBS PESs for $NH_2(1\,^2A')$ with those of other potentials, especially the most recent RKHS form of Ref. 19. The predicted geometry of the stationary points is seen to be basically coincident with those reported by Pederson *et al.*,[19] who have based their PES on MRCI calculations using AVTZ basis set. Such a good agreement is not entirely unexpected as the DMBE/SEC surface has been obtained from a fit to SEC/MRCI with AVQZ raw energies, while the DMBE/CBS surface has been obtained from a fit to CBS(T,Q)/MRCI(Q) raw energies. This may also explain the fact that the DMBE/CBS PES predicts a slightly deeper well depth than the DMBE/SEC one. Moreover, Table 3 shows that the features of the other transition states in the DMBE/SEC PES are in quite good agreement with the results from DMBE/CBS, although this predicts a slightly deeper well depth. As for the harmonic frequencies, they are predicted from the DMBE/SEC PES to be 3641, 3956, and 985 $\mathrm{cm^{-1}}$, whereas the corresponding values calculated from a fit to a dense grid of SEC/MRCI/AVQZ points

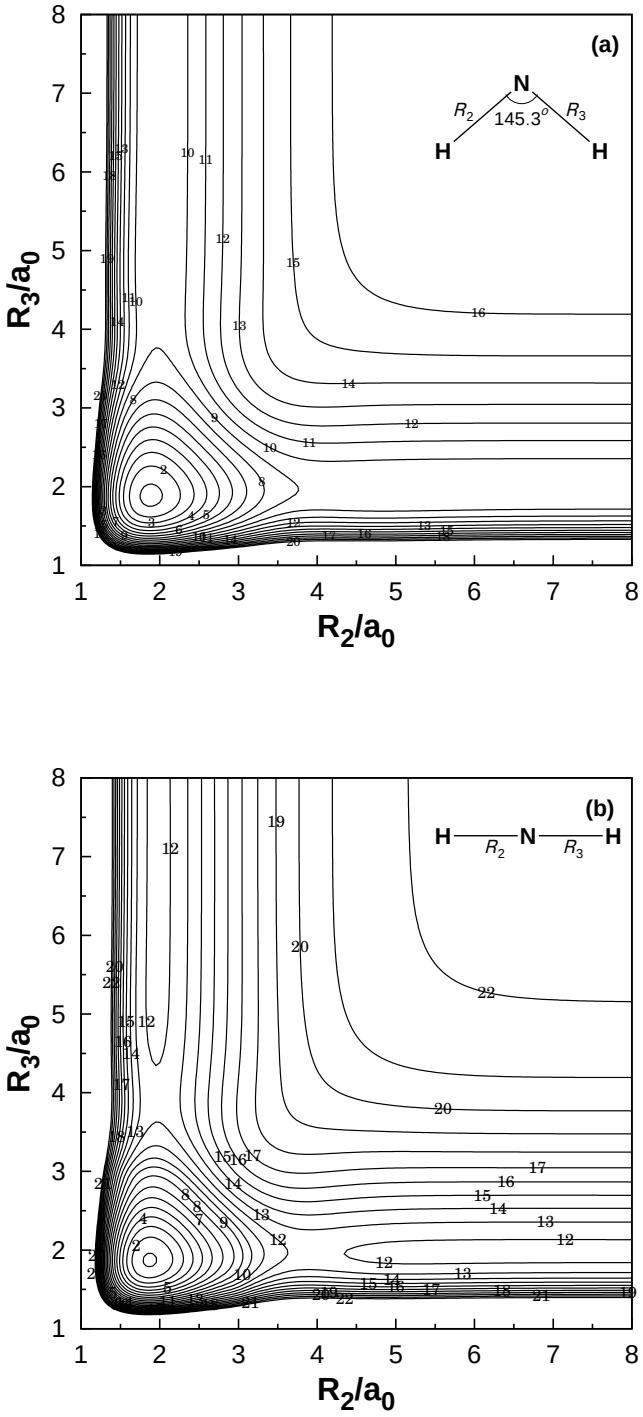

Figure 3. Contour plot for bond stretching in $H-N-H$, (a) included angle fixed at 145.3^o; (b) included angle fixed at 180^o. Contours are equally spaced by $0.02\,E_h$ in plot (a)and $0.015\,E_h$ for (b), starting at $-0.32\,E_h$. The energy zero is defined at the $N(^2D) + H(^2S) + H(^2S)$ asymptote.

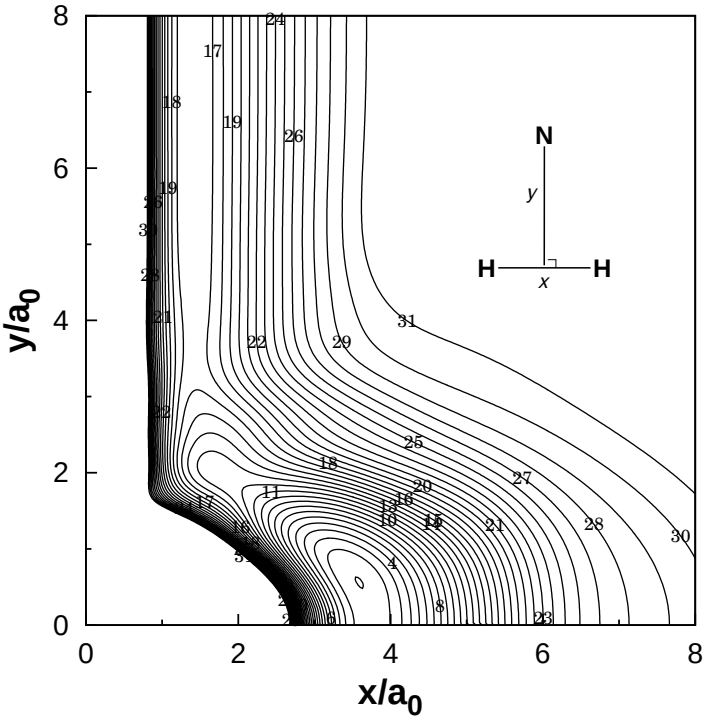

Figure 4. Contour plot for the C_{2v} insertion of the N atom into H_2. Contours are equally spaced by $0.01\,E_h$, starting at $-0.325\,E_h$. The energy zero is defined at the $N(^2D) + H(^2S) + H(^2S)$ asymptote.

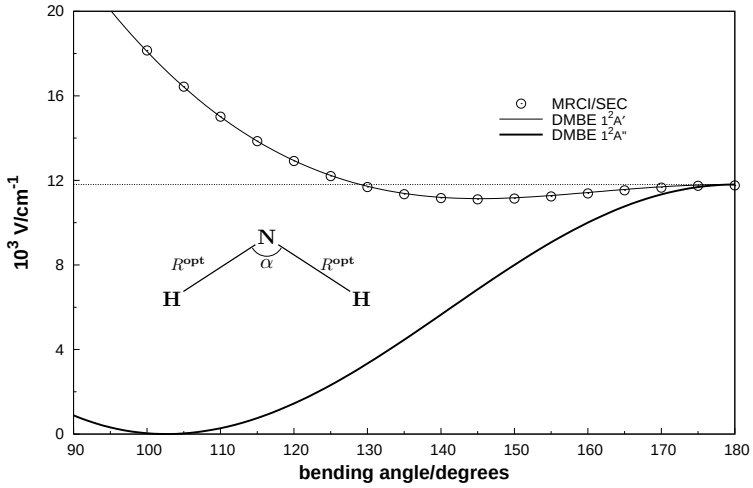

Figure 5. Optimized C_{2v} bending curve: circles, SEC/MRCI/AVQZ; dark solid line, DMBE $1\,^2A''$; thin solid line, DMBE/SEC $1\,^2A'$(this work). The energy zero is defined at the global minimum of the DMBE $1\,^2A''$ PES.

near the equilibrium geometry are 3639, 3953, and 978 cm^{-1}. Clearly, both sets of values show an excellent agreement with each other. Table 3 also shows that the harmonic frequencies are very similar for the CBS and DMBE/CBS surfaces, with the differences being smaller than $10\,cm^{-1}$. We emphasize that a dense grid of points has been calculated in the vicinity of the global minimum, with the rmsd of the DMBE least-squares fit to such points being $\sim 0.03\,cm^{-1}$ and a maximum deviation of $< 0.034\,kcal\,mol^{-1}$ (see Table 2). For C_{2v} insertion of $N(^2D)$ into H_2, the DMBE/SEC PES predicts a barrier height only $0.1\,kcal\,mol^{-1}$ lower than the one of Ho *et al.*[19] In fact, Table 3 shows that a fairly good agreement also exists between the DMBE/CBS and RKHS[19] PESs as far the vibrational frequencies are concerned: the largest absolute deviations do not generally exceed 75 cm^{-1}. The deviations remain small when comparing the DMBE/SEC and DMBE/CBS results, which corroborates the high quality of both fits. The barrier height of the saddle point at $C_{\infty v}$ (N − H − H) geometries is seen to be larger than the previous best theoretical value. Perhaps not surprisingly, somewhat larger differences are also observed for the corresponding harmonic frequencies. Unfortunately, no results are available for comparison for the $D_{\infty h}$ (H − N − H) barrier. Despite this, there is a fairly good agreement between the results obtained from the DMBE/SEC and DMBE/CBS forms. So, we may judge the DMBE function here reported as providing an accurate representation of the true PES at the chosen level of theory. A technical detail to note that the dense grids of *ab initio* points near the stationary points have been highly weighted in the fitting procedure, thus warranting an accurate description of the topographical features of the PES at such regions.

Figures 3 to 13 illustrate the topographical features of the $NH_2(1\,^2A')$ DMBE/SEC PES (the corresponding Figures for DMBE/CBS are shown in Figures 1-11 of the SI). Clearly, it has a smooth and correct behavior over the whole configuration space. Also visible from these plots are its major stationary points: C_{2v}, $C_{\infty v}$ and $D_{\infty h}$ barriers, and the global minimum. Specifically, Figure 3 shows a contour plot for bond stretching in H-N-H keeping the included angle fixed at 145.3 deg. The prominent feature is the global minimum, which corresponds to the point of minimum energy at 145.3 deg in the optimized bending plot of Figure 5. It is observed that the ground state $1\,^2A''$ and excited state $1\,^2A'$ PESs become

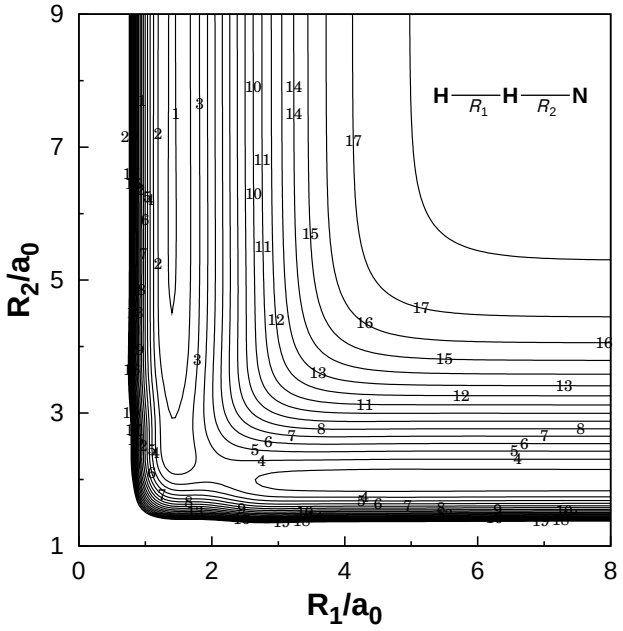

Figure 6. Contour plot for bond stretching in linear $N-H-H$ configurations. Contours are equally spaced by $0.01\,E_h$, starting at $-0.174\,E_h$. The energy zero is defined at the $N(^2D)+H(^2S)+H(^2S)$ asymptote.

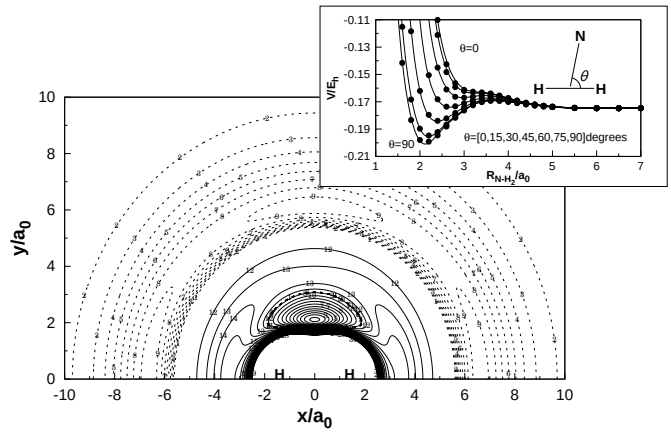

Figure 7. Contour plot for a N atom moving around a H_2 molecule fixed at the equilibrium geometry $R_1 = 1.401a_0$ and lying along the X-axis with the center of the bond fixed at the origin. Contours are equally spaced by $0.0025\,E_h$, starting at $-0.20\,E_h$. Shown in dash are contours equally spaced by $-32.5\,\mu E_h$, starting at $-0.1744747\,E_h$. Shown in the inset are cuts along the atom-diatom radial coordinate for selected values of the Jacobi angle. The reference energy refers to $N(^2D)+H_2$. The energy zero is defined at the $N(^2D)+H(^2S)+H(^2S)$ asymptote.

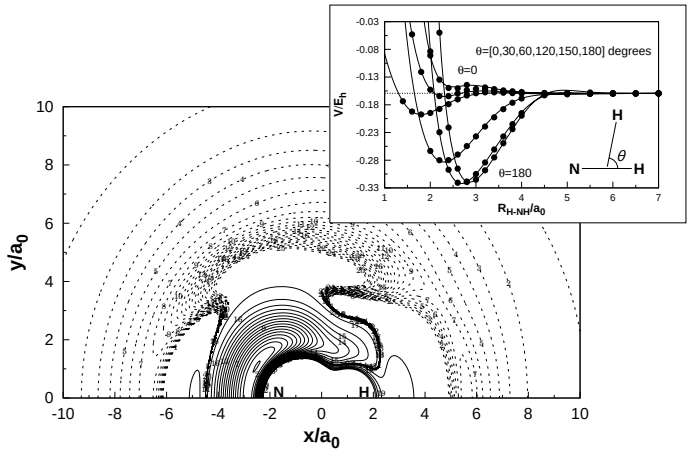

Figure 8. Contour plot for a H atom moving around a NH molecule fixed at the equilibrium geometry $R_{NH} = 1.974\,a_0$ and lying along the X-axis with the center of the bond fixed at the origin. Contours are equally spaced by $0.01\,E_h$, starting at $-0.323\,E_h$. Shown in dash are contours equally spaced by $-50\,\mu E_h$, starting at $-0.159241\,E_h$. The insert shows cuts along the atom-diatom radial coordinate for selected values of the Jacobi angle. The reference energy refers to $H + NH(a^1\Delta)$. The energy zero is defined at the $N(^2D) + H(^2S) + H(^2S)$ asymptote.

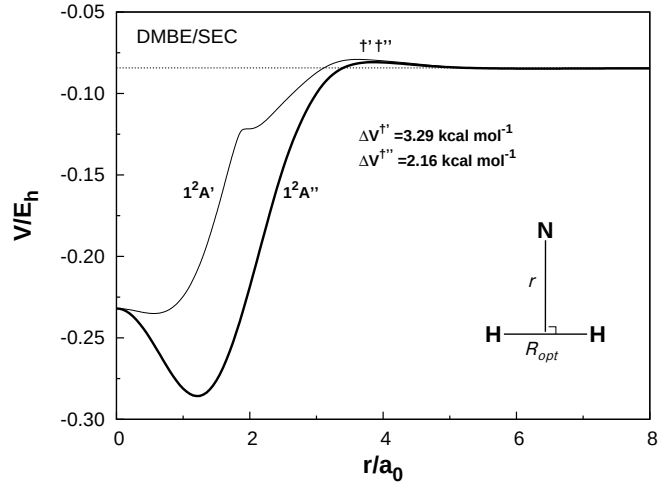

Figure 9. Minimum energy path as a function of r (distance between the N atom and the center of the HH diatom), with the HH bond length optimized at each value of r. dark solid line, DMBE $1\,^2A''$; thin solid line, DMBE/SEC $1\,^2A'$ (this work). The energy zero is defined at the $N(^4S) + H(^2S) + H(^2S)$ asymptote.

degenerate at the $^2\Pi$ line of linear geometries, as they should according to the

MRCI calculations for small bond lengths. Not surprisingly, the excited state $1\,^2A'$ predicts the same optimum energy and bond length at $D_{\infty h}$ geometry as the ground state $1\,^2A''$ PES; such a structure corresponds to the maximum at 180 deg in the optimized bending plot of Figure 5. The notable feature from this plot is the fairly good agreement between our optimized bending curve and the one we have directly optimized at SEC/MRCI/AVQZ level. In turn, Figure 4 shows a contour plot for the C_{2v} insertion of the nitrogen atom into the hydrogen molecule. Visible from this plot are the stationary points corresponding to C_{2v} and $D_{\infty h}$ barriers, and the global minimum.

Figures 7 and 8 illustrate the long range regions of the DMBE/SEC PES which have been fitted such as to provide a reliable description of the van der Waals minimum for the $N - H_2$ interaction. Note that it shows a flat van der Waals valley, with two minima: one at a C_{2v} geometry and the other at a $C_{\infty v}$ one. Of these, the deepest minimum refers to the T-shaped structure, although the well depth is only $0.0004\,\mathrm{kcal\,mol^{-1}}$ ($0.14\,\mathrm{cm^{-1}}$) larger than the collinear one; see Table 4 for other attributes. As shown in the insert of Figures 7 and 8, the final DMBE/SEC form reproduces quite satisfactorily all such topographical features. Thus, the $NH_2(1\,^2A')$ PES shows a topography rather similar to the ground state when evaluated at the same level of theory. It should be noted at this point that the single-state CAS self-consistent-field (CASSCF) reference wave function that has been utilized for the CI should, in principle, yield a better description of the PES than usually do[16] state-averaged CASSCF ones, although this by no means implies that the latter approach cannot be useful when aiming at a more uniform description of the various electronic states under theoretical scrutiny. The minimum energy paths of the DMBE/SEC PESs for C_{2v} insertion of N(^{2}D) into H_2 are shown in Figure 9; r is the distance from N to the center of HH, with the HH bond length optimized at each value of r. visible from this plot are the small maxima corresponding to the C_{2v} saddle points, the minima, and $D_{\infty h}$ barriers for linearity. Also visible is, of course, the RT degeneracy of the $1\,^2A''$ and $1\,^2A'$ PESs at linearity .

Figure 10 shows the isotropic and leading anisotropic components of the N-H_2 interaction potential, two important quantities of relevance in atom-diatom scattering.[57] Specifically, the isotropic potential V_0 determines how close on av-

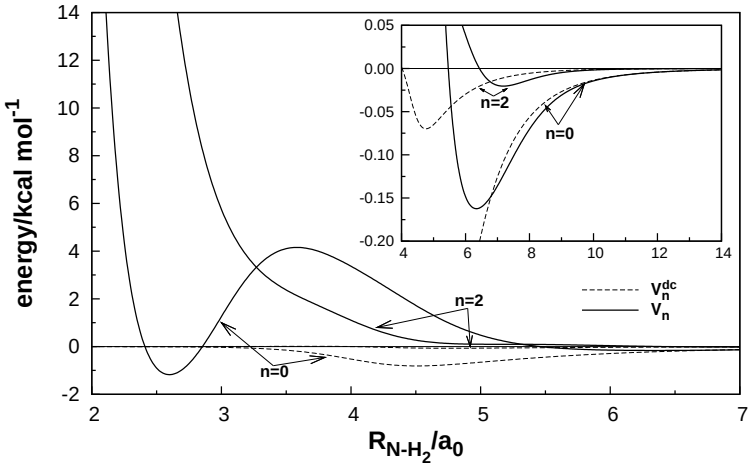

Figure 10. Isotropic (V_0) and leading anisotropic (V_2) components of the N − H_2 interaction potential, with the diatomic molecule fixed at the equilibrium geometry. solid line, DMBE; dashed line, three-body dynamical correlation term (leading to asymptotic atom-diatom dispersion interaction at large distances) in Eq. (20). The axes in all panels have the same units.

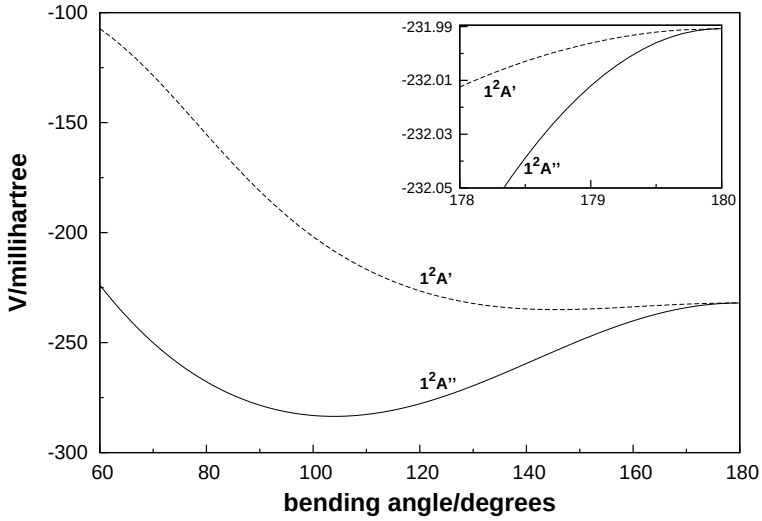

Figure 11. One-dimensional cuts of the PESs of $1\,^2A''$(Ref.14) and $1\,^2A'$ states of NH_2 along the bending angle with the bond lengths fixed at $1.8695\,a_0$. Shown in the insert are the cuts of regions with bending angles from 178 to 180 deg. The energy zero is defined at the $N(^4S) + H(^2S) + H(^2S)$ asymptote.

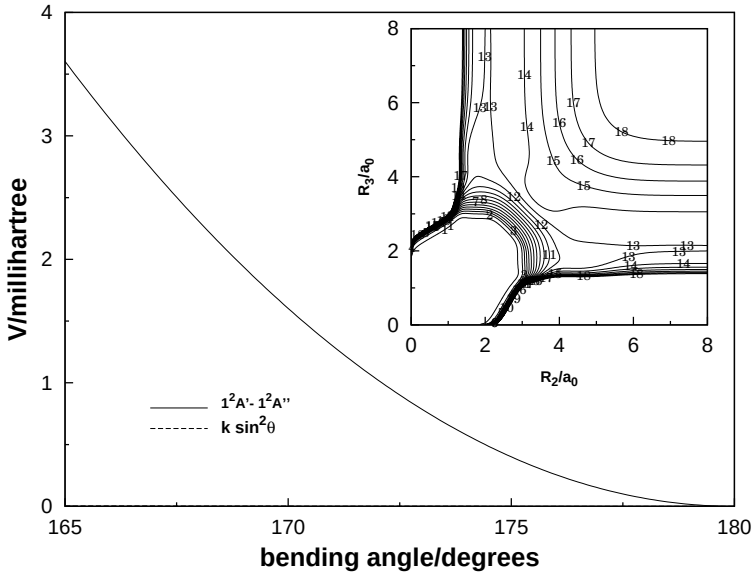

Figure 12. Energy difference between the excited ($1\,^2A'$) and ground state ($1\,^2A''$) DMBE/SEC PESs as a function of bending angle, with the bond lengths fixed at $1.8695\,a_0$. Shown in the inset is the energy difference between both PESs in linear $H-N-H$ configurations. Contours are equally spaced by $0.005\,E_h$, starting at $0.001\,E_h$.

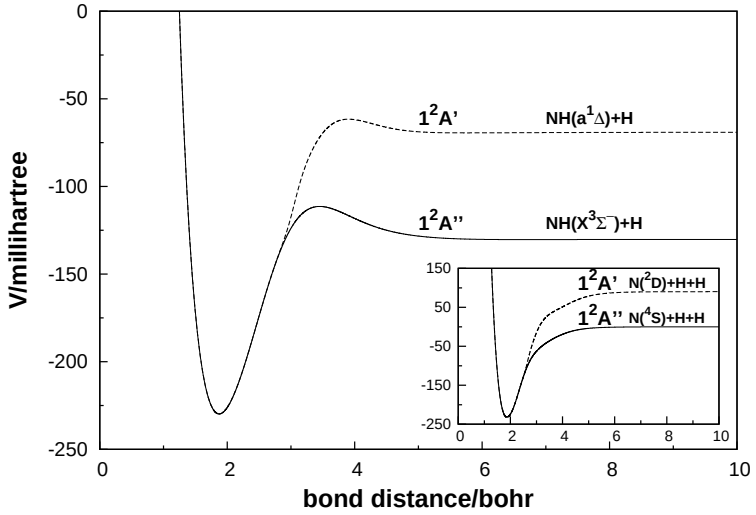

Figure 13. One-dimensional cuts of the PESs of $1\,^2A''$(Ref.14) and $1\,^2A'$ states of NH_2 along the bending length with the bond angle fixed at 180 deg and other bond length fixed at $1.965\,a_0$. Shown in the inset are the cuts along the bending length with the bond angle fixed at 180 deg and the two bond lengths fixed same values. The energy zero is defined at the $N(^4S)+H(^2S)+H(^2S)$ asymptote.

erage the atom and molecule can approach each other, while the magnitude of V_2 indicates whether or not the molecule prefers to orient its axis along the direction of the incoming atom: a negative value favors the collinear approach while a positive value favors the approach through an isosceles triangular geometry. The barrier in V_0 located near 3.58 a_0 (see Figure 10) corresponds to the C_{2v} transition state, as corroborated by the positive value of V_2 at such a distance. Correspondingly, the sign of V_2 at distances larger than 7.18 a_0 is negative favoring a collinear atom-diatom approach, but become positive at $\sim 6.34\,a_0$ where the van der Waals minimum of the isotropic curve occurs. This conforms with the fact that the deepest well is associated to the T-shaped van der Waals structure. Note that the $N + H_2$ reaction has been shown to display a preference for the insertion mechanism, and hence such subtle details may have practical implications for scattering calculations, especially at low collision energies.

The interaction between electronic states of NH_2 is intricate,[2, 13] especially in the NH+H channel. As noted elsewhere,[13, 56] by stretching a N−H bond in linear H−N−H, the $^2\Pi$ state will intersect conically with a $^2\Sigma^-$, a $^2\Delta$, and a $^2\Sigma^+$ state; these correlate with different states of the NH + H products. Because of these conical intersections, the ground state $1\,^2A''$ correlates to $^2\Pi$ or to $^2\Sigma^-$, and hence may dissociate to form NH($X^3\Sigma^-$)+H products. Similarly, the excited state $1\,^2A'$ correlates to $^2\Pi$ or $^2\Delta$, and with the NH($a^1\Delta$)+H dissociation channel. Thus, for linearity, the ground state $1\,^2A''$ and the excited state $1\,^2A'$ become degenerate for small HN − H bond distances.

Figure 11 illustrates $1D$ cuts of $1\,^2A''$ and $1\,^2A'$ DMBE/SEC PESs of NH_2 as a function of the bending angle for a bond length fixed at $1.8695\,a_0$. Clearly, the $1\,^2A''$ and $1\,^2A'$ states become degenerate at linearity. The potential well in the $1\,^2A'$ state DMBE/SEC PES toward the linear H − N − H geometry is also seen to be very shallow, with a barrier height for linearity of only 673 cm^{-1}. This compares well with the value of 674 cm^{-1} obtained on the DMBE/CBS PES. In turn, this is in good agreement with the theoretical value of 693 cm^{-1} obtained from the PES of Qu *et al.*,[13] and the recent theoretical value of 719 cm^{-1} by Zhou *et al.*[21] In turn, Figure 12 illustrates a $1D$ cut of the energy difference between the $1\,^2A'$ and the ground state ($1\,^2A''$) PESs as a function of the bending angle, keeping the bond lengths fixed at $1.8695\,a_0$. Shown in the insert of Figure 12

is the energy difference between both PESs in linear H − N − H configurations. As noted elsewhere,[58, 59] such a difference should have the form $\Delta V = k\sin^2\theta$, where θ is the bending angle. The agreement is shown from Figure 12 to be good, with the 1D cut of the energy difference being nearly indistinguishable from the fit for small deviations from linearity. Two further points should be noted: first, the form $k\sin^2\theta$ ensures that the states $1\,^2A''$ and $1\,^2A'$ become strictly degenerate at all linear configurations for small HN − H bond distances; second, the energy split between the $1\,^2A'$ and $1\,^2A''$ PESs is proportional to θ^2 at small HN − H bond distances and small deviations from linearity, as it should for electronic Π states. Such a behavior is depicted graphically in Figure 13, which shows $1D$ cuts of the $1\,^2A''$ and $1\,^2A'$ DMBE/SEC PESs of NH_2 as a function of the stretched bond distance, with the bond angle fixed at 180 deg and the other bond length at $1.965\,a_0$. Clearly, the degeneracy at linearity is lifted such as to allow that the $1\,^2A''$ state correlates with $NH(X^3\Sigma^-) + H$, while $1\,^2A'$ does with $NH(a\,^1\Delta) + H$. This is consistent with the PESs of Qu *et al.*[13] and Zhou *et al.*[21] Moreover, Figure 13 shows that, for small N − H distances, the $1\,^2A''$ and $1\,^2A'$ PESs become degenerate while, for large N − H distances, $1\,^2A''$ correlates with $N(^4S) + 2H$ and $1\,^2A'$ with $N(^2D) + 2H$.

5 Concluding remarks

We have reported a single-sheeted DMBE/SEC PES for the excited state of NH_2 based on a realistic representation of the long-range forces and a fit to accurate *ab initio* energies calculated at the MRCI level with the AVQZ basis set, after slightly correcting semiempirically the dynamical correlation by the DMBE-SEC method. The resulting function has been compared in detail with the DMBE/CBS PES obtained by extrapolating the calculated raw energies to the CBS limit. The various topographical features of both DMBE/SEC and DMBE/CBS PESs have been carefully examined, and compared with previous results for the title system. Regarding accuracy attributes, the two forms can hardly be discriminated since they have rather similar rmsd. Of course, the DMBE/CBS PES has been constructed in a purely *ab initio* fashion, whereas the DMBE/SEC one here reported entails a small degree of empiricism via scaling of the external (or dynamical)

correlation. The fact that they are so similar in topography and accuracy can therefore be regarded as an asset on the consistency of both schemes. Since the DMBE functions from the present work fit accurately the *ab initio* energies, they can both be recommended for dynamics studies of the $N(^2D) + H_2$ reaction and as building blocks for constructing the PESs of larger nitrogen/hydrogen containing systems. Their use for ro-vibrational calculations both with inclusion or without inclusion of nonadiabatic effects may help on further judging some minute but subtle (such as core correlation) effects that have been neglected (DMBE/CBS) or corrected empirically (DMBE/SEC) in the present work.

Acknowledgments

Y.Q. Li thanks the Liaoning University for leave of absence during his PhD Studies. This work has the financial support of Fundação para a Ciência e a Tecnologia, Portugal.

References and Notes

[1] Wright, A. N.; Winkler, C. A. *Active Nitrogen;* Academic: New York, 1968.

[2] Takayanagi, T.; Kurosaki, Y.; Yokoyama, K. *Chem. Phys. Lett.* **2000**, *321*, 106.

[3] Dodd, J. A.; Lipson, S. J.; Flanagan, D. J.; Blumberg, W. A. M.; Pearson, J. C.; Green, B. D. *J. Chem. Phys.* **1991**, *94*, 4301.

[4] Umemoto, H.; Matsumoto, K. *J. Chem. Phys.* **1996**, *104*, 9640.

[5] Umemoto, H.; Asai, T.; Kimura, Y. *J. Chem. Phys.* **1997**, *106*, 4985.

[6] Alagia, M.; Balucani, N.; Cartechini, L.; Cachavecchia, P.; Volpi, G. G.; Pederson, L. A.; Schatz, G. C.; Lendvay, G.; Harding, L. B.; Hollebeek, T.; Ho, T.-S.; Rabitz, H. *J. Chem. Phys.* **1999**, *110*, 8857.

[7] Buenker, R. J.; Perić, M.; Peyerimhoff, S. D.; Marian, R. *Mol. Phys.* **1981**, *43*, 987.

[8] Jensen, P.; Buenker, R. J.; Hirsch, G.; Rai, S. N. *Mol. Phys.* **1990**, *70*, 443.

[9] Funken, K.; Engels, B.; Peyerimhoff, S. D.; Grein, F. *Chem. Phys. Lett.* **1990**, *172*, 180.

[10] Suzuki, T.; Shihira, Y.; Sato, T.; Umemoto, H.; Tsunashima, S. *J. Chem. Soc. Faraday Trans.* **1993**, *89*, 995.

[11] Vetter, R.; Zülicke, L.; Koch, A.; van Dishoeck, E. F.; Peyerimhoff, S. D. *J. Chem. Phys.* **1995**, *104*, 5558.

[12] Takayanagui, T.; Kobayashi, H.; Tsunashima, S. *J. Chem. Soc. Faraday Trans.* **1996**, *92*, 1311.

[13] Qu, Z.; Zhu, H.; Schinke, R.; Adam, L.; Hack, W. *J. Chem. Phys.* **2005**, *122*, 204313.

[14] Varandas, A. J. C.; Poveda, L. A. *Theor. Chem. Acc.* **2006**, *116*, 404.

[15] Adam, L.; Hack, W.; McBane, G. C.; Zhu, H.; Qu, Z.-W.; Schinke, R. *J. Chem. Phys.* **2007**, *126*, 034304.

[16] Zhou, S. L.; Xie, D.; Lin, S. Y.; Guo, H. *J. Chem. Phys.* **2008**, *128*, 224316.

[17] Saxon, R. P.; Lengsfield III, B. H.; Liu, B. *J. Chem. Phys.* **1983**, *78*, 312.

[18] Pederson, L. A.; Schatz, G. C.; Ho, T.; Hollebeek, T.; Rabitz, H.; Harding, L. B. *J. Chem. Phys.* **1999**, *110*, 9091.

[19] Pederson, L.; Schatz, G.; Hollebeek, T.; Ho, T.-S.; Rabitz, H.; Harding, L. B. *J. Phys. Chem. A* **2000**, *104*, 2301.

[20] Honvault, P.; Launay, J. *J. Chem. Phys.* **1999**, *111*, 6665.

[21] Zhou, S. L.; Li, Z.; Xie, D.; Lin, S. Y.; Guo, H. *J. Chem. Phys.* **2009**, *130*, 184307.

[22] Gamallo, P.; Defazio, P. *J. Chem. Phys.* **2009**, *131*, 044320.

[23] Varandas, A. J. C. *Adv. Chem. Phys.* **1988**, *74*, 255.

[24] Varandas, A. J. C. *Chem. Phys. Lett.* **1992**, *194*, 333.

[25] Varandas, A. J. C. *Lecture Notes in Chemistry*; Laganá, A., Riganelli, A., Eds.; Springer: Berlin, 2000; Vol. 75, pp 33–56.

[26] Varandas, A. J. C.; World Scientific Publishing, 2004; chapter 5, p 91; Advanced Series in Physical Chemistry.

[27] Werner, H.-J.; Knowles, P. J. *J. Chem. Phys.* **1988**, *89*, 5803.

[28] Knowles, P. J.; Werner, H.-J. *Chem. Phys. Lett.* **1988**, *145*, 514.

[29] Varandas, A. J. C. *J. Chem. Phys.* **1989**, *90*, 4379.

[30] Varandas, A. J. C. *Physica Scripta; Comm. At. Opt. Mol. Phys.* **2007**, *76*, C28.

[31] Dunning Jr., T. H. *J. Chem. Phys.* **1989**, *90*, 1007.

[32] Kendall, R. A.; Dunning Jr., T. H.; Harrison, R. J. *J. Chem. Phys.* **1992**, *96*, 6796.

[33] Varandas, A. J. C. *J. Chem. Phys.* **2007**, *126*, 244105.

[34] Varandas, A. J. C. *J. Chem. Phys.* **2007**, *127*, 114316.

[35] Werner, H.-J.; Knowles, P. J., MOLPRO is a package of *ab initio* programs written by H.-J. Werner, P. J. Knowles, with contributions from J. Almlf, R. D. Amos, M. J. O. Deegan, S. T. Elbert, C. Hampel, W. Meyer, K. A. Peterson, R. Pitzer, A. J. Stone, P. R. Taylor, R. Lindh, (1998).

[36] Basis sets were obtained from the extensible computational chemistry environment basis set database, version 02/25/04, as developed and distributed by the molecular science computing facility, environmental and molecular sciences laboratory which is part of the pacific northwest laboratory, p.o. box 999, richland, washington 99352, usa, and funded by the u.s. department of energy. the pacific northwest laboratory is a multi-program laboratory operated by battelle memorial institute for the u.s. department of energy under

contract de-ac06-76rlo 1830. contact karen schuchardt for further information.

[37] Varandas, A. J. C.; Rodrigues, S. P. J. *J. Phys. Chem A* **2006**, *110*, 485.

[38] Varandas, A. J. C.; Rodrigues, S. P. J. *Spectrochim. Acta A* **2002**, *58*, 629.

[39] Karton, A.; Martin, J. M. L. *Theoret. Chim. Acta* **2006**, *115*, 330–333.

[40] Helgaker, T.; Klopper, W.; Koch, H.; Noga, J. *J. Chem. Phys.* **1997**, *106*, 9639.

[41] Varandas, A. J. C. *J. Chem. Phys.* **2000**, *113*, 8880–8887.

[42] Varandas, A. J. C. *Chem. Phys. Lett.* **2007**, *443*, 398.

[43] Varandas, A. J. C. *J. Chem. Phys.* **2008**, *129*, 234103.

[44] Varandas, A. J. C. *Chem. Phys. Lett.* **2008**, *463*, 225–229.

[45] Varandas, A. J. C. *J. Comput. Chem.* **2009**, *30*, 379.

[46] Varandas, A. J. C. *J. Chem. Phys.* **2009**, *131*, 124128.

[47] Song, Y. Z.; Varandas, A. J. C. *J. Chem. Phys.* **2009**, *130*, 134317.

[48] Varandas, A. J. C. *J. Phys. Chem. A* **2008**, *112*, 1841–1850.

[49] Poveda, L. A.; Varandas, A. J. C. *Phys. Chem. Chem. Phys.* **2005**, *7*, 2867.

[50] Varandas, A. J. C.; Silva, J. D. *J. Chem. Soc. Faraday Trans.* **1992**, *88*, 941.

[51] Varandas, A. J. C. *J. Mol. Struct. Theochem.* **1985**, *120*, 401.

[52] Varandas, A. J. C. *J. Chem. Phys.* **1996**, *105*, 3524.

[53] Herzberg, G. *Molecular Spectra and Molecular Structure. I. Spectra of Diatomic Molecules, (2nd edition);* Van Nostrand: New York, 1950.

[54] Owono Owono, L. C.; Jaidane, N.; Kwato Njock, M. G.; Ben Lakhdar, Z. *J. Chem. Phys.* **2007**, *126*, 244302.

[55] Martínez-Núñez, E.; Varandas, A. J. C. *J. Phys. Chem. A* **2001**, *105*, 5923.

[56] Santoro, F.; Petrongolo, C.; Schatz, G. C. *J. Phys. Chem. A* **2002**, *106*, 8276.

[57] Varandas, A. J. C. *J. Chem. Phys.* **1979**, *70*, 3786.

[58] Gabriel, W.; Chambaud, G.; Rosmus, P.; Carter, S.; Handy, N. *Mol. Phys.* **1994**, *6*, 1445–1461.

[59] Carter, S.; Mills, I. M.; Dixon, R. N. *J. Mol. Spectrosc.* **1984**, *106*, 411.

J. Phys. Chem. A. **114**, 9644-9654 (2010).

Accurate potential energy surface for the $1\,^2A'$ state of NH_2: scaling of the external correlation versus extrapolation to complete-basis-set limit

Y. Q. Li and A.J.C. Varandas

Departamento de Química, Universidade de Coimbra
3004-535 Coimbra Codex, Portugal.

(Received: January 11, 2010; In final form: February 22, 2010)

Table 1. Parameters of two-body potential energy curves in Eqs. (17)-(21).

Parameter	NH($a^1\Delta$)/SEC	NH($a^1\Delta$)/CBS	$H_2(X^1\Sigma_g^+)$
R_e/a_0	1.974	1.974	1.401
D/E_h	0.287545	0.289261	0.22979439
α_1/a_0^{-1}	2.95556	3.00041	1.82027480
α_2/a_0^{-2}	2.61308	2.76841	0.52437767
α_3/a_0^{-3}	0.94138	1.11775	0.36999610
γ_0/a_0^{-1}	2.39092	2.43535	1.094670
γ_1/a_0^{-1}	-0.104357	-0.108428	1.009737
γ_2/a_0^{-1}	0.872534	0.83125	0.235856
$\widetilde{A}/E_h a_0^{-\widetilde{\alpha}}$			-0.8205
$\widetilde{\alpha}_1/a_0^{-1}$			0
$\widetilde{\alpha}$			2.5
$\widetilde{\gamma}/a_0^{-1}$			2.0
R_0/a_0	6.75306911	6.75306911	6.9282
$C_6/E_h a_0^{-6}$	12.2568025	12.2568025	6.499
$C_8/E_h a_0^{-8}$	232.171547	232.171547	124.4
$C_{10}/E_h a_0^{-10}$	5761.18842	5761.18842	3286.0
$C_{11}/E_h a_0^{-11}$			-3475
$C_{12}/E_h a_0^{-12}$			121,500
$C_{13}/E_h a_0^{-13}$			-291,400
$C_{14}/E_h a_0^{-14}$			6,061,000
$C_{15}/E_h a_0^{-15}$			-23,050,000
$C_{16}/E_h a_0^{-16}$			393,800,000

Table 2. Parameters and reference geometries of DMBE/SEC PES, which used in the extended Hartree-Fock energy in Eq. (25).

Coefficients	$P^{(1)}$	$P^{(2)}$	$P^{(3)}$
$\gamma_1^{(j)}/a_0^{-1}$	0.6	0.7	0.4
$\gamma_2^{(j)}/a_0^{-1}$	0.9	1.2	0.7
$\gamma_3^{(j)}/a_0^{-1}$	0.9	1.2	0.7
$R_1^{(j),\mathrm{ref}}/a_0$	1.4	3.0	3.8
$R_2^{(j),\mathrm{ref}}/a_0$	3.0	2.5	3.0
$R_3^{(j),\mathrm{ref}}/a_0$	3.0	2.5	3.0

Table 3. Numerical values of DMBE/SEC PES, which used in the extended Hartree-Fock energy in Eq (25).

Coefficients	$P^{(1)}$	$P^{(2)}$	$P^{(3)}$
C_1/a_0^0	−6.9445959097	−5.5684576070	8.0562556558
C_2/a_0^{-1}	−1.7927064363	−0.0921728439	−1.9212102554
C_3/a_0^{-1}	−2.9575063858	−0.9467948710	3.3690640150
C_4/a_0^{-2}	−1.3789061843	−1.8685057139	1.3428713667
C_5/a_0^{-2}	−5.6313400809	−2.2254865846	1.0588315775
C_6/a_0^{-2}	−0.6114974820	0.0602872726	−1.6922359646
C_7/a_0^{-2}	−0.9313499675	−0.5394573895	0.4417090677
C_8/a_0^{-3}	−0.9788813868	0.2145292865	−0.4164956241
C_9/a_0^{-3}	−1.9632265192	−0.1575448392	−0.4961067906
C_{10}/a_0^{-3}	−0.2319561504	−0.0717234500	0.1025783652
C_{11}/a_0^{-3}	−0.6942913490	−0.9465433525	0.8205176191
C_{12}/a_0^{-3}	−0.8458066353	−0.2048421685	0.3049074208
C_{13}/a_0^{-3}	−0.1967963412	0.1728623412	0.0300097218
C_{14}/a_0^{-4}	−0.1167264334	−0.0435984955	0.0266474104
C_{15}/a_0^{-4}	−0.8604045368	0.3189057226	0.1486118124
C_{16}/a_0^{-4}	−0.7603144931	−0.1295109714	0.0794020260
C_{17}/a_0^{-4}	0.1829632546	0.7572422535	−0.1095224714
C_{18}/a_0^{-4}	−0.2536737245	−0.5839199519	−0.1263369415
C_{19}/a_0^{-4}	−0.0239919396	0.3669381234	−0.1686466736
C_{20}/a_0^{-4}	0.2221192090	−0.2226917895	−0.1506082583
C_{21}/a_0^{-4}	−0.0102403648	−0.1012786080	0.0023450421
C_{22}/a_0^{-4}	−0.1214021487	0.0456579932	−0.0167790935
C_{23}/a_0^{-5}	−0.1020845467	0.0420090597	0.0007373850
C_{24}/a_0^{-5}	−0.2285650035	−0.0379090133	0.0079077236
C_{25}/a_0^{-5}	−0.0517933419	−0.0003347071	−0.0406340355
C_{26}/a_0^{-5}	0.0652027555	0.1325356120	0.0226837555
C_{27}/a_0^{-5}	0.0037405057	−0.1141356883	0.0042373292
C_{28}/a_0^{-5}	−0.0605324041	−0.1806920748	0.0016049046
C_{29}/a_0^{-5}	0.0331982080	0.0213174833	0.0231696709
C_{30}/a_0^{-5}	−0.1020675226	0.0700799290	0.0133072547
C_{31}/a_0^{-5}	0.1064745080	0.0375400782	−0.0083895850
C_{32}/a_0^{-5}	0.0511797840	0.0297835613	−0.0000352599
C_{33}/a_0^{-5}	0.0111683227	0.0517592845	0.0095717982
C_{34}/a_0^{-5}	0.0145297278	−0.0189105035	−0.0026133257

Table 3. Continue

C_{35}/a_0^{-6}	0.0081269194	−0.0032076815	0.0010249946
C_{36}/a_0^{-6}	−0.0473490834	0.0173321542	−0.0039180850
C_{37}/a_0^{-6}	0.0250649111	−0.0907315433	0.0039100752
C_{38}/a_0^{-6}	−0.0027992599	−0.0188465554	−0.0016320073
C_{39}/a_0^{-6}	0.1343414718	−0.0396089649	−0.0001736353
C_{40}/a_0^{-6}	−0.0467524285	−0.0122739602	0.0007328184
C_{41}/a_0^{-6}	−0.0078997965	−0.0197150866	−0.0001770807
C_{42}/a_0^{-6}	0.0039297282	−0.0612294775	−0.0016894302
C_{43}/a_0^{-6}	0.0206051561	−0.0188237837	−0.0030572589
C_{44}/a_0^{-6}	0.0276523706	0.0306767777	0.0032857405
C_{45}/a_0^{-6}	0.0640472759	0.0457656741	−0.0001861065
C_{46}/a_0^{-6}	0.0210728652	−0.0249278274	0.0032151326
C_{47}/a_0^{-6}	0.0263247691	0.0524694210	−0.0020500867
C_{48}/a_0^{-6}	0.0318038343	−0.0291167015	0.0000791760
C_{49}/a_0^{-6}	−0.0120735502	0.0387865172	0.0009577033
C_{50}/a_0^{-6}	0.0085901250	0.0347687759	−0.0011679920

Table 4. Parameters and reference geometries of DMBE/CBS PES, which used in the extended Hartree-Fock energy in Eq. (25).

Coefficients	$P^{(1)}$	$P^{(2)}$	$P^{(3)}$
$\gamma_1^{(j)}/a_0^{-1}$	0.4	1.1	0.3
$\gamma_2^{(j)}/a_0^{-1}$	0.8	1.1	1.0
$\gamma_3^{(j)}/a_0^{-1}$	0.8	1.1	1.0
$R_1^{(j),\mathrm{ref}}/a_0$	1.4	3.0	3.8
$R_2^{(j),\mathrm{ref}}/a_0$	3.0	2.5	3.0
$R_3^{(j),\mathrm{ref}}/a_0$	3.0	2.5	3.0

Table 5. Numerical values of DMBE/CBS PES, which used in the extended Hartree-Fock energy in Eq (25)

Coefficients	$P^{(1)}$	$P^{(2)}$	$P^{(3)}$
C_1/a_0^0	−3.6131972688	0.3760584069	−0.6860940355
C_2/a_0^{-1}	2.9666268115	−4.5627139245	−1.6911850193
C_3/a_0^{-1}	3.1215115473	1.4424371349	0.8011838070
C_4/a_0^{-2}	−0.5205026667	−0.2006234339	0.3108837620
C_5/a_0^{-2}	−2.9831322753	1.6368742123	0.3776487116
C_6/a_0^{-2}	6.4488244481	−1.2740257882	0.0422197152
C_7/a_0^{-2}	1.1458357022	0.2419043688	0.3449741514
C_8/a_0^{-3}	0.1120465134	−1.4746155401	−0.3883259919
C_9/a_0^{-3}	0.7593129119	−0.9671194428	−0.0698625723
C_{10}/a_0^{-3}	0.0730449815	0.0151285248	−0.0080766897
C_{11}/a_0^{-3}	−3.1908835012	−0.1560954544	0.6632400741
C_{12}/a_0^{-3}	−0.7271789435	0.5536927327	0.1626496747
C_{13}/a_0^{-3}	0.1180967295	0.6112777464	−0.1053223907
C_{14}/a_0^{-4}	−0.2162315779	0.0484250638	0.0000764501
C_{15}/a_0^{-4}	−0.5351393200	0.2741114831	0.1550747827
C_{16}/a_0^{-4}	−0.0685644754	0.4755437521	0.0397547565
C_{17}/a_0^{-4}	0.0734380694	−0.2690044939	0.0304861775
C_{18}/a_0^{-4}	1.1296697016	−0.6106116765	−0.2137131744
C_{19}/a_0^{-4}	0.2260557885	0.0338385631	−0.0333037206
C_{20}/a_0^{-4}	0.1701897329	−0.1916249959	−0.2385923058
C_{21}/a_0^{-4}	0.1863295909	−0.0191648907	0.0357985511
C_{22}/a_0^{-4}	0.3331721694	−0.2066966169	−0.0045116868
C_{23}/a_0^{-5}	0.0657062662	−0.0798665536	−0.0206898392
C_{24}/a_0^{-5}	0.1892115137	0.2568403100	−0.0279094371
C_{25}/a_0^{-5}	0.1749574467	0.0133052300	−0.0186132823
C_{26}/a_0^{-5}	−0.0275895315	0.1896437944	−0.0505683079
C_{27}/a_0^{-5}	0.0464722081	−0.0110111489	−0.0138122739
C_{28}/a_0^{-5}	−0.1304480250	−0.0933590085	0.0469671912
C_{29}/a_0^{-5}	0.0457090716	−0.1780393787	−0.0447799456
C_{30}/a_0^{-5}	−0.2107451688	0.0624583375	−0.0031670710
C_{31}/a_0^{-5}	0.0396907213	−0.1602592181	0.0032894809
C_{32}/a_0^{-5}	0.0556221672	−0.0717004410	−0.0767850139
C_{33}/a_0^{-5}	−0.0198254315	0.0356267712	−0.0111882971
C_{34}/a_0^{-5}	0.0119651016	−0.0092445159	−0.0082091075

Table 5. Continue

C_{35}/a_0^{-6}	−0.0033602831	0.0124044227	−0.0029235211
C_{36}/a_0^{-6}	−0.0014478444	−0.0047737372	0.0097427445
C_{37}/a_0^{-6}	−0.0370250796	0.0182942487	0.0002676181
C_{38}/a_0^{-6}	0.0163520828	0.0734165847	−0.0228759016
C_{39}/a_0^{-6}	−0.0187157856	−0.0824216458	−0.0160575555
C_{40}/a_0^{-6}	0.0044380247	0.0231785175	−0.0077463751
C_{41}/a_0^{-6}	−0.0009654444	−0.0038012199	−0.0015454905
C_{42}/a_0^{-6}	0.0055733645	−0.0454288037	−0.0034241896
C_{43}/a_0^{-6}	0.0042103082	−0.0215890360	−0.0145315359
C_{44}/a_0^{-6}	0.0120908784	0.1105230068	−0.0183163390
C_{45}/a_0^{-6}	−0.0011304861	−0.0169523064	0.0324410188
C_{46}/a_0^{-6}	−0.0191218740	−0.0269179141	0.0015208468
C_{47}/a_0^{-6}	0.0201236095	−0.0182798082	0.0006936851
C_{48}/a_0^{-6}	−0.0054523062	−0.0124714156	0.0040623792
C_{49}/a_0^{-6}	−0.0108391916	0.0076398845	0.0008196160
C_{50}/a_0^{-6}	−0.0024657372	−0.0073187637	−0.0164326558

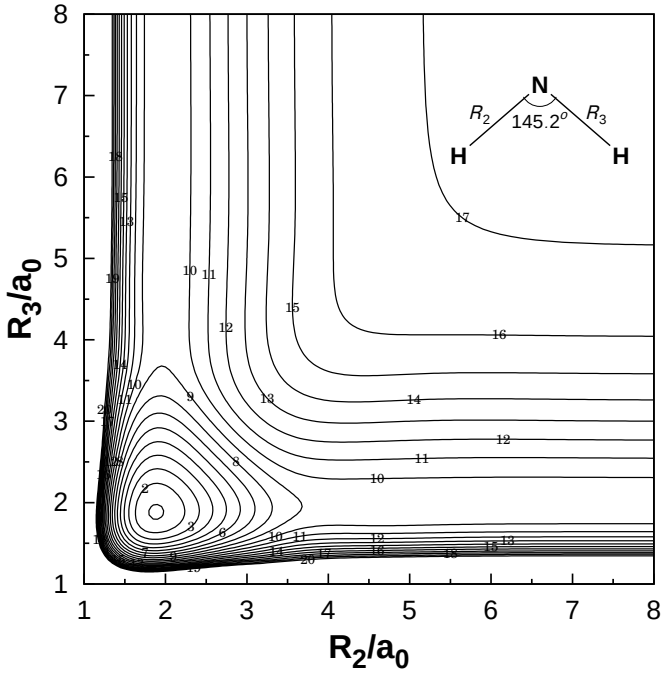

Figure 1. Contour plot for bond stretching in H-N-H, keeping the included angle fixed at 145.2^0. Contours are equally spaced by $0.02\,\mathrm{E_h}$, starting at $-0.325\,\mathrm{E_h}$. The energy zero is defined at the $\mathrm{N}(^2D) + \mathrm{H}(^2S) + \mathrm{H}(^2S)$ asymptote.

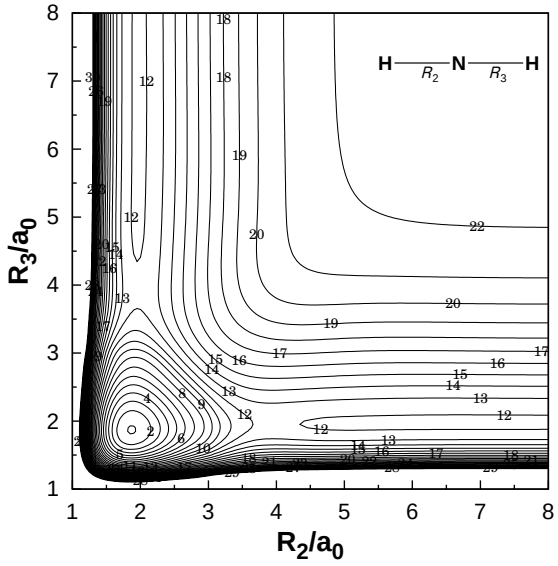

Figure 2. Contour plot for bond stretching in linear H-N-H configurations. Contours are equally spaced by $0.015\,\mathrm{E_h}$, starting at $-0.323\,\mathrm{E_h}$. The energy zero is defined at the $\mathrm{N}(^2D) + \mathrm{H}(^2S) + \mathrm{H}(^2S)$ asymptote.

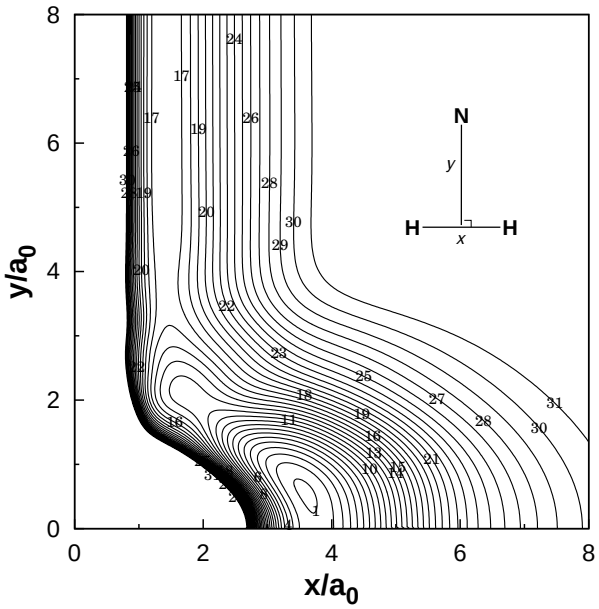

Figure 3. Contour plot for the C_{2v} insertion of the N atom into H_2. Contours are equally spaced by 0.01 Eh, starting at $-0.325\,\mathrm{E_h}$. The energy zero is defined at the $\mathrm{N}(^2D) + \mathrm{H}(^2S) + \mathrm{H}(^2S)$ asymptote.

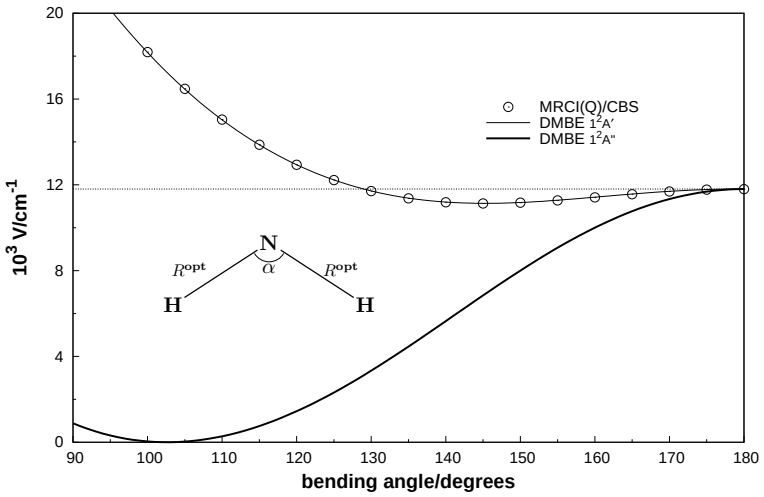

Figure 4. Optimized C_{2v} bending curve: circles, CBS/MRCI(Q)/AVXZ; dark solid line, DMBE $1\,^2A''$; thin solid line, DMBE/CBS $1\,^2A'$(this work).

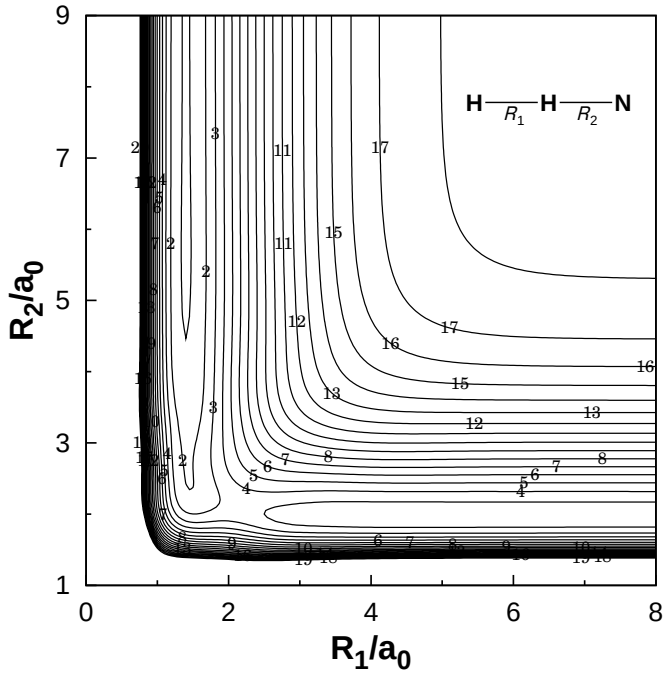

Figure 5. Contour plot for bond stretching in linear N-H-H configurations. Contours are equally spaced by $0.01\,\mathrm{E_h}$, starting at $-0.174\,\mathrm{E_h}$. The energy zero is defined at the $\mathrm{N}(^2D) + \mathrm{H}(^2S) + \mathrm{H}(^2S)$ asymptote.

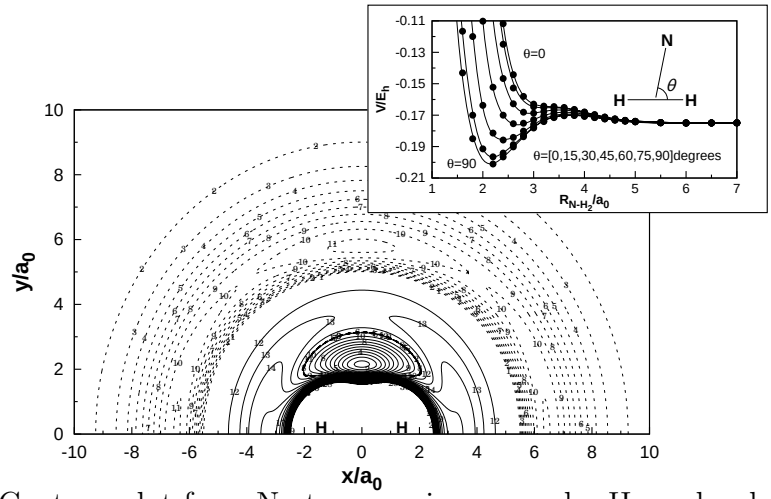

Figure 6. Contour plot for a N atom moving around a H_2 molecule fixed at the equilibrium geometry $R_1 = 1.401 a_0$ and lying along the X-axis with the center of the bond fixed at the origin. Contours are equally spaced by $0.0025\,E_h$, starting at $-0.20\,E_h$. Shown in dash are contours equally spaced by $-0.00005\,E_h$, starting at $-0.1744747\,E_h$. Shown in the inset are cuts along the atom-diatom radial coordinate for selected values of the Jacobi angle. The reference energy refers to $N(^2D) + H_2$.The energy zero is defined at the $N(^2D) + H(^2S) + H(^2S)$ asymptote.

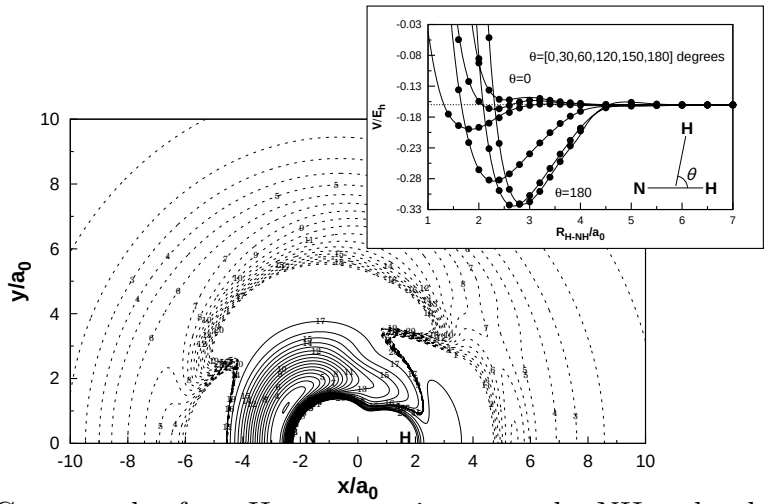

Figure 7. Contour plot for a H atom moving around a NH molecule fixed at the equilibrium geometry $R_{NH} = 1.974\,a_0$ and lying along the X-axis with the center of the bond fixed at the origin. Contours are equally spaced by $0.01\,E_h$, starting at $-0.3252\,E_h$. Shown in dash are contours equally spaced by $-0.00005\,E_h$, starting at $-0.16011\,E_h$. The inset shows reference along the atom-diatom radial coordinate for selected values of the Jacobi angle. The reference energy refers to $H + NH(a^1\Delta)$. The energy zero is defined at the $N(^2D) + H(^2S) + H(^2S)$ asymptote.

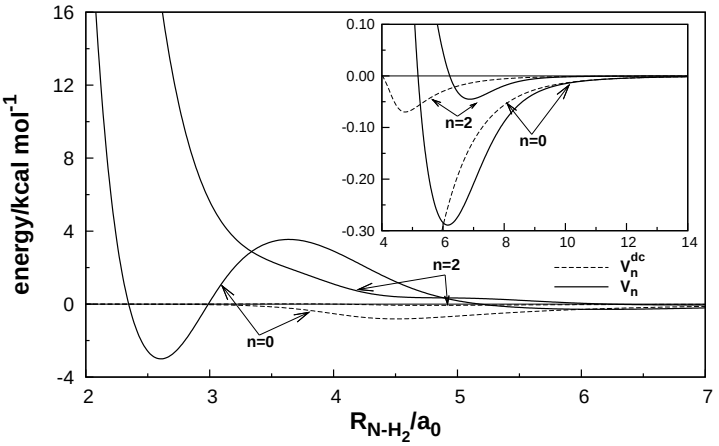

Figure 8. Isotropic (V_0) and leading anisotropic (V_2) components of the $N - H_2$ interaction potential, with the diatomic molecule fixed at the equilibrium geometry. *continuous line*, DMBE; *dashed line*, three-body dynamical correlation term (leading to asymptotic atom-diatom dispersion interaction at large distances) in Eq. (22). The axes in all panels have the same units.

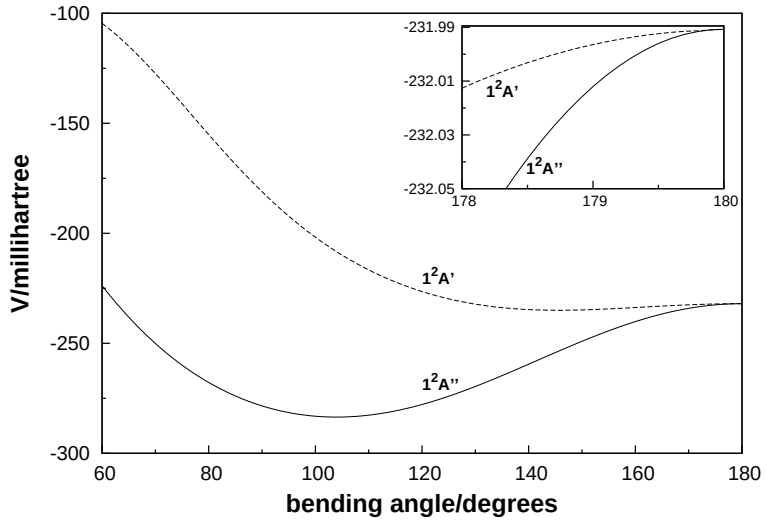

Figure 9. One-dimensional cuts of the PESs of $1\,^2A''$ and $1\,^2A'$ states of NH_2 along the bending angle with the bond lengths fixed at $1.8695\,a_0$. Show in the inset are the cuts of region with bending angle from 178 deg to 180 deg. The energy zero is defined at the $N(^4S) + H(^2S) + H(^2S)$ asymptote. One-dimensional cuts of the PESs of $1\,^2A''$ and $1\,^2A'$ states of NH_2 along the bending angle with the bond lengths fixed at $1.8695\,a_0$. Show in the inset are the cuts of region with bending angle from 178 deg to 180 deg. The energy zero is defined at the $N(^4S) + H(^2S) + H(^2S)$ asymptote.

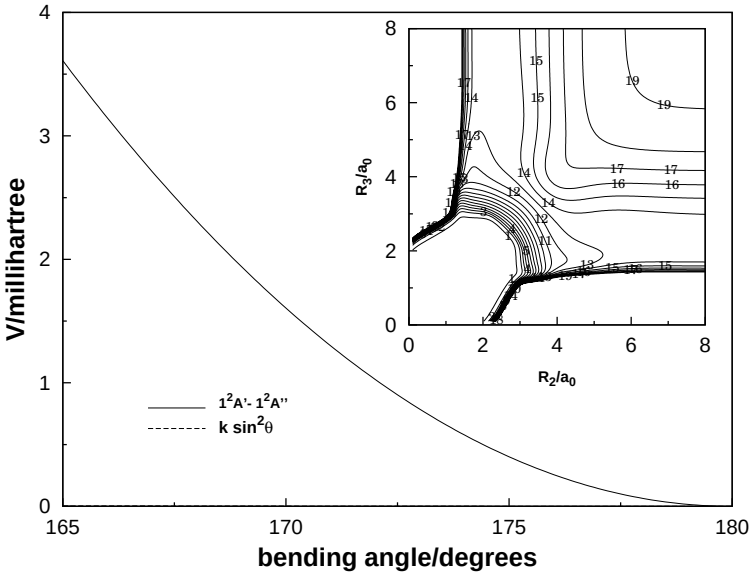

Figure 10. One-dimensional cuts of the PESs of $1\,^2A''$ and $1\,^2A'$ states of NH_2 along the bending length with the bond angle fixed at 180 deg and other bond length fixed at $1.965\,a_0$. Show in the inset are the cuts along the bending length with the bond angle fixed at 180 deg and the two bond lengths fixed same values. The energy zero is defined at the $N(^4S) + H(^2S) + H(^2S)$ asymptote.

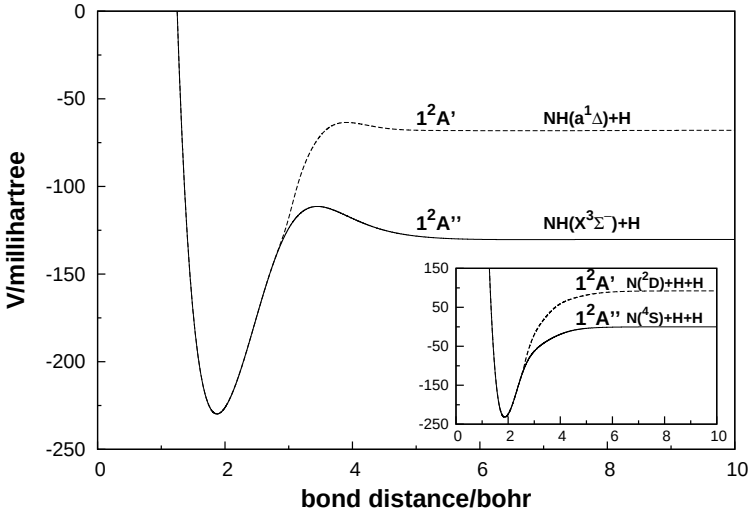

Figure 11. One-dimensional cut energy difference of the excited state $1\,^2A'$ and the ground state $1\,^2A''$ PESs along the bending angle with the bond lengths fixed at $1.8695\,a_0$. Shown in the inset is the energy difference between both PESs in linear H−N−H configurations. Contours are equally spaced by $0.005\,E_h$, starting at $0.001\,E_h$.

Chapter 5

DMBE-PES for ground state of the ammonia

J. Phys. Chem. A. **114**, 6669-6680 (2010).

Ab initio-based double many-body expansion potential energy surface for the electronic ground state of the ammonia molecule

Y. Q. Li and A.J.C. Varandas

Departamento de Química, Universidade de Coimbra
3004-535 Coimbra Codex, Portugal.

(Received: March 4, 2010; In final form: April 21, 2010)

Abstract

We report a single-sheeted global double many-body expansion potential energy surface for the ground electronic state of NH_3 that has been calibrated from newly calculated ab initio energies. It employs realistic double many-body expansion functions previously reported from accurate *ab initio* data for the triatomic fragments plus four-body energy terms that have been calibrated from multireference configuration calculations carried out in the present work for the title system using the full valence complete active space wave function as reference and a basis set of the correlation consistent type. The major attributes of the NH_3 double many-body expansion potential energy surface have also been characterized, and found to be in good agreement both with the calculated ones from the raw *ab initio* energies and theoretical results available in the literature. It can then be recommended both as a reliable functional form on which dynamics calculations can be performed and as a model for improvement that is open to refinement through further accurate *ab initio* calculations, vibrational calculations, or both.

1 Introduction

The availability of potential energy surfaces for small molecules is key for reaction dynamics and kinetics studies. Amongst the tetratomic systems, the potential energy surface (PES) of NH_3 [1–10] assumes special relevance because this species is a major constituent of some planetary atmospheres whose Boltzmann temperatures require for their determination an accurate knowledge of the ro-vibrational transition energies, and hence of its potential energy surface. Moreover, NH_3 is an important intermediate in atmospheric chemistry and combustion processes, and a prototype pyramidal molecule that provides a benchmark system for theoretical spectroscopic models. In particular, its complicated low-frequency large amplitude inversion motion makes it a challenge to understanding.

It is therefore not surprising that ammonia has been extensively studied [1], with related topics being MASER action [11], microwave and infrared spectroscopy [12–16], chirality [17],and time-dependent multidimensional quantum wave packet dynamics under coherent laser excitation [18]. Moreover, ammonia and its isotopomers have been interesting prototypical systems for the studying of photodissociation dynamics [8, 9, 19–21] and the role of atomic insertion versus molecular abstraction reactions [22, 23]. Having a relatively small number of electrons, NH_3 further allows calculations of its electronic structure with accurate ab initio methods and large basis sets, although being still too large to permit a dense exploration of its entire PES.

Recently, quite accurate experiments and calculations have been reported for the ammonia molecule. [1–4, 18, 24–29] Theoretically, representations of the PES have mostly utilized high-order Taylor expansions in the neighborhood of the equilibrium molecular structure, although some [1, 27] can describe large amplitude vibrations. Therefore, adiabatic representations of the PES reported thus far from ab initio calculations are either accurate but local or global but not sufficiently accurate to describe the complete set of experimental data. In particular, such adiabatic PESs often fail to show the correct behavior at all dissociation channels related to the global PES. An alternative to adiabatic representations is to have diabatic representations. [28, 29] Although these offer generally smoother features and hence may be easier to model than adiabatic ones, especially when

aiming at multisheeted forms, there are also cons associated with difficulties in defining proper dissociation limits (ref 30 and references therein). This situation prompted us to carry out electronic structure calculations extensively enough to cover the major features of the full six-dimensional ($6D$) configuration space of the ammonia molecule and to model globally the PES using double many-body expansion (DMBE) theory [31–33]. This approach has been successfully applied to a wealth of triatomic systems (including all ground-state triatomic fragments arising from dissociation of ammonia, namely NH_2 [34, 35], and H_3 [36]) as well as tetratomic (O_4 [37], HO_3 [38], and HSO_2 [39]) and N_2H_2 [40], and even larger polyatomic (HO_4 [41] and HO_5 [42]) systems, and can provide a physically motivated form to model accurate *ab initio* calculations in both at valence and and long-range interaction regions. Because single-valued DMBE PESs have been reported for the NH_2 and H_3 molecules, such a work has paved the way for obtaining a similar form for the larger NH_3 molecule by providing the involved two-body and three-body energy terms that arise in the cluster expansion of the molecular potential energy. In turn, $NH_3(1\,^1A_1)$ can serve as a building-block for the PESs of larger N_xH_y species such as those of relevance in the synthesis of ammonia, and hence the current study may to construct global DMBE forms for such polyatomic systems.

A final remark to note that proper dissociation at all asymptotes is warranted by employing a generalization of the Varandas-Poveda [34] switching function approach originally reported for triatomic species. As calibration data, 476 ab initio energies calculated at the multi-reference configuration interaction with the popular quasi-degenerate Davidson correction [MRCI(Q) [43, 44]] level have been utilized. Such calculations employed the full valence complete active space (FVCAS) wave function as reference, and the aug-cc-pVTZ (AVTZ) basis set of Dunning. [45, 46] We emphasize that the PES so obtained shows the correct long-range behavior at all dissociation channels while providing a realistic representation at all interatomic separations. The small number of required *ab initio* points is clearly an asset of DMBE theory (obviously of any cluster expansion [47]) by allowing the use of work previously done for the molecular fragments.Naturally, electronic structure calculations of higher accuracy are nowadays feasible for the title molecule, with the PES here reported then serving as a starter toward more

ambitious and expensive endeavors along such a direction. Of course, if combined with vibrational calculations, it may also serve as an *ab initio* 6D model that may afford sufficiently flexibility to fit available spectroscopic data, much on line with what has be done in the past with triatomic potentials [48–53].

The paper is organized as follows. Section 2 describes the results of new ab initio calculations carried out for NH_3, while the DMBE methodology is discussed and applied in Section 3 by focusing on the title system. The characterization of the novel DMBE PES is then presented in Section 4. Section 5 gathers the major conclusions.

2 Ab initio calculations

All *ab initio* calulations have been carried out at the MRCI(Q) [43, 44]level using the FVCAS [43] wave function as reference. The AVTZ atomic basis set of Dunning [45, 46] has been employed, and the calculations carried out using the Molpro [54] package. The most important regions of the PES for spectroscopic studies are the two symmetry equivalent global minima (C_{3v}) and the region around the saddle point (D_{3h}) for the umbrella motion. However, because the aim is to obtain a fully six-dimensional PES, there is the need to consider also the description of the PES away from such regions. A total of 476 *ab initio* points has been calculated, of which 205 concentrated in the region of the two equivalent C_{3v} minima and D_{3h} saddle point for the umbrella motion that connects them. The remainder 271 *ab initio* points have been necessary to remove an unphysical minimum that occurs in the absence of the four-body energy correction, and to refine the entrance barrier associated to the $H + NH_2$ channel. Since one seeks a reliable description of the inversion barrier, the above 205 raw *ab initio* energies there located have been carried out using state averaging of the two lowest states of the same symmetry. All others that have been employed to model the V_S and V_L contributions that will be discussed later (see section 3.4) have been generated at the cheaper single state level. Note that the dissociation limit of $H + NH_2$ has been calculated by keeping NH_2 frozen at the geometry reported in Ref. 34 while moving away the hydrogen atom. Similarly, the dissociation energy of $N + H_3$ has been calculated by keeping H_3 frozen at its optimum FVCAS/AVTZ collinear ge-

ometry (the well established saddle point in $3D$) while moving away the nitrogen atom, and so on (see Table 5).

3 Single-sheeted DMBE potential energy surface

Within the framework of DMBE theory as applied to four-atom systems [38, 39], a single-sheeted PES for ground state NH_3 (labelled ABCD in the following) is written as

$$V_{NH_3}(\mathbf{R}) = \sum_{i=1}^{4} V^{(i)}(\mathbf{R}) \tag{1}$$

where $\mathbf{R}$ is the vector of the six internuclear coordinates $[R_j\,(j = 1, \ldots, 6)]$, $V^{(1)} = V^{(1b)}_{N(^2D)} f^{(4)}(R)$ is a (pseudo-) one-body term, $V^{(4)}_{N(^2D)}$ represents the energy difference between the ^2D and ^4S states of atomic nitrogen: $V^{(1b)}_{N(^2D)} = 0.091225\,E_h$. In turn, $f^{(4)}(R)$ is a $6D$ switching function, and $V^{(2)}$, $V^{(3)}$ and $V^{(4)}$ are two-body, three-body, and four-body terms in the cluster expansion of the molecular potential energy. The details of the analytical forms employed to represent the various n-body energy terms that are involved will be given in the following subsections.

3.1 Two-body energy terms

The potential energy curves for the two-body fragments are based on the extended Hartree-Fock approximate correlation energy method for diatomic molecules including the united atom limit [55] (EHFACE2U)which show the correct behavior at both asymptotic limits $R \to 0$ and $R \to \infty$. For the j-th diatomic, it assumes the form

$$V^{(2)}(R_j) = V^{(2)}_{EHF}(R_j) + V^{(2)}_{dc}(R_j) \tag{2}$$

where $V^{(2)}_{EHF}$, $V^{(2)}_{dc}$ are two-body terms of the extended Hartree-Fock and dynamical correlation types, respectively; Eq. (2) applies to all six diatomic fragments. The two-body extended Hartree-Fock energy term $V^{(2)}_{EHF}$ is written as

$$V^{(2)}_{EHF}(R) = -\frac{D}{R}\left(1 + \sum_{i=1}^{n} \alpha_i r^i\right) \exp(-\gamma r) + \chi_{exc}(R) V^{asym}_{exc}(R) \tag{3}$$

where

$$\gamma = \gamma_0[1 + \gamma_1 \tanh(\gamma_2 r)] \tag{4}$$

and

$$V_{\rm exc}^{\rm asym}(R) = -\widetilde{A}R^{\widetilde{\alpha}}(1 + \widetilde{\alpha}_1 R + \widetilde{\alpha}_2 R^2)\exp(-\widetilde{\gamma}R) \tag{5}$$

is the asymptotic exchange energy, and $\chi_{exc}(R)$ is a convenient damping function that accounts for charge overlap effects, r denotes the displacement coordinate relative to equilibrium geometry of the diatomic, $r = R - R_e$. In turn, the two-body dynamical correlation energy term $V_{\rm dc}^{(2)}$ is written as

$$V_{\rm dc}^{(2)}(R) = -\sum_{i=6,8,10} C_n \chi_n(R) R^{-n} \tag{6}$$

where

$$\chi_n(R) = \left[1 - \exp\left(-A_n \frac{R}{\rho} - B_n \frac{R^2}{\rho^2}\right)\right]^n \tag{7}$$

is a charge-overlap dispersion damping function. Moreover, $A_n = \alpha_0 n^{-\alpha_1}$ and $B_n = \beta_0 \exp(-\beta_1 n)$ are auxiliary functions [31, 56] ; $\alpha_0 = 16.36606$, $\alpha_1 = 0.70172$, $\beta_0 = 17.19338$, and $\beta_1 = 0.09574$. for a given pair of atoms (say, XY), $\rho = 5.5 + 1.25(\langle r_X^2 \rangle^{1/2} + \langle r_Y^2 \rangle^{1/2})$ is a scaling parameter. Finally, the coefficients appearing in Eqs. (2)-(7) are chosen such as to reproduce available theoretical (and experimental, although this will not be done here) data in diatomic as described elsewhere [31, 55]. In this work, we employ the accurate EHFACE2U potential energy curve of ground state $H_2(X^1\Sigma_g^+)$ reported in Ref. 48, and the curve of ground-state imidogen, $NH(X^3\Sigma^-)$, reported in Ref. 57. As shown in Figure 2 of Ref. 34, both potential curves mimic accurately the calculated *ab initio* energies.

3.2 Three-body energy terms

The three-body energy is written as

$$V^{(3)}(\mathbf{R}) = \sum_{i=1}^{4} [V_{\rm EHF}^{(3)}(\mathbf{R}^3) + V_{\rm dc}^{(3)}(\mathbf{R}^3)] \tag{8}$$

where $V_{\rm EHF}^{(3)}$, $V_{\rm dc}^{(3)}$ are the three-body terms of extended Hartree-Fock and dynamical correlation energy, respectively; $\mathbf{R}^3$ specifies the set of the three interatomic distances referring to each triatomic fragment.

The three-body energy terms employed in Eq. (8) have been taken from Ref. 34 and 36 for NH_2 and H_3, respectively. In turn, the three-body dynamical correlation of NH_2 is modeled by the form [48]

$$V^{(3)}_{\mathrm{dc-NH_2}} = -\sum_i \sum_n f_i(R) C^{(i)}_n(R_i, \theta_i) \chi_n(r_i) r_i^{-n} \tag{9}$$

where r_i, θ_i and R_i are the Jacobi coordinates corresponding to a specific geometry of the triatomic and $f_i = \frac{1}{2}\{1 - \tanh[\xi(\eta R_i - R_j - R_k)]\}$ is a convenient switching function. Following recent work on NH_2 [34], we have fixed $\eta = 6$, $\xi = 1.0 a_0^{-1}$ and $\rho = 16.125 a_0$. Regarding, the damping function $\chi_n(r_i)$, we still adopt Eq. (7) but replace R by the center-of-mass separation for relevant atom-diatom channel of NH_2. The atom-diatom dispersion coefficients in Eq. (9) assume their usual form

$$C^{(i)}_n(R_i) = \sum_L C^L_n(R) P_L(\cos\theta_i) \tag{10}$$

where $P_L(\cos\theta_i)$ denotes the L-th Legendre polynomial. The expansion in Eq. (9) has been truncated by considering only the coefficients C^0_6, C^2_6, C^0_8, C^2_8, C^4_8 and C^0_{10}. As noted elsewhere, [48] Eq. (9) causes an overestimation of the dynamical correlation energy at the atom-diatom dissociation channels. To correct such a behavior, we have multiplied the two-body dynamical correlation for the i-th pair by $\prod_{j\neq i}(1 - f_j)$. This ensures [34, 48, 52] that the only two-body contribution at the i-th channel belongs to the JK atom-pair (in an obvious notation IJK is any triatomic formed from atoms A to D).

The three-body extended Hartree-Fork energy for the NH_2 fragments has been modeled via a three-body distributed-polynomial [34, 58] form

$$V^{(3)}_{\mathrm{EHF-NH_2}} = \sum_{j=1}^{5} \left\{ P^{(j)}(Q_1, Q_2, Q_3) \prod_{i=1}^{3} \left\{ 1 - \tanh[\gamma^{(j)}_i (R_i - R^{(j),\mathrm{ref}}_i)] \right\} \right\} \tag{11}$$

where all the polynomials $P^{(j)}(Q_1, Q_2, Q_3)$ are written in terms of symmetry coordinates, $\gamma^{(j)}_i$ is a nonlinear range-determining parameter, and $R^{(j),\mathrm{ref}}_i$ a reference geometry.

Following earlier work [36] , the three body dynamical correlation of H_3 as-

sumes the form

$$V^{(3)}_{\mathrm{dc-H_3}} = \sum_{i=1}^{3}\sum_{n=6,8,10} C_n\{1-\frac{1}{2}[\mathrm{g}_n\left(R_{i+1(\mathrm{mod}\,3)}\right)h_n\left(R_{i+2(\mathrm{mod}\,3)}\right) + \mathrm{g}_n\left(R_{i+2(\mathrm{mod}\,3)}\right)h_n\left(R_{i+1(\mathrm{mod}\,3)}\right)]R_i^{-n}\} \quad (12)$$

where

$$g_n(R) = 1 + k_n \exp[-k_n^{'}(R - R_m)] \quad (13)$$

and

$$h_n(R) = [\tanh(k_n^{'})R]^{\eta^{'}} \quad (14)$$

The constants $k_n^{'}$ and $\eta^{'}$ control the rate of decay of the g_n and h_n functions, and these constants and the k_n are determined, for a given $\eta^{'}$, by the requirement that the model reproduces the $\mathrm{H-H_2}$ dispersion coefficients [59] $C_n^{\mathrm{H-H_2}}$ at r_e for $n = 6$, 8, and 10.

Note that the Eq. (9) and (12) represent dynamical correlation terms for different three-body interaction fragments. Specifically, Eq. (9) account for $\mathrm{N-H_2}$ and $\mathrm{H-NH}$ long range energies whereas the the Eq. (12) describe the $\mathrm{H-H_2}$ dissociation channels. As noted in Ref. 39, due to an overestimation of the dynamical correlation energy, each $V^{(2)}_{\mathrm{dc}}(R_i)$ term in the DMBE PES of NH_2 has been multiplied by a switching function $\prod_{j\neq i}(1-f_j)$ for the i-th pair [34], which transforms such contributions into three-body-like ones. Thus, an extra three-body energy term should be added to Eq. (8). Taking into account the properties of the switching function $\prod_{j\neq i}(1-f_j)$, such an additional term should be written as follows:

$$V^{(3)}_{\mathrm{add}} = \sum_{1}^{12} V^{(2)}_{\mathrm{dc}}(R_i)(\prod_{j\neq i}(1-f_j) - 1) \quad (15)$$

which, when taken into account, reproduces all the asymptotic limits of the tetratomic PES (*i.e.*, if one of the atoms is placed far away from the remaining triatomic, the resulting PES matches exactly that of the triatomic fragment. As shown in Figure 14, the resulting PES matches exactly that of the NH_2 DMBE PES when one of the H atoms is placed far away from the remaining NH_2). We should also note that the diatomic potential (H_2) originally employed in the H_3

DMBE PES which has been constructed using an earlier formalism somewhat simpler than that used for NH_2 DMBE PES. For consistency, we have replaced it by corresponding updated diatomic curves [34, 48], which has been used for NH_2 DMBE PES. As shown in Table 5, The dissociation energy at the $N(^2D)+H_3(^2A')$ limit is $-0.0680\,E_h$, If one then removes from this amount the energy difference between the ^2D and ^4S states of atomic nitrogen, we predict the energy of $H_3(^2A')$ at reference geometries to be $-0.1592\,E_h$, which in good agreement with the one of $-0.1591\,E_h$ that we have calculated using the original form. Thus, the update does not affect significantly the attributes of the H_3 PES in comparison with its original form.

Finally, the three-body extended Hartree-Fork energy of H_3 is written by the form [36]

$$V^{(3)}_{\mathrm{EHF}-\mathrm{H_3}} = s^2(1 + s^3 cos(3\phi))(b_{61} + b_{62}q)\exp[-b^2_{63}(q - q_0)^2] \qquad (16)$$

where q, s and ϕ are defined in Eqs. (4), (40) and (41) of Ref. 36, respectively. Finally, the parameters appearing in Eqs. (8)-(16) have been taken from Refs. 34 and 36 for NH_2 and H_3, respectively; for clarity, the notations of such equations has been kept unchanged, with the reader being referred to the original papers for the numerical values of the coefficients.

3.3 The switching function

The use of switching function to approximate the multivalued nature of a PES (*i.e.*, to replace a crossing by an avoided crossing, and hence allow proper dissociation with a single-sheeted form) has first been proposed by Murrell and Carter [60], who applied the formalism in the construction of an approximate PES for the ground state of H_2O. However, as noted in their paper, their switching function cannot reach a unique value at the three-atom limit. To solve this inconsistency and get a smooth three-body energy term, Varandas and Poveda [34] proposed an improved switching-function formalism and applied it successfully to the ground-state of NH_2. A similar situation holds for the title system, where

the following dissociation scheme applies:

$$\begin{aligned} NH_3(^1A_1) &\rightarrow H_2(X^1\Sigma_g^+) + N(^2D) + H(^2S) && (17)\\ &\rightarrow NH(X^3\Sigma^-) + H(^2S) + H(^2S) && (18)\\ &\rightarrow NH(a^1\Delta) + H_2(X^1\Sigma_g^+) && (19)\\ &\rightarrow NH_2(1^2A'') + H(^2S) && (20)\\ &\rightarrow N(^2D) + H_3(^2A') && (21) \end{aligned}$$

Since $NH(X^3\Sigma^-)$ dissociates to ground-state atoms, it will be necessary to introduce a switching function that removes the $N(^2D)$ state from the channel as $NH(X^3\Sigma^-)$ dissociates to nitrogen and hydrogen atoms in their ground electronic states, respectively $N(^4S)$ and $H(^2S)$. By comparing the PES that is obtained by using only two-body and three-body terms with the *ab initio* calculations here carried out, we have established the major changes to warrant the proper dissociation limits. This was followed by modeling a convenient switching function that could also ensure the proper atom-permutational symmetry. Although not unique (for a similar extension that has been found convenient for the N_2H_2 molecule, see Ref. 40), of course, a form that satisfies such criteria is

$$f^{(4)}(\mathbf{R}) = \sum_{\alpha\beta\gamma} h(R_{\alpha\beta}) g(R_{A-\alpha\beta}) k(R_{A\gamma}) \tag{22}$$

where

$$h(R_{\alpha\beta}) = \frac{1}{4}\sum_{i=1}^{2}\left\{1 - \tanh[\alpha_i(R_{\alpha\beta} - R_{\alpha\beta}^{i0}) + \beta_i(R_{\alpha\beta} - R_{\alpha\beta}^{i1})^3]\right\} \tag{23}$$

$$g(R_{A-\alpha\beta}) = \frac{1}{2}\left\{1 + \tanh[\alpha_0(R_{A-\alpha\beta} - R_{A-\alpha\beta}^0)]\right\} \tag{24}$$

$$k(R_{A\gamma}) = \gamma_0 + \frac{(1-\gamma_0)}{2}\left\{1 + \tanh[\gamma_1(R_{A\gamma} - R_{A\gamma}^0)]\right\} \tag{25}$$

with $R_{\alpha\beta}$ representing the $H-H$ distance, $R_{A-\alpha\beta}$ the distance of the N atom to the center of mass of reference H_2, $R_{A\gamma}$ the distance of the N atom to another H atom, and A and $(\alpha\beta\gamma)$ stand for the nitrogen and hydrogen atoms. Thus, $h(R_{\alpha\beta})$ in Eq. (23) will allow the $N(^2D)$ state to appear in the $H_2(X^1\Sigma_g^+)+N(^2D)+H(^2S)$ channel while being absent in the $NH(X^3\Sigma^-)+H(^2S)+H(^2S)$ one (see the panel

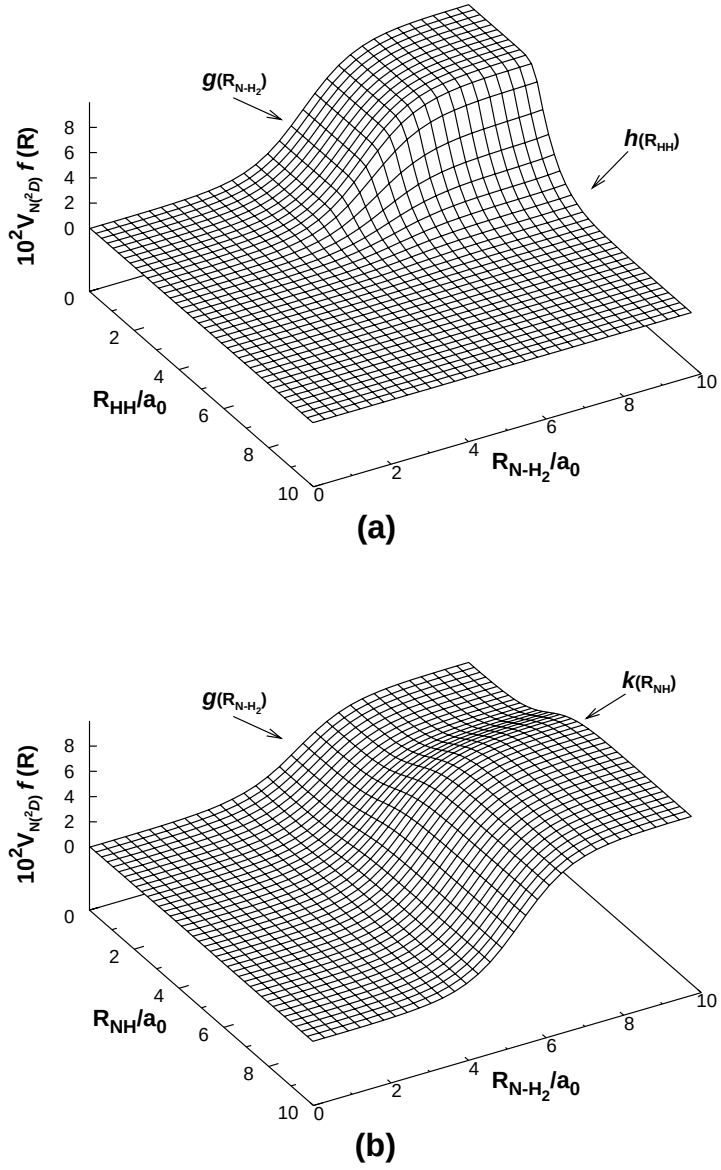

Figure 1. Switching function used to model the single-sheeted NH_3 DMBE PES. Where $R_{NH} = 20\,a_0$ in panel (a) and $R_{HH} = 1.401\,a_0$ in panel (b).

(a) of Fig. 1). Note that α_i and β_i (i=1,2) are parameters to be obtained as described elsewhere [34], while the values of the $R^{i0}_{\alpha\beta}$ and $R^{i1}_{\alpha\beta}$ are chosen from the requirement that the PES have the correct energy dissociation limit at $N(^2D) + H_3(^2A')$ asymptote. Similarly, the value of the γ_0 in Eq. (25) is chosen from the requirement that the PES displays the correct energy dissociation limit at the $NH(a^1\Delta) + H_2(X^1\Sigma_g^+)$ asymptote (see the panel (b) of Fig.1). Taking into

account the conform between the four-atom and threeatom cases, we adopt to represent the final one-body term $V^{(1)}(\mathbf{R})$ the following generalized form

$$V^{(1)}(\mathbf{R}) = V^{(1b)}_{\mathrm{N}(^2D)} f^{(4)}(\mathbf{R})[1 - f(\mathbf{R})] + V^{(1a)}_{\mathrm{N}(^2D)} f^{(3)}(\mathbf{R}) f(\mathbf{R}) \tag{26}$$

with $V^{(1a)}_{\mathrm{N}(^2D)} f^{(3)}(\mathbf{R})$ represents the one-body term of $NH_2(^2A'')$, and $f(\mathbf{R})$ is a function of the internuclear coordinates that varies smoothly between 0 and 1 in such a way that $V^{(1b)}_{\mathrm{N}(^2D)} f^{(4)}(\mathbf{R})$ and $V^{(1a)}_{\mathrm{N}(^2D)} f^{(3)}(\mathbf{R})$ switched on/off conveniently in different regions of the configuration space. An appropriate function that describes approximately the desired behavior is

$$f(\mathbf{R}) = \prod_{i=1,2,4} \frac{1}{2} \left\{1 - \tanh[\alpha(R_i - R_0^{\mathrm{f}}]\right\} \prod_{j=3,5,6} \frac{1}{2} \left\{1 + \tanh[\alpha(R_j - R_0^{\mathrm{f}}]\right\} \tag{27}$$

where $\alpha = 1.0$ and $R_0^{\mathrm{f}} = 12\, a_0$. Note that the summation in Eq. (22), Eq. (26) and Eq. (27) run over the three terms to the ABCD, ACDB, and ADBC species, such as to keep the correct permutational symmetry on the H atoms. Finally, to get a smooth four-body energy term, the coefficients α_0, $R^0_{A-\alpha\beta}$ in Eq. (24) and γ_1, $R^0_{A\gamma}$ in Eq. (25) have been calculated using a trial-and-error procedure. The numerical values of all parameters in Eq. (22) are collected in Table 3. As a check to the switching function, we have calculated the energy dissociation limits by using $V^{(1)}$, $V^{(2)}$ and $V^{(3)}$ (hereafter referred to as DMBE_{1+2+3} PES) and our own *ab initio* calculations. As seen from Table 5, the switching function imposes the correct behavior at every dissociation channel while providing a realistic representation at all interatomic separations.

3.4 Four-body energy term

As a first step toward the four-body energy term $V^{(4)}$, we have examined in detail all the features predicted by the PES when truncated at the $V^{(1)} + V^{(2)} + V^{(3)}$ level. As already noted in the previous section, this DMBE_{1+2+3} PES shows the correct behavior while providing a fair representation at all interatomic separations. Thus, it has been found to qualitatively describe the NH_3 PES. By comparing the DMBE_{1+2+3} surface with our own *ab initio* calculations, we have established the major differences that ought to be corrected by adding four-body

energy terms. We have found convenient the following correction:

$$V^{(4)} = \sum_{i=1}^{4} V_{Si}^{(4)} + \sum_{l=1}^{3} V_{l}^{(4)} + P^{(4)}T^{(4)} \tag{28}$$

where $V_{Si}^{(4)}$ is a Gaussian-type function

$$\begin{aligned} V_{Si}^{(4)} = & \sum_{\alpha\beta\gamma} \big\{ d_i[1 + a_{i1}(R_{A\alpha} - R_{A\alpha}^{i0}) + a_{i2}(R_{A\alpha} - R_{A\alpha}^{i0})^2 + a_{i3}(R_{A\alpha} - R_{A\alpha}^{i0})^3] \\ & \exp[-b_{i1}(R_{A\alpha} - R_{A\alpha}^{i0})] exp[-b_{i2}(R_{A\alpha} - R_{A\alpha}^{i0})^2] \big\} T_{\alpha\beta\gamma}^{(i)} \end{aligned} \tag{29}$$

the $T_{\alpha\beta\gamma}^{(i)}$ in Eg. (29) is the range function defined by

$$\begin{aligned} T_{\alpha\beta\gamma}^{(1)} = & \exp[-\gamma_{11}(2R_{A\alpha} - R_{A\beta} - R_{A\gamma})^2] \\ & \exp\big\{ -\gamma_{12}[(R_{\alpha\beta} - R_{\alpha\beta}^0)^2 + (R_{\alpha\gamma} - R_{\alpha\gamma}^0)^2 + (R_{\beta\gamma} - R_{\beta\gamma}^0)^2] \big\} \end{aligned} \tag{30}$$

$$\begin{aligned} T_{\alpha\beta\gamma}^{(2)} = & \exp[-\gamma_{21}(R_{A\beta} - R_{A\gamma})^2] \\ & \exp\big\{ -\gamma_{22}[(R_{\alpha\beta} - R_{\alpha\beta}^0)^2 + (R_{\alpha\gamma} - R_{\alpha\gamma}^0)^2 + (R_{\beta\gamma} - R_{\beta\gamma}^0)^2] \big\} \end{aligned} \tag{31}$$

$$\begin{aligned} T_{\alpha\beta\gamma}^{(3)} = & \exp[-\gamma_{31}(R_{A\beta}^2 - R_{A\alpha}^2 - R_{\beta\gamma}^2 + R_{A\alpha}R_{\beta\gamma})^2] \\ & \exp[-\gamma_{31}(R_{A\beta}^2 - R_{A\alpha}^2 - R_{\beta\gamma}^2 - R_{A\alpha}R_{\beta\gamma})^2] \\ & \exp\big\{ -\gamma_{32}[(R_{\alpha\beta} - R_{\alpha\beta}^0)^2 + (R_{\alpha\gamma} - R_{\alpha\gamma}^0)^2 + (R_{\beta\gamma} - R_{\beta\gamma}^0)^2] \big\} \end{aligned} \tag{32}$$

$$\begin{aligned} T_{\alpha\beta\gamma}^{(4)} = & \exp[-2(R_{\alpha\beta} - R_{\alpha\gamma})^2 - 2(R_{A\beta} - R_{A\gamma})^2] exp[-\gamma_{41}(R_{\beta\gamma} - R_{\beta\gamma}^{0'})^2] \\ & \exp\big\{ -\gamma_{42}[(R_{A\beta} - R_{A\beta}^0)^2 - (R_{A\gamma} - R_{A\gamma}^0)^2] \big\} \end{aligned} \tag{33}$$

In turn, $V_{S1}^{(4)}$, $V_{S2}^{(4)}$ and $V_{S3}^{(4)}$ have been chosen to correct the energy at the $N + H_3$ channel, with the parameters in $V_{S1}^{(4)}$, $V_{S2}^{(4)}$ and $V_{S3}^{(4)}$ calibrated by fitting *ab initio* points that cover the regions that the dissociation process $NH_3 \rightarrow N + H_3$. In turn, $V_{S4}^{(4)}$ is rather localized, and hence chosen to remove a small unphysical minimum that occurred in the $H + N + H_2$ channel, while the parameters of $V_{S4}^{(4)}$ were fitted to *ab initio* points in the vicinity of the corresponding geometry. In turn, the terms $V_l^{(4)}$ that appear in Eq. (28) are local Gaussian functions defined by

$$V_1^{(4)} = \sum_{\alpha\beta\gamma} \sum_{j=1}^{6} C_1 \exp[-\gamma_{51}(R_j - R_j^0)^2] \tag{34}$$

Table 1. Stationary points (in Å and degrees) and harmonic frequencies (in cm^{-1}) computed using different methods and available experimental results. Uncertainties are given in parentheses where applicable.

Symmetry	method	R_{NH}	θ_{HNH}	ω_1	ω_2	ω_3	ω_4
C_{3v}	Global PES[a]	1.0155	105.85	3482	1039	3569	1500
	Dense-grid[a]	1.0160	105.95	3747	1025	3892	1821
	B97-1/TZ2P [62]	1.0138	106.49	3485	1066	3606	1677
	CCSD(T)/ccVTZP [6]	1.0141	105.64	3471.9	1109.2	3597.5	1687.9
	CCSD(T)/ccVQZP [6]	1.0124	106.18	3480.5	1084.1	3608.8	1679.6
	QCISD(T)/[5s4p2dlf,3s2p]+core [6]	1.0132	106.6	3486	1075	3616	1684
	MP4/6-31G** [67]	1.035	105.9	3546.2	1140.8	3687.3	1733.19
	CISDTQ/DZP [68]	1.0173	106.3	3528	1121	3676	1706
	Hoy et al. [69]	1.025	107	3503	1030	3591.6	1689.9
	Duncan and Mills [70]	1.0116	106.7	3504	1022	3577	1691
	Coy and Lehmann [71]			3485(11)		3624(12)	1678(6)
	Lehmann and Coy [72]			3478(12)		3597(8)	1684(8)
D_{3h}	Global PES[a]	0.9983	120.0	3704	870i	3845	1572
	Dense-grid[a]	0.9983	120.0	3636	868i	3779	1561
	B97-1/TZ2P [62]	0.9971	120.0	3637	822i	3835	1577
	MC-QDPT [64]	0.998	120.0	3252	903i	3523	1596
	CCSD(T)/cc-pVDZ [10]	1.0051	120.0				
	CCSD(T)/aug-cc-pVDZ [10]	1.0054	120.0				
	CEPA-1/[9s6p4d2f/5s3p] [73]	0.9940	120.0				

[a]This work.

Table 2. Inversion energy (in cm^{-1}) of ammonia computed using different methods and available experimental results.

method	$\Delta E_{inv}(cm^{-1})$	$E_{min}(E_h)$	$E_{TS}(E_h)$
PES			
Global PES[a]	2033.5	−0.4660	−0.4567
Dense-grid[a]	2029.4	−0.4660	−0.4567
DFT [65]	2013.5		
B97-1/TZ2P [62]	1820		
ab initio			
Focal-point scheme [3]	2021		
CCSD(T)/aug-cc-pVDZ [10]	2033.4		
CCSD(T)/aug-cc-pVTZ [10]	1936.5		
CCSD(T)/aug-cc-pVQZ [10]	1866.9		
CCSD(T)/cc-pVDZ [10]	3104.5		
CCSD(T)/cc-pVTZ [10]	2237.9		
CCSD(T)/cc-pVQZ [10]	2025.6		
Experiment			
Swalen and Ibers [66]	2018		
Špirko and Kraemer. [13]	1885		
Špirko. [12]	1834		

[a]This work.

Table 3. Parameters in the switching function of Eq. (22).

Parameter	numerical value
α_1	0.718244
α_2	0.719351
β_1	0.493967
β_2	0.066742
$R^{10}_{\alpha\beta}$	3.17557
$R^{11}_{\alpha\beta}$	5.11353
$R^{20}_{\alpha\beta}$	4.19386
$R^{21}_{\alpha\beta}$	6.27869
α_0	0.75
$R^0_{A-\alpha\beta}$	5.35
γ_0	0.6478
γ_1	0.8
$R^0_{A\gamma}$	3.6

Table 4. Geometries(in a_0 and degree) and harmonic frequencies(in cm^{-1}) for $NH\cdots H_2$ transition state(TS), calculated from full DMBE PES, where ΔE (in kcal mol^{-1}) denotes the energy difference relative to the $NH+H_2$ asymptote.

	R_{NH_a}	R_{NH_b}	R_{NH_c}	$R_{H_bH_c}$	$R_{H_aH_b}$	$R_{H_aH_c}$	ΔE	**Frequencies**
$NH\cdots H_2$	1.983	4.860	4.860	1.405	5.361	5.361	13.1	$657i$ 3219 330 222 4257 914
$NH+H_2$	1.9565			1.401			0.0	

$$V_2^{(4)} = \sum_{\alpha\beta\gamma} \sum_{j=1}^{6} C_2 \exp[-\gamma_{61}(R_j - R_{j'}^0)^2] \exp[-\gamma_{62}(|cos\phi| - 1)] \tag{35}$$

$$V_3^{(4)} = \sum_{\alpha\beta\gamma} \big\{ G_1 G_2 G_3 C_2 \exp[-2(R_{\alpha\beta} - R_{\alpha\gamma})^2 - 2(R_{A\beta} - R_{A\gamma})^2] \exp[-\gamma_{71}(R_{A\alpha} - R_{A\alpha}^{50})] \big\} \tag{36}$$

where

$$G_1 = \frac{1}{2}\big\{1 + \tanh\big\{\alpha_1'[\frac{1}{4}(R_{A\beta} + R_{A\gamma})^2 - (\frac{1}{4}R_{\beta\gamma})^2 - R_1']\big\}\big\} \tag{37}$$

$$G_2 = \frac{1}{2}\big\{1 - \tanh[\alpha_2'(R_{\beta\gamma} - R_2')]\big\} \tag{38}$$

$$G_3 = \frac{1}{2}\big\{1 + \tanh[\alpha_3'(R_{\beta\gamma} - R_3')]\big\} \tag{39}$$

Moreover, $V_1^{(4)}$ and $V_2^{(4)}$ have been chosen to refine the entrance barrier of $H+NH_2$ channel, $V_3^{(4)}$ is rather localized and chosen to remove the unphysical minimum in NH + H + H channel, and the parameters of $V_l^{(4)}$ were chosen from a fit to the *ab initio* points in the vicinity of the corresponding geometry. In summary, the addition of such local terms $V_l^{(4)}$ has been found necessary particularly to eliminate spurious unphysical minima during the fitting procedure. Table 6 gathers the parameter values in Eqs. (28)-(39). Recall that A and $(\alpha\beta\gamma)$ stand for the nitrogen and hydrogen atoms, and note that the summation in $V_{Si}^{(4)}$ and $V_l^{(4)}$ runs over the three equivalent terms (ABCD, ACDB, ADBC) such as to keep the correct permutational symmetry on the H atoms. Note further that $T^{(4)}$ in Eg. (28) is a range-determining factor chosen to be of the Gaussian type [39]

$$T^{(4)} = \sum_{\alpha} exp\big\{ - [g_{\rm NH}(R_{A\alpha} - R_{\rm NH}^{\rm ref})^2 + g_{\rm HH}(R_{\alpha\beta} - R_{\rm HH}^{\rm ref})^2]\big\} \tag{40}$$

where $P^{(4)}$ is a fourth-order polynomial written as [61]

$$P^{(4)} = \sum_{i,j,k_p} a_{i,j,k_p} S_1^i S_4^j \prod_{p=1}^{8} t_p^{k_p} \tag{41}$$

with S_1, S_4 and

$$t_p = \left\{ S_2^2 + S_3^2, S_5^2 + S_6^2, S_2 S_5 + S_3 S_6, S_3^3 - 3 S_3 S_2^2, S_6^3 - 3 S_6 S_5^2, S_6(S_3^2 - S_2^2) \right.$$
$$\left. -2 S_2 S_3 S_5, S_3(S_6^2 - S_5^2) - 2 S_2 S_5 S_6, (S_3 + S_6)^3 - 3(S_3 + S_6)(S_2 + S_5)^2 \right\} \tag{42}$$

being 10 totally symmetric integrity functions [38, 61], which are invariant under permutation operation of any two equivalent H atoms of NH_3. Consequently, the NH_3 PES is totally symmetric under permutation of any two H atoms of NH_3. Note that S_i are the D_{3h} symmetric coordinates defined as Eq. (43) of Ref. 38 but using a different set of reference geometries ($R_{\rm NH}^{\rm ref}$, and $R_{\rm HH}^{\rm ref}$). In turn, the coefficients $R_{\rm NH}^{\rm ref}$, $R_{\rm HH}^{\rm ref}$, $g_{\rm NH}$, $g_{\rm HH}$ in Eq. (40) have been calculated using a trial-and-error procedure, their numerical values are reported in Table 7. The linear coefficients appearing in Eq. (41) have been calibrated from a least-squares fitting procedure to our own 205 *ab initio* points. Table 7 gathers the values of the 54 liner coefficients a_{i,j,k_p} appearing in Eq. (41). The fitted surface shows a root-mean-square deviation (rmsd) of $0.065\,\mathrm{kcal\,mol^{-1}}$ with a maximum error of $0.420\,\mathrm{kcal\,mol^{-1}}$. The stratified rmsd of the final PES with respect to all fitted *ab initio* energies are reported in Table 2. The DMBE form is seen to fit the ab initio date with chemical accuracy, with a stratified rmsd $\ll 1\%$ of the reference energy.

4 Features of the NH_3 potential energy surface

The reaction path with C_{3v} symmetry connects on the title system the D_{3h} transition state with the C_{3v} minimum [62]. Table 1 shows the results of the *ab initio* calculations and DMBE PES for the D_{3h} structure. As shown, the D_{3h} transition state structure on the DMBE PES shows the characteristic a bond length in very good agreement with the one predicted *ab initio*. In turn, Table 1 reports the properties of the DMBE PES at the C_{3v} equilibrium structure. Besides our own results, we give for comparison the results from other theoretical and experimental works. Here too, the DMBE PES predicts bond lengths in good agreement

Table 5. Energy dissociation limits (in E_h) of NH_3 PES.

Fragments[a]	R_1/a_0	R_2/a_0	R_3/a_0	R_4/a_0	R_5/a_0	R_6/a_0	$DMBE_{1+2+3}$	DMBE	*ab initio*[b]	error[c]
$N(^4S) + 3\,H(^2S)$	19.0000	19.0000	19.0000	32.9090	32.9090	32.9090	-0.000001	-0.000001	0.000000	0.000001
$H_2(X^1\Sigma_g^+) + N(^2D) + H(^2S)$	10.0000	10.0245	10.0245	20.0123	20.0123	1.4010	-0.083330	-0.083330	-0.083311	0.000019
$NH(X^3\Sigma^-) + 2H(^2S)$	1.9650	10.0245	10.0245	10.3491	10.3491	20.0000	-0.130233	-0.130233	-0.128466	0.001767
$NH(a^1\Delta) + H_2(X^1\Sigma_g^+)$	1.9565	15.0163	15.0163	16.9710	16.9710	1.4010	-0.243414	-0.243414	-0.243997	0.000583
$NH_2(1^2A'') + H(^2S)$	15.0000	1.9405	1.9405	16.2839	16.2839	3.0289	-0.285765	-0.285765	-0.282517	0.003248
$N(^2D) + H_3(^2A')$	20.0000	20.0773	20.0773	1.7605	1.7605	3.5210	-0.067950	-0.067950	-0.067262	0.000688

[a] H_3 is taken here at the collinear saddle point geometry ($D_{\infty h}$), although it is a well known van der Waals species. [b]Energy calculated using FVCAS/MRCI(Q)/AVTZ. [c]Taken as the difference between the DMBE PES and the calculated *ab initio* energy.

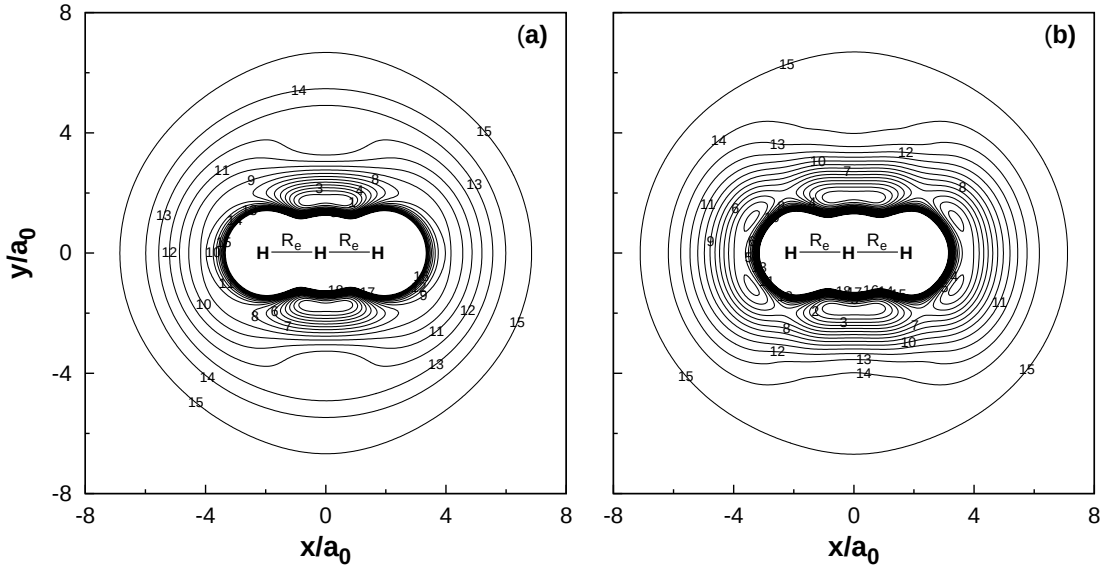

Figure 2. Contour plot for N moving in a coplanar manner around a partially relaxed H_3 molecule, where $R_e = 1.7605\,a_0$. Contour in panels (a) and (b) start at $-0.21\,E_h$, being equally spaced by $0.01\,E_h$. Panel (a) shows the $DMBE_{1+2+3}$ surface, while panel (b) refers to the full DMBE PES.

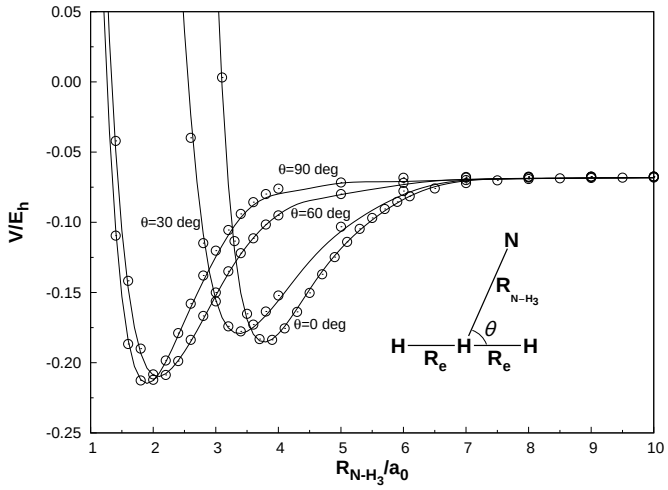

Figure 3. Comparison of the DMBE PES with the MRCI(Q)/AV*T*Z energies for N moving in a coplanar manner around a partially relaxed H_3 species, where $R_e = 1.7605\,a_0$. R_{N-H_3} refers the distance between N and the mass center of the H_3 molecule, and θ is the NHH bond angle indicated in the plot.

Table 6. Coefficients in $V_{Si}^{(4)}$ and $V_l^{(4)}$ of four-body energy term defined by Eqs. (28)-(39).

V_{S1}	V_{S2}	V_{S3}	V_{S4}	V_1	V_2	V_3
$d_1 = -0.108983$	$d_2 = 0.0198257$	$d_3 = 0.0022601$	$d_4 = -0.023724$	$C_1 = 0.035$	$C_2 = 0.025$	$C_3 = -0.050$
$a_{11} = 2.24483$	$a_{21} = 1.2956$	$a_{31} = 2.37549$	$a_{41} = 0.423244$	$R_1^0 = 3.5$	$R_1^0 = 3.7$	$\alpha_1' = 0.6$
$a_{12} = 0.678106$	$a_{22} = 0.909194$	$a_{32} = 1.23576$	$a_{42} = 0.737368$	$R_2^0 = 1.9405$	$R_2^0 = 1.9405$	$R_1' = 4.4$
$a_{13} = 0.582107$	$a_{23} = 0.622791$	$a_{33} = 0.181617$	$a_{43} = 0.273109$	$R_3^0 = 1.9405$	$R_3^0 = 1.9405$	$\alpha_2' = 2.0$
$b_{11} = 2.12763$	$b_{21} = 1.04963$	$b_{31} = 1.56864$	$b_{41} = 1.40199$	$R_4^0 = 2.742728$	$R_4^0 = 5.141385$	$R_2' = 3.2$
$b_{12} = 0.0$	$b_{22} = 0.919367$	$a_{32} = 0.0$	$a_{42} = 0.639717$	$R_5^0 = 2.742728$	$R_5^0 = 5.141385$	$\alpha_3' = 2.0$
$\gamma_{11} = 9.1$	$\gamma_{21} = 0.1$	$\gamma_{31} = 0.1$	$\gamma_{41} = 1.0$	$R_6^0 = 3.028850$	$R_6^0 = 3.028850$	$R_3' = 2.5$
$\gamma_{12} = 100$	$\gamma_{22} = 100$	$\gamma_{32} = 100$	$\gamma_{42} = 0.5$	$\gamma_{51} = 0.75$	$\gamma_{61} = 1.05$	$\gamma_{71} = 5.0$
$R_{A\alpha}^{10} = 2.9072$	$R_{A\alpha}^{20} = 4.4$	$R_{A\alpha}^{30} = 4.58303$	$R_{A\alpha}^{30} = 3.69261$		$\gamma_{62} = 10$	$R_{A\alpha}^{50} = 1.965$
$R_{\alpha\beta}^0 = 1.7605$	$R_{\alpha\beta}^0 = 1.7605$	$R_{\alpha\beta}^0 = 1.7605$	$R_{A\beta}^0 = 3.080698$			
$R_{\alpha\gamma}^0 = 1.7605$	$R_{\alpha\gamma}^0 = 1.7605$	$R_{\alpha\gamma}^0 = 1.7605$	$R_{A\gamma}^0 = 3.080698$			
$R_{\beta\gamma}^0 = 3.5210$	$R_{\beta\gamma}^0 = 3.5210$	$R_{\beta\gamma}^0 = 3.5210$	$R_{\beta\gamma}^{0'} = 1.401$			

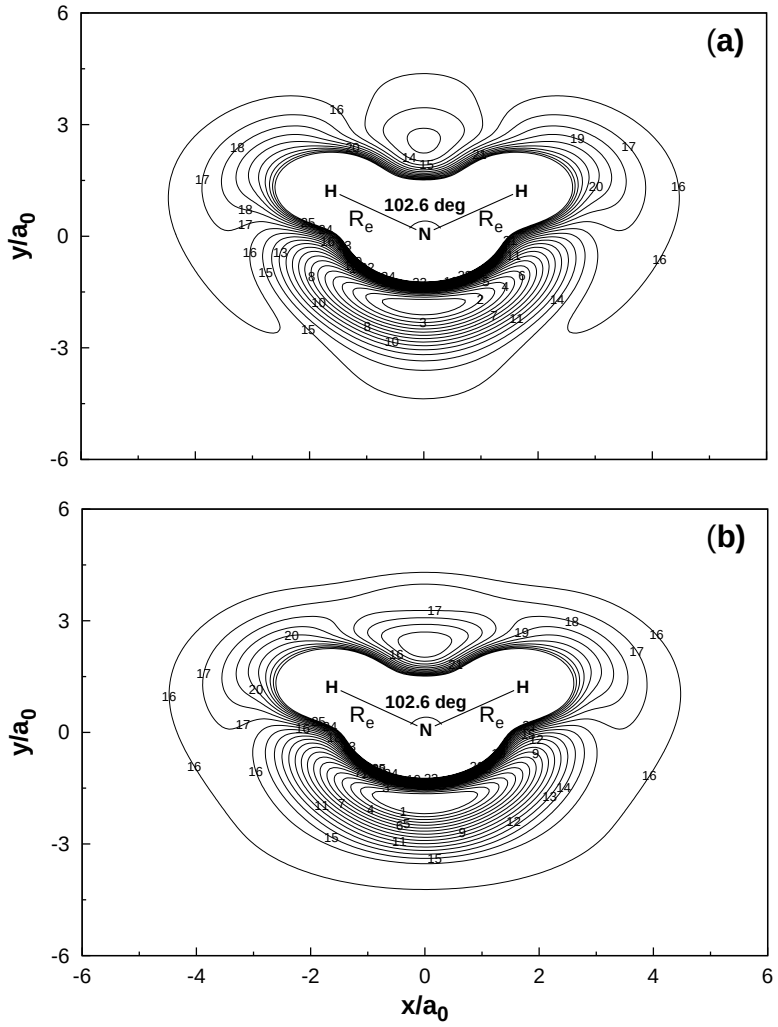

Figure 4. Contour plot for H moving in a coplanar manner around a partially relaxed NH_2 molecule, where $R_e = 1.9405\,a_0$. Contours in panels (a) and (b) start at $-0.458\,E_h$, being equally spaced by $0.01\,E_h$. Panel (a) shows the $DMBE_{1+2+3}$ surface, while panel (b) refers to the full DMBE PES.

with other results. Furthermore, the predicted bond angle from DMBE agrees with other predictions within 2 deg. These two facts suggest that the harmonic frequencies should also be in good agreement with one another, as is indeed observed from Table 1. Figures 2 to 15 illustrate the major topographical features of the $NH_3(^1A_1)$ DMBE PES. Clearly, it has a smooth and correct behavior over the whole configuration space. Also visible are its global minimum and the D_{3h} transition state. Specifically, Figure 2 shows energy contours for N

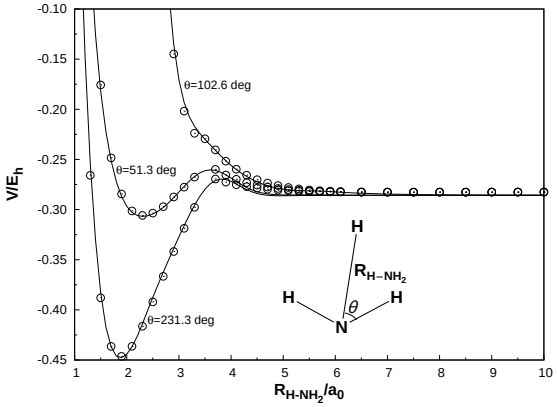

Figure 5. Comparison of the DMBE PES with the MRCI(Q)/AV*T*Z energies for H moving in a coplanar manner around a partially relaxed NH_2 molecule (by keeping NH_2 frozen at the geometry reported in Ref. 34). R_{H-NH_2} refers the distance between H and the N in the NH_2 molecule, and θ is the HNH bond angle.

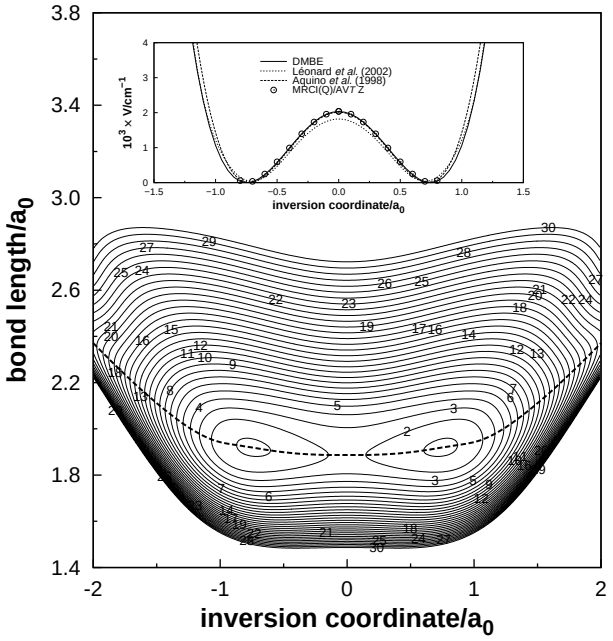

Figure 6. Two-dimensional section of the DMBE PES of NH_3 including the two minima and the saddle point of the six-dimensional space considered in the present work. Contours start at $-0.4650\,E_h$, being equally spaced by $0.0075\,E_h$. Shown in the inset is the optimized inversion potential curve: *dashed line* taken from Ref 65, *dotted line* taken from Ref 62, *continuous line*, DMBE (this work).

moving in a coplanar manner around a partially relaxed H_3 (this is frozen at its optimum FVCAS/AV*T*Z geometry) with the central H atom fixed at the origin. Note that H_3 is not a stable species, with the chosen structure corresponding to a well established saddle point of $D_{\infty h}$ symmetry for the hydrogen-atom exchange reaction. [36, 63] From Figures 2(a) and 2(b) we can see that both the $DMBE_{1+2+3}$ and DMBE PESs predictions for the dissociation limit at the N+H_3 dissociation limit are in good agreement with our *ab initio* results (see also the fifth entry of Table 5). However, inclusion of the four-body energy term make the full DMBE PES significantly improves the accuracy by improving the description of other regions at the N+H_3 channel.

Figure 3 compares the DMBE PES with the *ab initio* energies at MRCI(Q)/AV*T*Z for N moving in a coplanar manner around a partially relaxed H_3 molecule. The curves obtained from the DMBE PES are seen to be in good agreement with the calculated values. A diagram showing contour plots for H moving in a coplanar manner around a partially relaxed NH_2 molecule (by keeping NH_2 frozen at the geometry reported in Ref. 34) is shown in Figure 4. As panel (a) of Figure 4 shows, the $DMBE_{1+2+3}$ PES cannot attain an unique value at the H+NH_2 limit. Fortunately, as illustrated in panel (b) of Figure 4, this inconsistency is overcome through the inclusion of the four body energy term (*i.e.*, in the full DMBE PES). Similarly, the accuracy in describing the C_{2v} insertion of H atom into NH_2 molecular is significantly enhanced by the full DMBE PES. Figure 5 compares the DMBE PES with the MRCI(Q)/AV*T*Z energies for H moving in coplanarary around a partially relaxed NH_2 molecule. As shown by this plot, The curves obtained from the DMBE PES are in good agreement with the calculated energies. The above referred discrepancies for the coplanar geometries are mainly caused by a sudden change in the MRCI(Q) energy with the R_{H-NH_2} distance . At those geometries, there are strong configuration-mixing effects [1, 64] due to a change in the lowest electronic configuration from $^1A_1$ to A_2'' as one approaches the strong-interaction regions. Thus, the lowest adiabatic PES exhibits complicated topographical features. As a result, a multivalued approach may be required to obtain a more realistic potential model.

Figures 6 show the two-dimensional section of the DMBE PES of NH_3 including the two minima and the saddle point for the umbrella inversion. The

optimized DMBE potential curve is shown in the inset of Figures 6, and compared with the other reported inversion potential curve [62, 65]. A notable feature from such a plot is the fairly good agreement between our optimized DMBE inversion potential curve and the one by Aquino et al [65], particularly for small values of the inversion coordinate where the optimized DMBE inversion potential curve is almost indistinguishable from their curve. Table 2 gives the results of the calculation for the inversion barrier computed using different methods and available experimental results. The predicted DMBE inversion barrier of $2033.5\,\mathrm{cm}^{-1}$ is clearly in very good agreement with the result of $2029.4\,\mathrm{cm}^{-1}$ obtained from the fit to the dense grid of *ab initio* points close to the equilibrium geometry and D_{3h} saddle point, being also in quite good agreement with the experiment value of $2018\,\mathrm{cm}^{-1}$ by Swalen and Ibers [66]. Figure 7 shows the global minimum, while illustrating that the DMBE PES is totally symmetric under permutation of any two H atoms of NH_3. Moreover, inclusion of the four-body energy term in the full DMBE PES makes the global minimum energy to be reduced to $-0.4660\,\mathrm{E_h}$, in good agreement with the result of $-0.4660\,\mathrm{E_h}$ from our *ab initio* prediction. To obtain more information of the global minimum, we compare the DMBE PES with the *ab initio* energies at MRCI(Q)/AVTZ. This is illustrated in Figures 8 where cuts are shown of the DMBE PES along one bond length. Values for the remaining coordinates are bond lengths (b) at $1.919\,\mathrm{a_0}$ and bond angles (α) at 105.85 deg, respectively the optimum equilibrium bond length and equilibrium bond angle based on the DMBE PES. Clearly, the 1D cuts of the DMBE PES show good agreement with the calculated *ab initio* energies. Figure 9 shows a contour plot of the full DMBE PES for the channel $NH_2 + H \rightleftharpoons NH_3 \rightleftharpoons NH + H + H$, with a $2D$ minimum being apparent from Figure 9 corresponding to the D_{3h} transition state structure which energy is $-0.4567\,\mathrm{E_h}$, in good agreement with the result of $-0.4567\,\mathrm{E_h}$ from our *ab initio* prediction. Moreover, as panels (a) and (b) of Figures 10 and 11 clearly show, both the DMBE_{1+2+3} and DMBE PESs predict a barrier for the $NH_3 \rightleftharpoons H_2 + NH$ channel in agreement with the calculated *ab initio* result. By comparing panels (a) and (b) of Figures 10 and 11, we stress the significant improvement obtained by eliminating the unphysical minimum with the addition of the proper four-body energy term as discussed above. Figure 12 and Figure 13 shows contour plot of the full DMBE PES for the

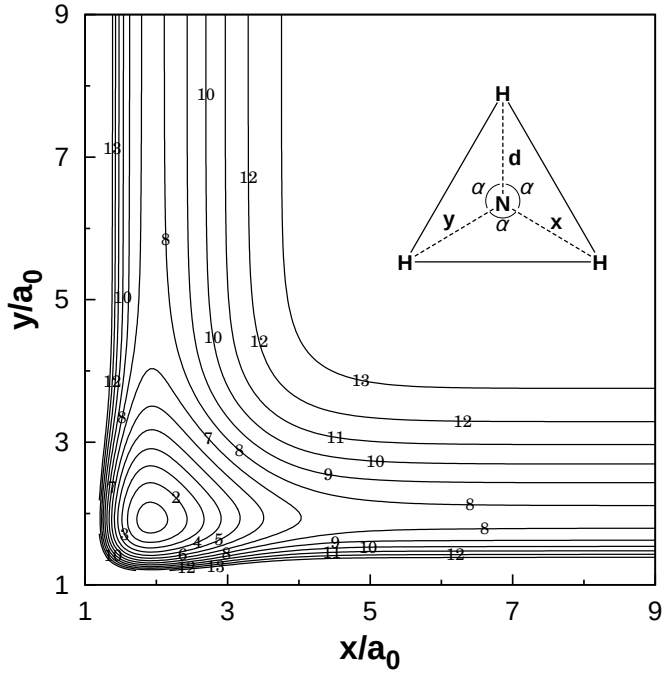

Figure 7. Contour plot of the full DMBE PES for the bond stretching in NH_3 where $d = 1.919\,a_0$ and keeping the included angle fixed at 105.85 deg. Contours start at $-0.455\,E_h$, being equally spaced by $0.025\,E_h$.

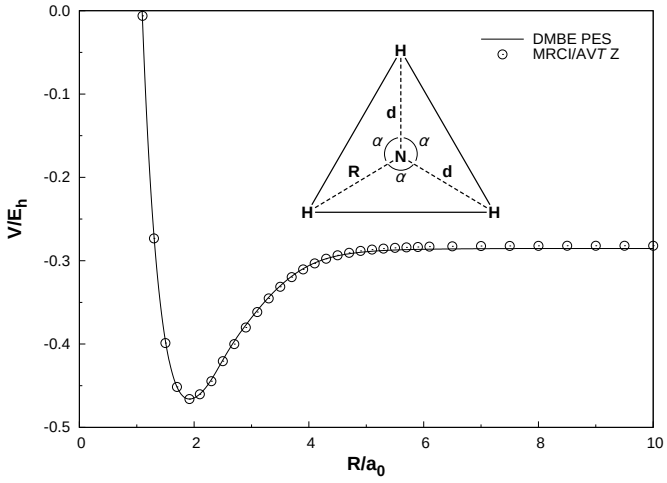

Figure 8. Cut of DMBE PES along one bond length, with values for the remaining coordinates being the bond lengths (b) at $1.919\,a_0$ and bond angles (α) at 105.85 deg, which are the optimum MRCI(Q)/AV*T*Z equilibrium bond length and equilibrium bond angle.

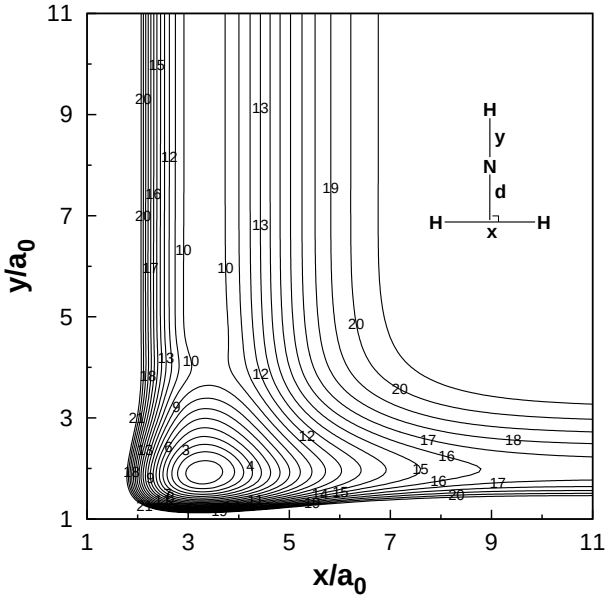

Figure 9. Contour plot of the full DMBE PES for the channel $NH_2 + H \rightleftharpoons NH_3 \rightleftharpoons NH + H + H$, where $d = 0.95\,a_0$. Contours start at $-0.4435\,E_h$, being equally spaced by $0.02\,E_h$. The corresponding plot for the $DMBE_{1+2+3}$ surface is nearly indistinguishable,and hence is not shown.

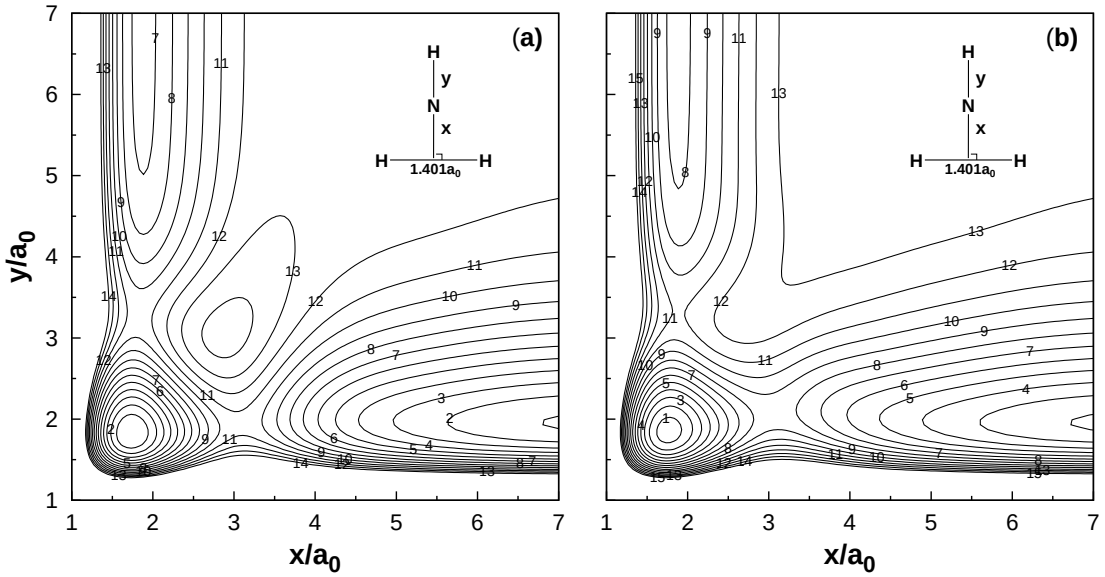

Figure 10. Contour plot for the channel H_2+N+H $\rightleftharpoons NH_3 \rightleftharpoons H_2$+NH. Contour in panels (a) and (b) start at $-0.252\,E_h$, being equally spaced by $0.0135\,E_h$. Panel (a) shows the $DMBE_{1+2+3}$ surface,while panel (b) refers to the full DMBE PES.

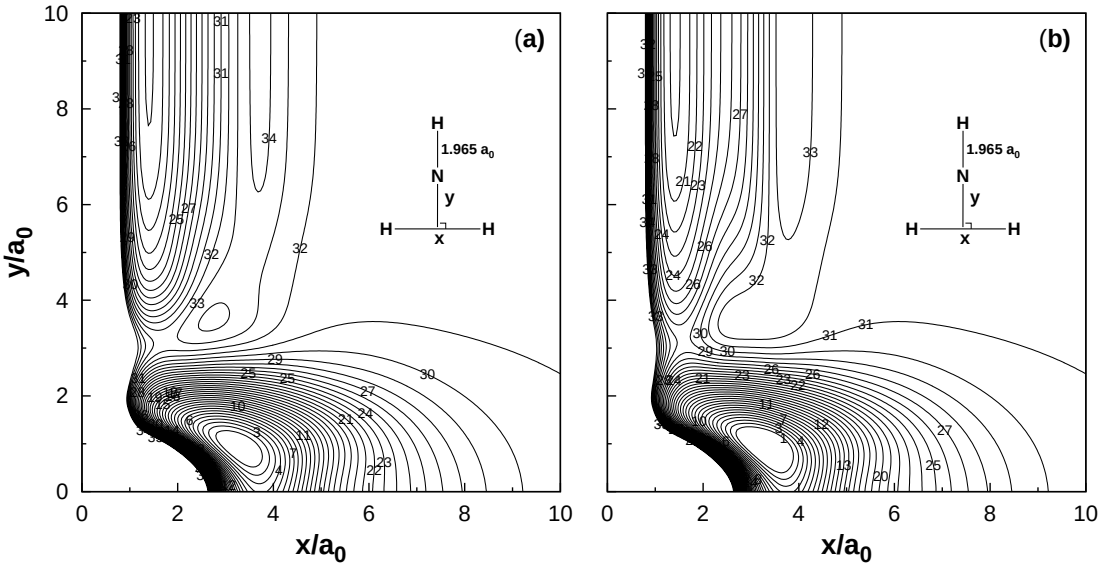

Figure 11. Contour plot for the channel $NH+H_2 \rightleftharpoons NH_3 \rightleftharpoons NH+H+H$. Contour in panels (a) and (b) start at $-0.432\,E_h$, being equally spaced by $0.01\,E_h$. Panel (a) shows the $DMBE_{1+2+3}$ surface, while panel (b) refers to the full DMBE PES.

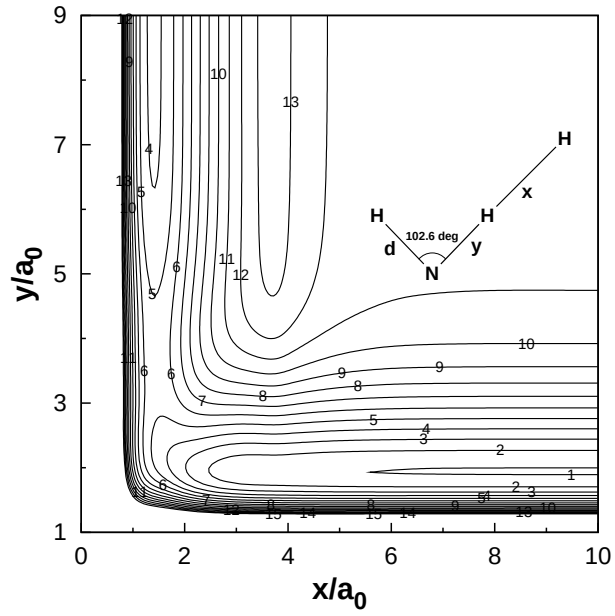

Figure 12. Contour plot of the full DMBE PES for the channel $NH_2 + H \rightleftharpoons NH + H_2$. where $d = 1.9405a_0$. Contour start at $-0.285\,E_h$, being equally spaced by $0.015\,E_h$. The corresponding plot for the $DMBE_{1+2+3}$ surface is nearly indistinguishable,and hence is not shown.

channel $NH_2 + H \rightleftharpoons NH + H_2$, the DMBE PES also predicts the barrier on the H_2+NH channel. Such a barrier has been found to be 13.1 kcal mol^{-1} higher than the NH+H_2 dissociate energy. Table 4 collects the the Geometries and harmonic frequencies for $NH\cdots H_2$ transition state , calculated from full BMBE PES. As shown in Figure 12 , there is no barrier for this geometry dissociates to $NH_2 + H$ geometry. in this direction, the H atom can more easily escapes, as can also be seen from Figure 5. Figure 15 shows a schematic diagram of energetics of the title system according to the DMBE PES reported in the present work, while table 5 summarizes the reference *ab initio* MRCI(Q)/AV*T*Z energy. In addition, as pointed out elsewhere, if one of the atoms is placed far away from the remaining triatomic, the resulting PES matches exactly that of the triatomic fragment. Finally, Figure 14 shows that the update does not affect significantly the attributes of the NH_2 PES in comparison with the original form [34].

5 Conclusions

We have reported a single-valued DMBE PES for the ground electronic state of NH_3, partly based on detailed MRCI(Q)/AV*T*Z calculations for the tetratomic also given in the present work. These have been shown to be in fair agreement with previously reported *ab initio* results. The DMBE PES shows the proper atom permutational symmetry. while being based on a modest number of *ab initio* energies (when judged from the popular X^{3N-6} law, which shows that the number of required energy points grows exponentially with the number of atoms, with X being the number of points typically required per dimension) at an affordable (relatively low) level of theory. Therefore, it may pave the way for an ab-initio-based study aiming at a more sophisticated level of *ab initio* theory, or else for improvement via a direct fit to spectroscopic data (ref 52 and references therein). Despite the above, The attributes of the function here reported have been found to be in generally good agreement with those from the fitted raw *ab initio* energies and the results from previous theoretical calculations and experiment. To warrant that the PES dissociates to the correct asymptotes, a generalization of the switching function proposed elsewhere [34] (see ref 40 for a related development for the N_2H_2 species)has been extended to the present four-

Table 7. Coefficients a_{n,i,j,k_p} appearing in Eqs. (40) and (41).

R_{NH}^{ref}	1.89	R_{HH}^{ref}	3.273411
g_{NH}	5.0	g_{HH}	2.0
$a_{0,0,0}$	−0.0149239509	$a_{2,0,1_1}$	−0.0000047329
$a_{1,0,0}$	0.0393566682	$a_{2,0,1_2}$	−0.0000249623
$a_{0,1,0}$	−0.0207103175	$a_{2,0,1_3}$	0.0000004764
$a_{2,0,0}$	−0.1460667641	$a_{1,1,1_1}$	−0.0000134270
$a_{1,1,0}$	0.0802288866	$a_{1,1,1_2}$	−0.0000655363
$a_{0,2,0}$	−0.0453661202	$a_{1,1,1_3}$	0.0000071649
$a_{0,0,1_1}$	−0.0956785052	$a_{1,3,0}$	−0.0221918415
$a_{0,0,1_2}$	−0.0399175663	$a_{1,0,1_4}$	0.0000145569
$a_{0,0,1_3}$	−0.0210753673	$a_{1,0,1_5}$	0.0000308448
$a_{3,0,0}$	0.0112004510	$a_{1,0,1_6}$	−0.0000055180
$a_{2,1,0}$	−0.0414751468	$a_{1,0,1_7}$	0.0000056313
$a_{1,2,0}$	−0.0186598337	$a_{1,0,1_8}$	0.0000457415
$a_{1,0,1_1}$	0.0003457716	$a_{0,4,0}$	−0.0717617678
$a_{1,0,1_2}$	0.0022309626	$a_{0,2,1_1}$	−0.0000314825
$a_{1,0,1_3}$	−0.0003883413	$a_{0,2,1_2}$	−0.0000927060
$a_{0,3,0}$	−0.0619437295	$a_{0,2,1_3}$	−0.0000167492
$a_{0,1,1_1}$	0.0008785003	$a_{0,1,1_4}$	0.0000332154
$a_{0,1,1_2}$	0.0017967763	$a_{0,1,1_5}$	0.0000834940
$a_{0,1,1_3}$	0.0009600578	$a_{0,1,1_6}$	−0.0000174075
$a_{0,0,1_4}$	−0.0004633714	$a_{0,1,1_7}$	−0.0000144196
$a_{0,0,1_5}$	−0.0056973880	$a_{0,1,1_8}$	0.0000212283
$a_{0,0,1_6}$	0.0004316154	$a_{0,0,2_{1,1}}$	−0.0000302394
$a_{0,0,1_7}$	0.0014237697	$a_{0,0,2_{1,2}}$	−0.0000088146
$a_{0,0,1_8}$	−0.0005946042	$a_{0,0,2_{1,3}}$	0.0000026353
$a_{4,0,0}$	0.0006812888	$a_{0,0,2_{2,2}}$	−0.0000500316
$a_{3,1,0}$	−0.0037633238	$a_{0,0,2_{2,3}}$	−0.0000417883
$a_{2,2,0}$	0.0153576383	$a_{0,0,2_{3,3}}$	0.0000005487

Table 8. Accumulated (acc.) and stratum (strat.) root-mean-square deviations (in kcal mol^{-1}) of DMBE PES[a]

Energy		N^b		max.dev.[c]		rmsd		$N^d_{>\text{rmsd}}$	
Acc.	strat.	acc.	strat.	acc.	strat.	acc.	strat.	acc.	strat.
10	0- 10	211	211	0.420	0.420	0.066	0.066	8	8
20	10- 20	212	1	1.215	1.215	0.106	1.215	8	0
30	20- 30	214	2	6.538	6.538	0.463	4.661	3	1
40	30- 40	215	1	6.538	4.734	0.563	4.734	4	0
50	40- 50	217	2	6.538	1.617	0.572	1.161	5	1
60	50- 60	219	2	6.538	2.915	0.615	2.425	7	1
70	60- 70	221	2	6.538	2.587	0.641	2.017	9	1
80	70- 80	223	2	6.538	1.983	0.654	1.525	11	1
90	80- 90	224	1	6.538	0.698	0.655	0.698	12	0
100	90-100	227	3	6.538	1.679	0.662	1.072	13	1
120	100-120	305	78	6.538	4.322	1.170	2.019	69	23
140	120-140	320	15	7.230	7.230	1.247	2.309	75	2
160	140-160	325	5	7.230	4.331	1.261	1.963	76	1
180	160-180	335	10	7.230	5.371	1.287	1.948	78	2
200	180-200	351	16	7.230	3.806	1.310	1.729	87	3
300	200-300	465	114	10.444	10.444	1.663	2.449	98	20
500	300-500	472	7	10.444	7.081	1.738	4.465	97	2
930	500-930	476	4	10.444	3.810	1.741	2.086	96	1

[a]Defined here by rmsd= $\{\sum_{i=1}^{N}[V(\boldsymbol{R}_i) - E(\boldsymbol{R}_i)]^2/N\}^{1/2}$, where $V(\boldsymbol{R}_i)$ and $E(\boldsymbol{R}_i)$ are the DMBE and calculated *ab initio* energies. [b] Number of calculated MRCI/AVTZ points up to the indicated energy range. [c] Maximum deviation up to the indicated energy range. [d] Number of calculated MRCI/AVTZ points with an energy deviation larger than the root-mean-square deviation.

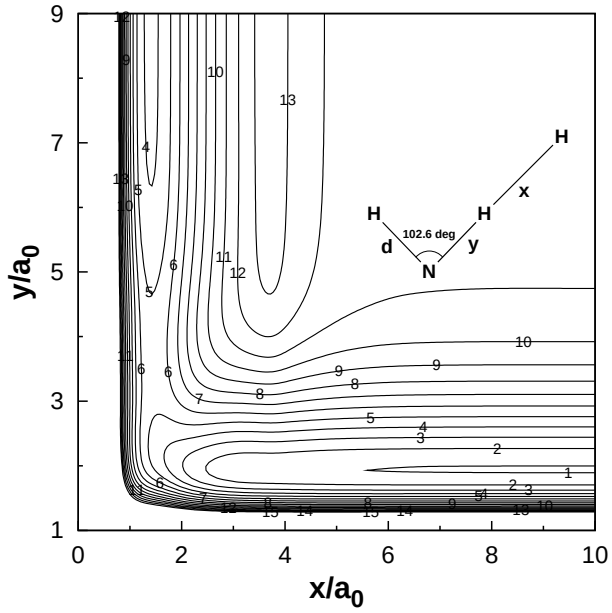

Figure 13. Contour plot of the full DMBE PES for the channel $NH_2 + H \rightleftharpoons NH + H_2$. where $d = 1.9405\,a_0$,the dihedral angle is 90 deg. Contour start at $-0.325\,E_h$, being equally spaced by $0.0125\,E_h$. The corresponding plot for the $DMBE_{1+2+3}$ surface is nearly indistinguishable, and hence is not shown.

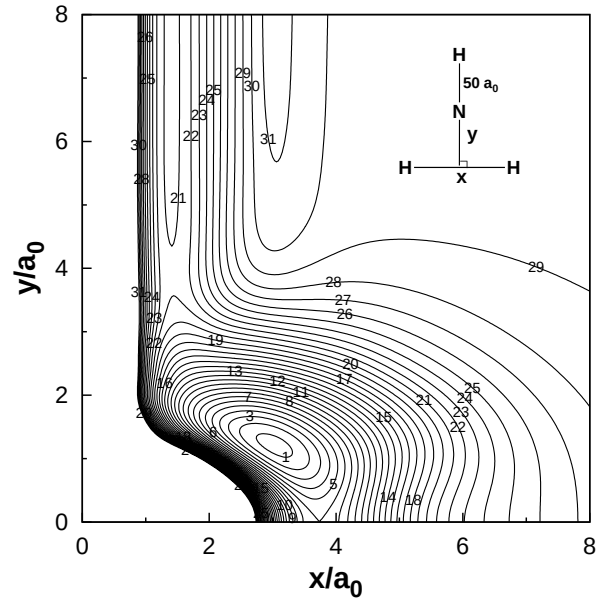

Figure 14. Contour plot of the NH_3 full DMBE PES for the C_{2v} insertion of the N atom into H_2, keeping the distance of the N to another H atom. Contour in start at $-0.282\,E_h$, being equally spaced by $0.01\,E_h$.

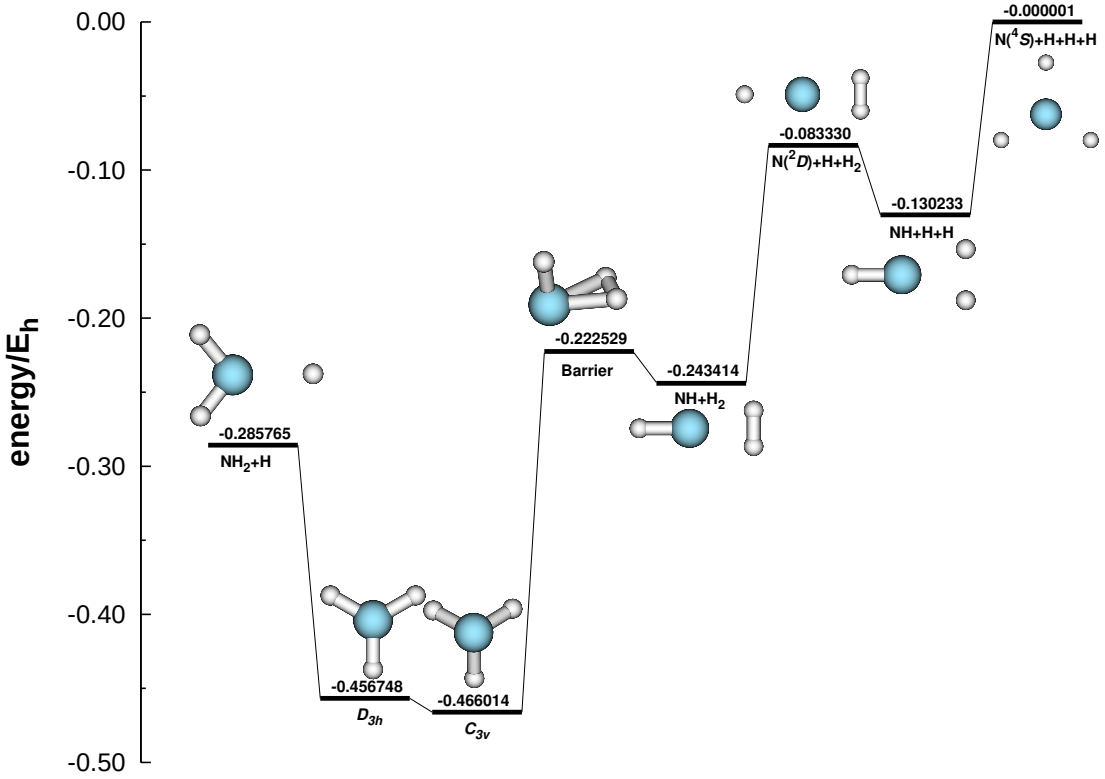

Figure 15. Energetics of full NH_3 DMBE PES reported in the present work.

atom species. As usual in DMBE theory, the PES is expected to mimic the correct behavior at all dissociation channels while providing a realistic representation at all interatomic separations. It can therefore be recommended both for dynamics studies and as a building block for construction of DMBE forms for largerN_xHy species. Such a work is currently in due course.

Acknowledgments

Y.Q. Li thanks the Liaoning University for leave of absence during his PhD Studies. This work has the financial support of Fundação para a Ciência e a Tecnologia, Portugal.

References

[1] Marquardt, R.; Sagui, K.; Klopper, W.; Quack, M. *J. Phys. Chem. B* **2005**, *109*, 8439.

[2] Rajamäki, T.; Miani, A.; Halonen, L. *J. Chem. Phys.* **2003**, *118*, 6358.

[3] Klopper, W.; Samson, C. C. M.; Tarczay, G.; Császár, A. G. *J. Comput. Chem.* **2001**, *22*, 1306.

[4] Lin, H.; Thiel, W.; Yurchenko, S. N.; Carvajal, M.; Jensen, P. *J. Chem. Phys.* **2002**, *117*, 11265.

[5] Canuto, S. *J. Phys. B: Atom. Molec. Phys.* **1979**, *12*, 3149.

[6] Martin, J. M. L.; Lee, T. J.; Taylor, P. R. *J. Chem. Phys.* **1992**, *97*, 8361.

[7] Yarkony, D. R. *J. Chem. Phys.* **2004**, *121*, 628.

[8] Biesner, J.; Schnieder, L.; Ahlers, G.; Xie, X.; Welge, K. H.; Ashfold, M. N. R.; Dixon, R. N. *J. Chem.Phys.* **1989**, *91*, 2901.

[9] McCarthy, M. I.; Rosmus, P.; Werner, H. J.; Botschwina, P.; Vaida, V. *J. Chem. Phys.* **1987**, *86*, 6693.

[10] Pesonen, J.; Miani, A.; Halonen, L. *J. Chem. Phys.* **2001**, *115*, 1243.

[11] Cheung, A. C.; Rank, D. M.; Townes, C. H.; Thornton, D. D.; Welch, W. J. *Phys. Rev. Lett.* **1968**, *21*, 1701.

[12] Špirko, V. *J. Mol. Spectrosc.* **1983**, *101*, 30.

[13] Špirko, V.; Kraemer, W. P. *J. Mol. Spectrosc.* **1989**, *133*, 331.

[14] Sasada, H.; Hasegawa, Y.; Amano, T.; Shimizu, T. *J. Mol. Spectrosc.* **1982**, *96*, 106.

[15] Snels, M.; Fusina, L.; Hollenstein, H.; Quack, M. *Mol. Phys.* **2000**, *98*, 837.

[16] Marshall, M. D.; Izgi, K. C.; Muenter, J. S. *J. Chem. Phys.* **1997**, *107*, 1037.

[17] Quack, M. *Angew. Chem. Int. Ed.* **2002**, *41*, 4618.

[18] Marquardt, R.; Quack, M.; Thanopulos, I.; Luckhaus, D. *J. Chem. Phys.* **2003**, *118*, 643.

[19] Biesner, J.; Schnieder, L.; Schmeer, J.; Ahlers, G.; Xie, X.; Welge, K. H.; Ashfold, M. N. R.; Dixon, R. N. *J. Chem. Phys.* **1988**, *88*, 3607.

[20] Mänz, U.; Reinsch, E. A.; Rosmus, P.; Werner, H. J.; Neil, S. O. *J. Chem. Soc., Faraday Trans.* **1991**, *87*, 1809.

[21] Bach, A.; Hutchison, J. M.; Holiday, R. J.; Crim, F. F. *J. Phys. Chem. A* **2003**, *107*, 10490.

[22] Rosmus, P.; Botschwina, P.; Werner, H. J.; Vaida, V.; Engelking, P. C.; McCarthy, M. I. *J. Chem. Phys.* **1987**, *86*, 6677.

[23] Mänz, U.; Rosmus, P.; Werner, H. J.; Botschwina, P. *Chem. Phys.* **1988**, *122*, 387.

[24] Snels, M.; Hollenstein, H.; Quack, M. *J. Chem. Phys.* **2003**, *119*, 7893.

[25] Léonard, C.; Handy, N. C.; Carter, S. *Chem. Phys. Lett.* **2003**, *370*, 360.

[26] Yurchenko, S. N.; Carvaial, M.; Jensen, P.; Lin, H.; Zheng, J. J.; Thiel, W. *Mol. Phys.* **2005**, *103*, 359.

[27] Huang, X.; Schwenke, D. W.; .; Leec, T. J. *J. Chem. Phys.* **2008**, *129*, 214304.

[28] Li, Z. H.; Valero, R.; Truhlar, D. G. *Theor. Chem. Acc.* **2007**, *118*, 9.

[29] Bonhommeau, D.; Valero, R.; Truhlar, D. G.; Jasper, A. W. *J. Chem. Phys.* **2009**, *130*, 234303.

[30] Mota, V. C.; Varandas, A. J. C. *J. Phys. Chem. A* **2008**, *112*, 3768.

[31] Varandas, A. J. C. *Adv. Chem. Phys.* **1988**, *74*, 255.

[32] Varandas, A. J. C. *Lecture Notes in Chemistry*; Laganá, A., Riganelli, A., Eds.; Springer: Berlin, 2000; Vol. 75, p 33.

[33] Varandas, A. J. C.; World Scientific Publishing, 2004; chapter 5, p 91; Advanced Series in Physical Chemistry.

[34] Varandas, A. J. C.; Poveda, L. A. *Theor. Chem. Acc.* **2006**, *116*, 404.

[35] Li, Y. Q.; Varandas, A. J. C. *J. Phys. Chem. A (to be published).*

[36] Varandas, A. J. C.; Brown, F. B.; Mead, C. A.; Truhlar, D. G.; Blais, N. C. *J. Chem. Phys.* **1987**, *86*, 6258.

[37] Varandas, A. J. C.; Llanio-Trujillo, J. L. *Chem. Phys. Lett.* **2002**, *356*, 585.

[38] Varandas, A. J. C.; Yu, H. G. *Mol. Phys.* **1997**, *91*, 301.

[39] Ballester, M. Y.; Varandas, A. J. C. *Phys. Chem. Chem. Phys.* **2005**, *7*, 2305.

[40] Poveda, L. A.; Biczysko, M.; Varandas, A. J. C. *J. Chem. Phys.* **2009**, *131*, 044309.

[41] Varandas, A. J. C.; Zhang, L. *Chem. Phys. Lett.* **2000**, *331*, 474.

[42] Varandas, A. J. C.; Zhang, L. *Chem. Phys. Lett.* **2004**, *385*, 409.

[43] Werner, H.-J.; Knowles, P. J. *J. Chem. Phys.* **1988**, *89*, 5803.

[44] Knowles, P. J.; Werner, H.-J. *Chem. Phys. Lett.* **1988**, *145*, 514.

[45] Dunning Jr., T. H. *J. Chem. Phys.* **1989**, *90*, 1007.

[46] Kendall, R. A.; Dunning Jr., T. H.; Harrison, R. J. *J. Chem. Phys.* **1992**, *96*, 6796.

[47] Murrell, J. N.; Carter, S.; Farantos, S. C.; Huxley, P.; Varandas, A. J. C. *Molecular Potential Energy Functions;* Wiley: Chichester, 1984.

[48] Varandas, A. J. C. *J. Chem. Phys.* **1996**, *105*, 3524.

[49] Varandas, A. J. C. *J. Chem. Phys.* **1997**, *107*, 867.

[50] Varandas, A. J. C.; Voronin, A. I.; Riganelli, A.; Caridade, P. J. S. B. *Chem. Phys. Lett.* **2000**, *331*, 331.

[51] Varandas, A. J. C.; Rodrigues, S. P. J. *Spectrochim. Acta A* **2002**, *58*, 629.

[52] Varandas, A. J. C.; Rodrigues, S. P. J. *J. Phys. Chem A* **2006**, *110*, 485.

[53] Galvao, B. R. L.; Rodrigues, S. P. J.; Varandas, A. J. C. **2008**, *112*, 3768.

[54] Molpro, version 2008.3, a package of *ab initio* programs. Werner, H. J.; Knowles, P. J.; Lindh, R.; Manby, F. R.; Schütz, M.; Celani, P.; Korona, T.; Mitrushenkov, A.; Rauhut, G.; Adler, T. B.; Amos, R. D.; Bernhardsson, A.; Berning, A.; Cooper, D. L.; Deegan, M. J. O.; Dobbyn, A. J.; Eckert, F.; Goll, E.; Hampel, C.; Hetzer, G.; Hrenar, T.; Knizia, G.; Köppl, C.; Liu, Y.; Lloyd, A. W.; Mata, R. A.; May, A. J.; McNicholas, S. J.; Meyer, W.; Mura, M. E.; Nicklass, A.; Palmieri, P.; Pflüger, K.; Pitzer, R.; Reiher, M.; Schumann, U.; Stoll, H.; Stone, A. J.; Tarroni, R.; Thorsteinsson, T.; Wang, M.; Wolf, A. **2008**.

[55] Varandas, A. J. C.; Silva, J. D. *J. Chem. Soc., Faraday Trans. 2* **1992**, *88*, 941.

[56] Varandas, A. J. C. *J. Mol. Struct. Theochem.* **1985**, *120*, 401.

[57] Varandas, A. J. C.; Rodrigues, S. P. J. *J. Chem. Phys.* **1997**, *106*, 9647.

[58] Martínez-Núñez, E.; Varandas, A. J. C. *J. Phys. Chem. A* **2001**, *105*, 5923.

[59] Torello, F.; Dondi, M. G. *J. Chem. Phys.* **1979**, *70*, 1564.

[60] Murrell, J. N.; Carter, S. *J. Phys. Chem.* **1984**, *88*, 4887.

[61] Yu, H. G.; Varandas, A. J. C. *Chem. Phys. Lett.* **2001**, *334*, 173.

[62] Léonard, C.; Handy, N. C.; Carter, S.; Bowman, J. M. *Spectrochim. Acta A* **2002**, *58*, 825.

[63] Varandas, A. J. C. *J. Chem. Phys.* **1979**, *70*, 3786.

[64] Nangia, S.; Truhlar, D. G. *J. Chem. Phys.* **2006**, *124*, 124309.

[65] Aquino, N.; Campoy, G.; Yee-Madeira, H. *Chem. Phys. Lett.* **1998**, *296*, 111.

[66] Swalen, J. D.; Ibers, J. A. *J. Chem. Phys.* **1962**, *36*, 1914.

[67] Hargiss, L. O.; Ermler, W. C. *J. Phys. Chem.* **1988**, *92*, 300.

[68] Lee, T. J.; Remington, R. B.; Yamaguchi, Y.; Schaefer III, H. F. *J. Chem. Phys.* **1988**, *89*, 408.

[69] Hoy, A. R.; Mills, I. M.; Strey, G. *Mol. Phys.* **1972**, *24*, 1265.

[70] Duncan, J. L.; Mills, I. M. *Spectrochim. Acta.* **1964**, *20*, 523.

[71] Coy, S. L.; Lehmann, K. K. *Spectrochim. Acta A* **1989**, *45*, 47.

[72] Lehmann, K. K.; Coy, S. L. *J. Chem. Soc. Fraday 2* **1988**, *84*, 1389.

[73] Botschwina, P. *J. Chem. Phys.* **1987**, *87*, 1453.

Chapter 6

Refining to near spectroscopic accuracy the DMBE-PES for ground-state NH_2

Chem. Phys. Lett. **516**, 17-22 (2011).

Refining to near spectroscopic accuracy the double many-body expansion potential energy surface for ground-state NH_2

S.P.J. Rodrigues, A.C.G. Fontes, Y.Q. Li and A.J.C. Varandas

Departamento de Química, Universidade de Coimbra
3004-535 Coimbra Codex, Portugal.

(Received: August 1, 2011; In final form: September 21, 2011)

Abstract

The single-sheeted double many-body expansion potential energy surface for the ground-state of NH_2 is refined to attain near spectroscopic accuracy from a multiproperty fit to accurate *ab initio* energies and experimental vibrational levels, including the Renner-Teller effect for total angular momentum (excluding spin) of $N = 0$. Quasiclassical trajectory calculations on both the original and newly reported potential energy surfaces suggest that the dynamical properties of the original form remain essentially unaltered as aimed.

1 Introduction

The amidogen (NH_2) radical plays a crucial role in atmospheric chemistry and combustion processes, being also a prototype in spectroscopic and reaction dynamics studies.

The spectrum of NH_2 has been first reported by Herzberg and Ramsey[1] in 1952. A more detailed analysis of that spectrum in 1959 by Dresseler and Ramsay[2] revealed the first experimental evidence of the Renner-Teller (RT) effect, a non-adiabatic effect due to the coupling of the electronic and total nuclear angular momenta that manifests on vibrational-rotational levels. Ever since, the spectrum of NH_2 and its isotopomers has been investigated by a large variety of spectroscopic and theoretical methods (see Refs. 3–6 and references therein). In addition, NH_2 is a well established prototype for the study of insertion reactions, with the reaction $N(^2D) + H_2(X^1\Sigma_g^+)$ playing also a key role in the combustion of nitrogen-containing materials.

Most studies of the title system have been carried out on its ground electronic adiabatic state potential energy surface (PES) and first excited state (labeled $1^2A''$ and $1^2A'$ in C_s symmetry, respectively). These PESs form a RT pair of $^2\Pi_u$ character at linear geometries, with both PESs becoming degenerate at some linear $D_{\infty h}$ and C_{2v} geometries and at the asymptote, $N(^2D) + H_2(X^1\Sigma_g^+)$.

Varandas and Poveda[7] reported a single-sheeted DMBE (double many-body expansion) PES for the ground state $1^2A''$ state of NH_2 from MRCI *ab initio* energies, using the double many-body expansion-scaled external correlation (DMBE/SEC)[8] to slightly correct semiempirically the calculated raw energies. To take care of the dissociation channels involving nitrogen in the ground $N(^4S)$ and first $N(^2D)$ excited states a switching-function formalism has been utilized. In addition, the barrier for $N(^2D) + H_2(X^1\Sigma_g^+)$ insertion has been calibrated. Moreover, quasiclassical[9] and quantum[10] studies of the $N(^2D) + H_2(X^1\Sigma_g^+)$ reaction as well as quasiclassical and quantum studies[11] of the reaction $H(^2S)+NH(X^3\Sigma^-) \rightarrow N(^2S) + H_2(X^1\Sigma_g^+)$ using this DMBE PES led to results in good agreement with the best available experimental and theoretical results. Li and Varandas[12] reported a single-sheeted DMBE PES for the $1^2A'$ state based on the DMBE/SEC method and complete basis set (CBS) extrapolation[13] with care taken to ensure

an accurate match of both PESs at linear $D_{\infty h}$ geometries and at asymptotic regions, since, as noted before, they form a RT pair.

Other PESs have been reported for the $1^2A''$ state,[14–16] $1^2A'$ state,[6, 17] as well as for both states[3, 18–20] of NH_2. Some of these PESs have also been used in reaction dynamics studies, both including the RT effect,[21–23] and without including it.[15, 16, 24] Spectroscopic studies have also been undertaken, both including the RT effect[3, 18, 19, 23] and without its inclusion.[15, 16, 20] Although the RT effect seems to have a relatively small influence in reaction dynamics, it is key in obtaining accurate spectroscopic attributes.

The main goal of the present work is to improve the spectroscopic properties of the single-sheeted DMBE PES of Varandas and Poveda for the ground-state of NH_2 (hereinafter referred to as DMBE I) by employing a multiproperty fit[25–27] to both the DMBE/SEC energies[7] and experimental vibrational levels.

To get a more clear picture of how much error can be ascribed to RT effect versus the error attributable to inaccuracies of the PES itself, fits have been done with and without the inclusion of RT effects. Following Zhou *et al.*,[6] these effects have been taken into account in the vibrational calculations considering an extra term on the PES that is dependent on $\hat{L}_z^2$, with $\hat{L}_z$ being the electronic angular momentum projection on the body-fixed (BF) z-axis. It assumes the form (in atomic units)[6]

$$V_{RT} = \left(\frac{1}{2\mu_R R^2} + \frac{1}{2\mu_r r^2}\right)\frac{\langle \hat{L}_z^2 \rangle}{\sin^2\gamma} - \frac{\langle \hat{L}_z^2 \rangle}{2\mu_r r^2} \tag{1}$$

where (R, r, γ) are Jacobi coordinates; $\mu_R = m_{\rm N}(m_{\rm H} + m_{\rm H})/(m_{\rm N} + m_{\rm H} + m_{\rm H})$ and $\mu_r = m_{\rm H}m_{\rm H}/(m_{\rm H} + m_{\rm H})$. Note that, for $N = 0$, with N the total angular momentum (excluding spin) quantum number, the coupling between the two potential energy sheets is absent and the vibrational calculations can be performed separately.[6, 19]

The paper is organized as follows. Section 2 describes the potential function and technical details of the fitting procedure, while the main features of the resulting PES are in Section 3. A brief description of the performed test dynamics studies will also be presented at this section. Finally, section 4 gathers the conclusions.

2 Potential energy surface recalibration

The Varandas-Poveda[7] single-sheeted DMBE PES for $NH_2(1^2A'')$ assumes the form

$$V(\mathbf{R}) = \sum_{i=1}^{3} V_i^{(2)}(R_i) + V_{\rm EHF}^{(3)}(\mathbf{R}) + V_{\rm dc}^{(3)}(\mathbf{R}) + V_{\rm N(^2D)}^{(1)} f(\mathbf{R}) \qquad (2)$$

where $V_i^{(2)}(R_i)$ are the two-body energy terms, $V_{\rm EHF}^{(3)}$ the three-body extended Hartree-Fock (EHF) energy term, $V_{\rm dc}^{(3)}$ the three-body dynamical correlation energy term, $V_{\rm N(^2D)}^{(1)}$ the difference in energy between ^2D and ^4S states of atomic nitrogen, and $f(\mathbf{R})$ is a switching function specially chosen to warrant the proper dissociation limits at all channels (see Ref. 7 for details).

For the multiproperty[25–27] recalibration, two approaches have been followed resulting in two slightly different new DMBE PESs, hereinafter dubbed as DMBE IIa and DMBE IIb. To obtain DMBE IIa, 18 experimental vibrational frequencies up to above the $D_{\infty h}$ barrier to linearity have been fitted including RT effects in the vibrational calculations, while, for DMBE IIb, only 9 experimental vibrational frequencies up to roughly half of the energy to linearity have been utilized but the RT effects have not been considered. A third fit using the same 18 experimental vibrational frequencies, but not including RT effects in the vibrational calculations, shows very similar results to DMBE IIa fit, except in what concerns the reproducing of the bending frequencies (see below), thus the results of this last fit are not presented.

2.1 Technical details

In the present work, a subset of coefficients of the three-body EHF energy term have been optimized in order to fit the experimental frequencies and the energy points. As in Ref. 7 this term is modeled via a distributed-polynomial[28] form

$$V_{\rm EHF}^{(3)} = \sum_{j=1}^{5} \left\{ P^{(j)}(Q_1,Q_2,Q_3) \prod_{i=1}^{3} \left\{ 1 - \tanh\left[\gamma_i^{(j)} \left(R_i - R_{i,\rm ref}^{(j)} \right) \right] \right\} \right\}$$

where for $j = 1-4$, $P^{(j)}(Q_1,Q_2,Q_3)$ is given by the sixth-order expansion,

$$P^{(j)}(Q_1,Q_2,Q_3) = C_1^{(j)} + C_2^{(j)}Q_1 + C_3^{(j)}Q_3 + C_4^{(j)}Q_1^2 + C_5^{(j)}S_{2a}^2 + C_6^{(j)}Q_1Q_3$$

$$
\begin{aligned}
&+ C_7^{(j)} S_{2b}^2 + C_8 Q_1^3 + C_9^{(j)} Q_1 S_{2a}^2 + C_{10}^{(j)} S_3^3 + C_{11}^{(j)} Q_1^2 Q_3 + C_{12}^{(j)} Q_1 S_{2b}^2 \\
&+ C_{13}^{(j)} Q_3 S_3^3 + C_{14}^{(j)} Q_1^4 + C_{15}^{(j)} Q_1^2 S_{2a}^2 + C_{16}^{(j)} S_{2a}^4 + C_{17}^{(j)} Q_1 S_3^3 \\
&+ C_{18}^{(j)} Q_1^3 Q_3 + C_{19}^{(j)} Q_1^2 S_{2b}^2 + C_{20}^{(j)} Q_1 Q_3 S_{2a}^2 + C_{21}^{(j)} Q_3 S_3^3 + C_{22}^{(j)} S_{2a}^2 S_{2b}^2 \\
&+ C_{23}^{(j)} Q_1^5 + C_{24}^{(j)} Q_1^3 S_{2a}^2 + C_{25}^{(j)} Q_1 S_{2a}^4 + C_{26}^{(j)} Q_1^2 S_3^3 + C_{27}^{(j)} S_{2a}^2 S_3^3 \\
&+ C_{28}^{(j)} Q_1^4 Q_3 + C_{29}^{(j)} Q_1^3 S_{2b}^2 + C_{30}^{(j)} Q_1^2 Q_3 S_{2a}^2 + C_{31}^{(j)} Q_1 Q_3 S_3^3 \\
&+ C_{32}^{(j)} Q_1 S_{2a}^2 S_{2b}^2 + C_{33}^{(j)} Q_3 S_{2a}^4 + C_{34}^{(j)} S_{2b}^2 S_3^3 + C_{35}^{(j)} Q_1^6 + C_{36}^{(j)} Q_1^4 S_{2a}^2 \\
&+ C_{37}^{(j)} Q_1^2 2 S_{2A}^4 + C_{38}^{(j)} Q_1^3 S_3^3 + C_{39}^{(j)} Q_1 S_{2a}^2 S_3^3 + C_{40}^{(j)} S_{2a}^6 + C_{41}^{(j)} S_3^6 \\
&+ C_{42}^{(j)} Q_1^5 Q_3 + C_{43}^{(j)} Q_1^4 S_{2b}^2 + C_{44}^{(j)} Q_1^3 Q_3 S_{2a}^2 + C_{45}^{(j)} Q_1^2 Q_3 S_3^3 \\
&+ C_{46}^{(j)} Q_1^2 S_{2a}^2 S_{2b}^2 + C_{47}^{(j)} Q_1 Q_3 S_{2a}^4 + C_{48}^{(j)} Q_1 S_{2b}^2 S_3^3 + C_{49}^{(j)} Q_3 S_{2a}^2 S_3^3 \\
&+ C_{50}^{(j)} S_{2a}^4 S_{2b}^2 \qquad (3)
\end{aligned}
$$

and for $j = 5$ only a fourth-order expansion is considered (up to $C_{22}^{(5)}$). Symmetry coordinates have been defined as[28–31]

$$
\begin{bmatrix} Q_1 \\ Q_2 \\ Q_3 \end{bmatrix} = \begin{bmatrix} \sqrt{1/3} & \sqrt{1/3} & \sqrt{1/3} \\ \sqrt{1/2} & -\sqrt{1/2} & 0 \\ -\sqrt{1/6} & -\sqrt{1/6} & \sqrt{2/3} \end{bmatrix} \begin{bmatrix} R_1 - R_{1,\mathrm{ref}}^{(j)} \\ R_2 - R_{2,\mathrm{ref}}^{(j)} \\ R_3 - R_{3,\mathrm{ref}}^{(j)} \end{bmatrix} \qquad (4)
$$

as well as $S_{2a}^2 = Q_2^2 + Q_3^2$, $S_{2b}^2 = Q_2^2 - Q_3^2$, and $S_3^3 = Q_3^3 - 3Q_2^2 Q_3$; for brevity, we omit any reference to the polynomial index in labeling the Q_i. As in Ref. 10, the complete set of parameters consists of 222 $C_i^{(j)}$, 5 $\gamma_i^{(j)}$, and 5 $R_{i,\mathrm{ref}}^{(j)}$ but, in the present work, only 50 of those parameters, corresponding to the $j = 3$ polynomial, centered near the equilibrium geometry, have been optimized. Our fitting code uses the routine LMDER of the package MINPACK,[32] which is a version[33] of the Levenberg-Marquardt method. The objective function

$$
F = \sum_{i=1}^{N_p} w_i \left(V\left[\mathbf{R}(i); C_k^{(j)}\right] - V_i^{\mathrm{ab}} \right)^2 + \sum_{v=1}^{M} w_v \left(E_v^{\mathrm{calc}}[C_k^{(j)}] - E_v^{\mathrm{exp}} \right)^2 \qquad (5)
$$

was minimized in order to fit $N_p = 1498$ energy points,[7] V_i^{ab}, and a maximum of $M = 18$ experimental vibrational frequencies,[3, 4] E_v^{exp}, with weights w_i and w_v respectively; w_v are given in Table 1 and $w_i = \max(1, w_i'/10^5)$ with w_i' being the original weights of Ref. 7. The theoretical vibrational spectra is calculated using

Table 1. Experimental and calculated vibrational energies (presented as the difference from calculated to experimental values, in cm^{-1}) for NH_2. For the DMBE potentials: the non-fitted frequencies are reported in italic; w_v are the weights used in the fitting procedure.

(n_1, n_2, n_3)	exp.[a]	calc.-exp. DMBE I[b]	calc.-exp. without RT[c]	calc.-exp. with RT[c]	calc.-exp. DMBE IIa[d]	calc.-exp. DMBE IIb[d]	$w_v/10^3$
(0 1 0)	1497.32	-6.28	7.37	9.64	-0.13	-0.11	10
(0 2 0)	2961.24	-3.18	-1.57	3.69	0.15	0.16	10
(1 0 0)	3219.37	-7.39	8.99	8.29	0.01	0.00	10
(0 0 1)	3301.11	-32.26	19.89	19.23	0.02	0.01	10
(0 3 0)	4391.35	2.99	1.15	10.73	-0.09	-0.10	10
(0 4 0)	5785.55	9.34	-3.87	11.72	-0.02	0.02	10
(1 2 0)	6151.95	-25.00	13.80	18.35	-0.79	-0.09	1
(2 0 0)	6335.15	-25.56	26.88	25.84	-0.69	0.18	1
(0 5 0)	7140.35	13.42	-15.30	10.45	0.54	0.05	1
(1 3 0)	7564.63	-18.08	15.05	23.64	0.03	*0.58*	1
(2 1 0)	7804.54	-48.79	32.39	33.54	0.84	*2.52*	1
(0 1 2)	8000.40	-70.30	47.35	48.19	-0.60	*-6.92*	0.1
(0 6 0)	8451.45	9.81	-35.36	10.58	0.94	*-3.89*	0.1
(1 4 0)	8942.59	-11.76	10.40	25.33	0.17	*-0.25*	1
(2 2 0)	9227.14	-41.48	33.15	36.73	-0.24	*0.09*	1
(0 2 2)	9421.50	-62.17	51.72	54.77	*1.54*	*0.67*	-
(0 7 0)	9716.90	-18.03	-86.88	8.07	-0.14	*-26.16*	0.01
(1 5 0)	10286.30	-13.03	-6.05	21.59	-3.16	*-8.21*	0.1
(2 3 0)	10609.00	-27.13	44.68	52.87	11.42	*8.93*	0.1
(0 8 0)	10948.00	-109.23	-198.66	8.88	*4.12*	*-101.84*	-
(0 10 0)	13448.60	-408.99	-446.26	20.74	*25.16*	*-396.45*	-
rmsd	-	96.76	110.96	26.60	6.16	89.56	

[a] Refs. 3, 4.[b] Ref. 7.[c] Ref. 6.[d] This work.

Table 2. Stratified root-mean-square deviations (in kcal mol^{-1}) between DMBE PESs and *ab initio* points.

Points	energy	DMBE I[a]	DMBE IIa[b]	DMBE IIb[b]
141	20	0.045	0.091	0.195
184	40	0.251	0.389	0.369
218	60	0.283	0.484	0.445
259	80	0.296	0.550	0.501
404	100	0.286	0.527	0.482
600	120	0.341	0.527	0.482
1421	200	0.428	0.514	0.491
1498	2400	0.474	0.566	0.539

[a] Ref. 7. [b] This work.

the DVR3D suite[34] in Radau coordinates; the assignment of vibrational states is based in the previously used scheme[25, 26] including a complementary harmonic progressions test. In each step of the iterative fitting process, the lowest 200 vibrational levels ($N = 0$) of the potential energy function were calculated in Radau coordinates using the DVR3D program suite[34] which uses a discrete variable representation (DVR) for each coordinate and is based on the Tennyson and Sutcliffe methodology.[35] For the radial coordinates, the number of the DVR grid points (based on Morse oscillator-like functions) have been set to 29 with the variational Morse parameters being optimized and set to $r_e = 2.00\,a_0$, $D_e = 0.17\,E_h$, and $\omega_e = 0.008\,E_h$. For the bending the number of grid DVR points (based on the associated Legendre polynomials) have been set to 80. According to the DVR3D methodology[34, 36] the calculation was set up as a series of diagonalizations using the order $r_2 \rightarrow r_1 \rightarrow \theta$ and using the lowest 500 $1D$ states together with an energy cutoff of 0.0 cm^{-1} (referred to the PES minimum of -62748 cm^{-1}), to obtain the final Hamiltonian matrix of dimension 2000×2000; as in previous studies[25, 26] even-odd symmetry was not considered for simplicity. Based on comparisons with calculations with larger Hamiltonian matrices and more functions per coordinate the calculated levels should be converged within 0.01 cm^{-1} or better. For the RT contributions to the potential in the vibrational calculations the extra term in Eq. (1) have been used; the angular variation of $\langle \hat{L}_z^2 \rangle$ has been taken (in atomic units) as $\langle \hat{L}_z^2 \rangle = [1 + s_1(\alpha - \pi)^4]s_2$ ($s_1 = 0.05(1 + \tanh[10(\alpha - \pi/4)])$,

Table 3. Experimental and calculated vibrational energies (presented as the difference from calculated to experimental values, in cm^{-1}) for NH_2 isotopomers (these frequencies have not been used in the calibration of the PES).

(n_1, n_2, n_3)	exp.[a]	calc.-exp. DMBE I[b]	calc.-exp. Zhou et al.[c]	calc.-exp. DMBE IIa[d]	calc.-exp. DMBE IIb[d]
ND_2					
(0 1 0)	1108.75	4.85	-13.50	1.97	0.31
NHD					
(0 1 0)	1321	7.89	-8.65	3.58	2.55
$^{15}NH_2$					
(0 1 0)	1495.5	8.39	-7.39	2.23	2.24
(1 0 0)	3215	7.66	-8.25	0.49	0.44

[a] Refs. 39, 42.[b] Ref. 7.[c] Ref. 6.[d] This work.

$s_2 = 0.5\,\{1 - \tanh[10(R_1 + R_2 + R_3 - 9.8)]\}$, and α is the bending angle between R_2 and R_3), which reproduces with reasonable accuracy the calculated *ab initio* values. Note that $\langle \hat{L}_z^2 \rangle = 1$ a.u. is the exact value at some linear geometries. The partial derivatives of the vibrational energy with respect to the parameters in the PES which are required for the least-squares fitting procedure have been calculated using the Hellmann-Feynman theorem

$$\frac{\partial E_n}{\partial C_i^{(j)}} = < n | \frac{\partial V\left(R_1, R_2, R_3; C_i^{(j)}\right)}{\partial C_i^{(j)}} | n > \tag{6}$$

using the wavefunction values at the grid points.[37] As in previous work,[25, 26] the attribution of the quantum numbers has been made automatically. The vibrational quantum numbers are first estimated as[38]

$$n_i = \frac{1}{2} \frac{< n | \Delta Q_i^2 | n >}{< 0 | \Delta Q_i^2 | 0 >} - \frac{1}{2} \tag{7}$$

where $\Delta Q_i^2 = Q_i^2 - < Q_i >^2$, with Q_i corresponding to the normal modes eigenvectors calculated at the equilibrium geometry. This assignment is then corrected using harmonic progressions of levels and monitorized by fitting the resulting fre-

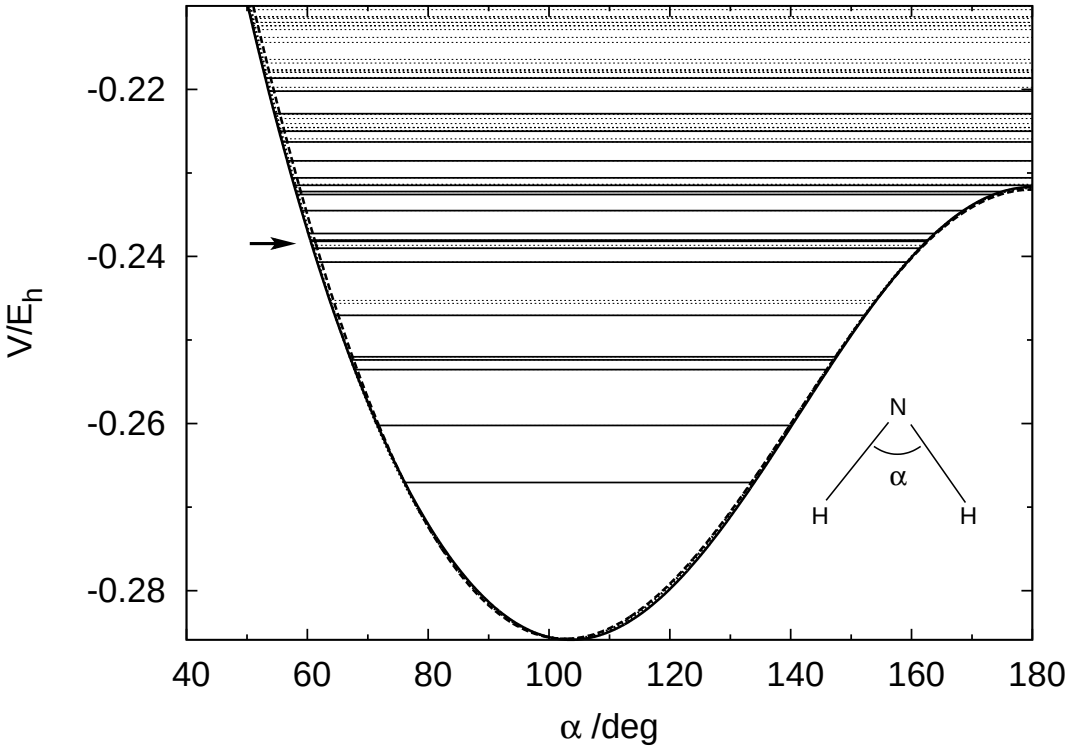

Figure 1. Optimized NH_2 C_{2v} bending curve: DMBE I[7] (*dashed line*); DMBE IIa (*solid*; this work); DMBE IIb (*dotted*, this work). Horizontal thin line segments show the calculated vibrational levels: fitted frequencies (*solid*); frequencies not fitted (*dotted*). The arrow indicates the approximate energy of the top fitted level in DMBE IIb PES.

quencies to a Dunham expansion

$$E_n = \sum_{i=1}^{3} \left(n_i + \frac{1}{2} \right) \omega_i + \sum_{i=1}^{3} \sum_{j=1}^{3} \left(n_i + \frac{1}{2} \right) \left(n_j + \frac{1}{2} \right) x_{ij}$$

and also by inspecting wavefunction plots. The fit started with the parameters from Ref. 7, with the final parameters reported as supplementary material. The root mean squared deviations of the fit to the energy points is shown in Table 2, while the initial and final deviations relative to the fitted vibrational levels is given in Table 1. In addition to the available experimental data, Table 1 gives the theoretical estimates based on other PESs. As Table 2 shows, the DMBE fits from the present work reproduce the *ab initio* energies only slightly poorer than the Varandas-Poveda potential.[7] However, this is compensated by the more

accurate description now reported of the vibrational levels, which are reproduced within $1\,\mathrm{cm}^{-1}$ or so for frequencies below the linear barrier (see Figure 1) when compared to the measured values. As also shown from Table 1, the current fits reproduce the spectroscopic data with a smaller root mean-squared deviation (rmsd) than the recently calculated PES of Zhou *et al.*[6]

The vibrational levels calculated for the isotopomers ND_2, NHD, and $^{15}NH_2$ are shown in Table 3. These have not been included in the fits here reported, and hence may serve as a test on the predictive capability of the present DMBE IIa and DMBE IIb forms. The agreement with experiment is quite satisfactory, although caution must be exercised by noting that such matrix-isolation infrared measurements of Milligan and Jacox[39] are expected to have an associated error of a few cm^{-1}. Rotational-vibrational term values have also been calculated up to $N = 3$ (presented as additional information) using the using the DVR3D and ROTLEV3 suite.[34] The agreement with experimental and other accurate calculations is good, showing that the present fit do not introduce any significant bias in the potential.

The fit without RT effects, including only 9 vibrational levels (DMBE IIb) shows a performance almost identical to the one including levels up to the top of the barrier and RT effects except in what concerns the bending levels. Indeed, the bending levels which are prone to be naturally affected by the RT effect cannot be fitted irrespective of the weights assigned to such levels provided that spurious features are avoided.

3 Features of potential energy function

The features of the new DMBE IIa and IIb potential energy surfaces (see Figure 2 for DMBE IIa) are very similar to the previous DMBE I ones, particularly at regions far from the global minimum (where the parameters optimized in the present work are centered). Indeed, one expects small deviations from the start, since the very purpose of a direct fitting technique is to convey spectroscopic accuracy without endangering the quality of the original fit to accurate *ab initio* points.[40] As can be seen from Table 4, which gathers the stationary

Table 4. Stationary points at the valence region of the $NH_2(1^2A'')$ potential energy surfaces.

Feature	property	ab initio[a]	RKHS[a]	ZXLG[b]	DMBE I[c]	DMBE IIa[d]	DMBE IIb[d]	exp.
Global	r_e(NH)/a_0	1.9445	1.94	1.923	1.9405	1.9377	1.9411	1.9377(23)[e]
minimum	∠HNH/deg	102.7	102.7	102.61	102.6	103.6	103.9	102.85(14)[e], 103.36[e]
	V/E_h				-0.2858	-0.2859	-0.2859	
	ΔE^h/kcal mol^{-1}	-126.4	-126.4	-128.93	-126.4	-126.47	-126.46	
	ω_s/cm^{-1}	3340	3350		3383	3381	3382	3374[f]
	ω_{as}/cm^{-1}	3435	3436		3457	3491	3491	3481[f]
	ω_b/cm^{-1}	1542	1559		1541	1548	1548	1524[f]
Linear	r_e(NH)/a_0	1.8695				1.8694	1.8657	
barrier	V/E_h					-0.23169	-0.23171	
	ΔE^i/cm^{-1}				11802	11894	11886	11914[f], 11774[g]
	ω_s/cm^{-1}	3676				3674	3706	
	ω_{as}/cm^{-1}	6979				4101	4122	
	ω_b/cm^{-1}	1544				1575i	1582i	
C_{2v} barrier	r_e(NH)/a_0	1.42	1.42	1.419	1.4198	1.4196	1.4202	
N(^2D)−H_2	R/a_0	3.99	3.99		3.8703	3.9444	3.9427	
	V/E_h				-0.0809	-0.08088	-0.08087	
	ΔE^e/kcal mol^{-1}	1.8	1.8	1.948	2.16	2.17	2.17	
	ω_s/cm^{-1}	4239	4240		4209	4215	4210	
	ω_{as}/cm^{-1}	501i	499i		499i	499i	500i	
	ω_b/cm^{-1}	324	325		282	285	278	
$C_{\infty v}$	r_e(HH)/a_0	1.539	1.54	1.55	1.5121	1.4836	1.4843	
barrier	r_e(NH)/a_0	2.913	2.93	2.869	2.9010	2.9787	2.9744	
	V/E_h				-0.0763	-0.07609	-0.07606	
	ΔE^e/kcal mol^{-1}	4.8	4.8	4.925	5.1	5.17	5.19	
	ω_s/cm^{-1}	3031	2616		2671	2920	2910	
	ω_{as}/cm^{-1}	1031i	1032i		1455i	814i	812i	
	ω_b/cm^{-1}	818i	764i		844i	817i	824i	

[a] Ref. 15.[b] Ref. 16.[c] Ref. 7.[d] This work.[e] Ref. 2, 41.[f] Ref. 3.[g] Ref. 4.[h] Relative to the N(^{2}D) + H_2 asymptote (−0.084335 E_h).[i] Relative to the global minimum.

points features of the PES, the C_{2v} and $C_{\infty v}$ barriers are nearly identical in all DMBE potentials. In fact, maintaining the topography of these barriers has been considered very important to warrant that the reactivity predicted from the original DMBE form of Varandas and Poveda (*i.e.*, DMBE I) will not be altered but, if possible, be even slightly improved. This was verified with exploratory quasiclassical trajectory (QCT) calculations that we have carried out for the reaction $N(^2D) + H_2(X^1\Sigma_g^+)$. Since the calculations are essentially identical to the ones reported for DMBE I,[10] we just mentioned that batches of 10^4 trajectories have been run on the new PESs at $T = 300\,K$ yielding a rotational specific ($j = 0$) rate constant (in units of $10^{-12}cm^3s^{-1}$) of $k_0 = 1.36 \pm 0.07$ for both DMBE IIa and DMBE IIb (the corresponding value for DMBE I is $k_0 = 1.42 \pm 0.06$), thus overlapping each other within their mutual uncertainties. At this temperature, the agreement extends to other rotational-specific rate constants. In order to test if the small differences in the wells of DMBE I and DMBE II surfaces manifest at lower temperature, thermalized calculations have also been done for $T = 200\,K$. At this temperature, the calculated rate constant is $k = 2.3 \pm 0.3 \times 10^{-13} cm^3\,s^{-1}$ which is slightly higher than the value of $k = 1.9 \pm 0.3 \times 10^{-13} cm^3\,s^{-1}$ obtained previously for DMBE I. Note that the Arrhenius forms presented in Ref. 10 have been misprinted, with a factor of 10^3 missing: the correct expressions are $k(T) = (9.8 \pm 0.8) \times 10^{-11} \exp[-(1247 \pm 26)/T] cm^3\,s^{-1}$ and $k(T) = (9.2 \pm 0.6) \times 10^{-11} \exp[-(1099 \pm 25)/T] cm^3\,s^{-1}$ for thermalized QCT and quantum closed coupling (CC) calculations, respectively. The results are found to be insentive to the addition of the RT-diagonal term in Eq. (1). At the global minimum, the equilibrium angle of the DMBE IIa and IIb PESs are slightly larger than the available experimental and theoretical results.[2, 41] This feature is consistent in DMBE IIa and DMBE IIb and appears to be a result of the inclusion of the vibrational frequencies in the optimization procedure; note that the DMBE I and all other PESs show equilibrium bond angles slightly smaller than the experimental value.[2, 41] Regarding the equilibrium internuclear distance, DMBE IIa has the value closest to the experimental result as surveyed in Ref. 41. As for the barrier to linearity, both the DMBE IIa and DMBE IIb PESs show close agreement with the Varandas-Poveda[7] prediction of $11802\,cm^{-1}$, and the value of Gabriel *et al.*[3] of $11914\,cm^{-1}$. Shown in Figures 3 and 4 are contour

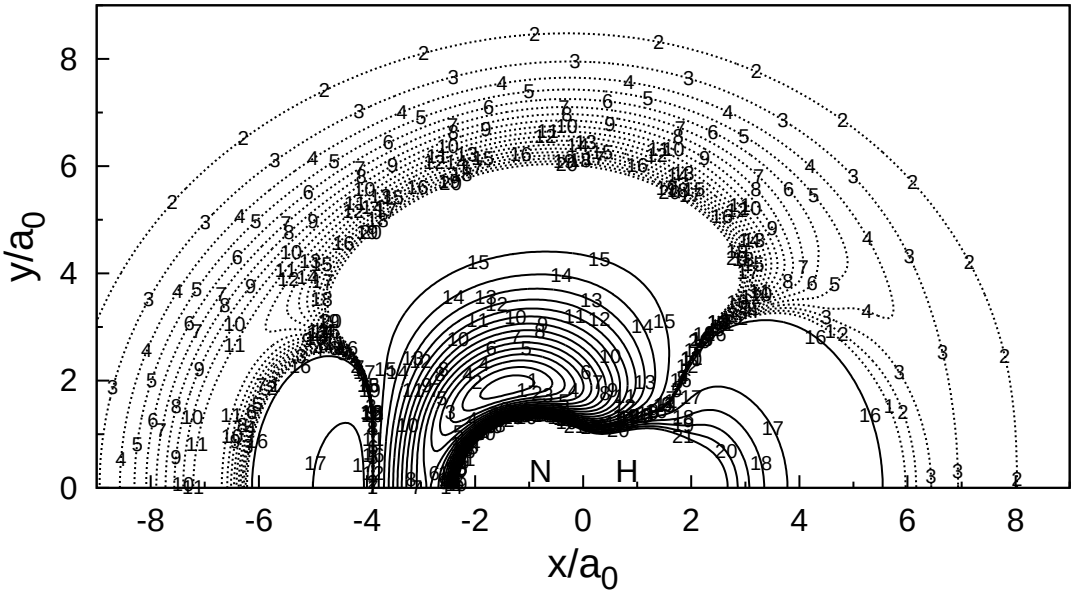

Figure 2. Contour plot for a H atom moving around a NH diatomic fixed at the equilibrium geometry, $1.965\,a_0$ for DMBE IIa PES. Solid contours start at $-0.29\,E_h$ with $\Delta E = 0.01\,E_h$. Dotted contours start at $-0.130208\,E_h$, with $\Delta E = -0.00005\,E_h$.

plots of the energy differences between DMBE I and DMBE IIa PESs. As it is observed, for the most relevant configurations such differences are of $< 10\,cm^{-1}$. Generically, they are $< 1\,kcal\,mol^{-1}$.

Finally, it must be stressed that to study RT coupling effects, the excited-state $1^2A'$ DMBE potential can easily be made degenerate with the present ground state $1^2A''$ DMBE potentials by using the switching function formalism reported in Ref. 12.

4 Concluding remarks

In this work we have recalibrated the spectroscopic properties of the single-sheeted DMBE PES for $NH_2(1^2A'')$ within $< 1\,cm^{-1}$ (below the barrier for linearity) while maintaining the quality of *ab initio*-based fit everywhere else. Our results, obtained including the Renner-Teller effect for $N = 0$ are consistent with the experimental[3, 4] data and recent theoretical studies.[6, 16] We expect to address the Renner-Teller effect for $N > 0$ and for studying reactivity in future work.

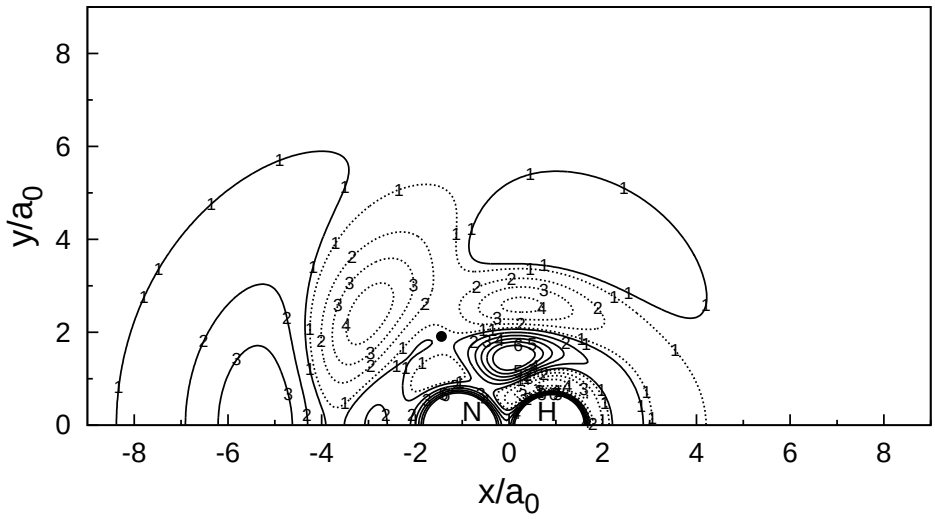

Figure 3. Contour plot of the energy difference between DMBE I and DMBE IIa PES for a H atom moving around a NH diatomic fixed at the equilibrium geometry, $1.965\,a_0$. Solid contours start at $0.0001\,E_h$ with $\Delta E = 0.0005\,E_h$. Dotted contours start at $-0.0001\,E_h$, with $\Delta E = -0.0005\,E_h$. The position of the minimum is indicated by a solid dot.

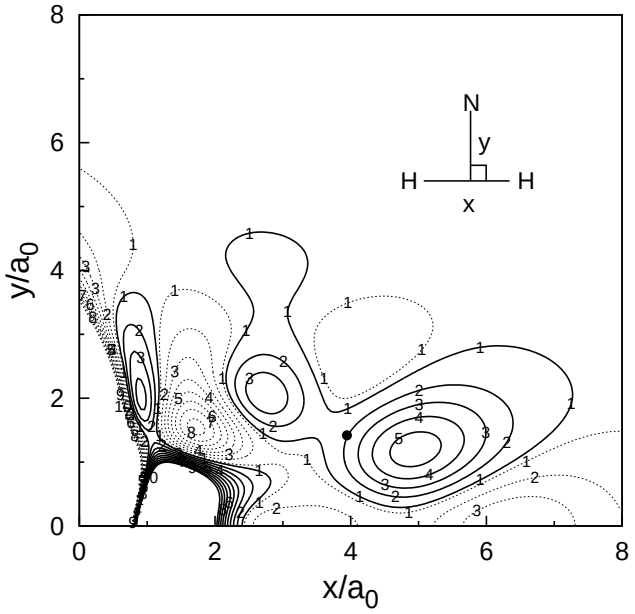

Figure 4. Contour plot of the energy difference between DMBE I and DMBE IIa PES for the C_{2v} insertion of a H atom into a H_2 molecule. Solid contours start at $0.0001\,E_h$ with $\Delta E = 0.0005\,E_h$. Dotted contours start at $-0.0001\,E_h$, with $\Delta E = -0.0005\,E_h$. The position of the C_{2v} barrier is indicated by a solid dot.

Acknowledgments

This work has the support of Fundação para a Ciência e Tecnologia, Portugal, under contracts PTDC/QUI-QUI/099744/2008 and PTDC/AAC-AMB/099737/2008.

References and Notes

[1] G. Herzberg and D. A. Ramsay, J. Chem. Phys. 20 (1952) 347.

[2] K. Dressler and D. A. Ramsay, Philos. Trans. R. Soc. London Ser. A 25 (1959) 553.

[3] W. Gabriel, G. Chambaud, P. Rosmus, S. Carter and N. C. Handy, Mol. Phys. 6 (1994) 1445.

[4] A. Alijah and G. Duxbury, J. Mol. Spectrosc. 211 (2002) 16.

[5] G. Duxbury and A. Alijah, J. Mol. Spectrosc. 211 (2002) 31.

[6] S. Zhou, Z. Li, D. Xie, S. Y. Lin and H. Guo, J. Chem. Phys. 130 (2009) 184307.

[7] A. J. C. Varandas and L. A. Poveda, Theor. Chem. Acc. 116 (2006) 404.

[8] A. J. C. Varandas, J. Chem. Phys. 90 (1989) 4379.

[9] T.-S. Chu, K.-L. Han and A. J. C. Varandas, J. Phys. Chem. A 110 (2006) 1666.

[10] A. J. C. Varandas, T.-S. Chu, K.-L. Han and P. J. S. Caridade, Chem. Phys. Lett. 421 (2006) 415.

[11] B. Han, H. Yang, Y. Zheng and A. J. C. Varandas, Chem. Phys. Lett. 493 (2010) 225.

[12] Y. Q. Li and A. J. C. Varandas, J. Phys. Chem. A 114 (2010) 9644.

[13] A. J. C. Varandas, J. Chem. Phys. 126 (2007) 244105.

[14] L. Pederson, G. Schatz, T.-S. Ho, T. Hollebeek, H. Rabitz, L. B. Harding and G. Lendvay, J. Chem. Phys. 110 (1999) 9091.

[15] T.-S. Ho, H. Rabitz, F. J. Aoiz, L. Bañares, S. A. Vázquez and L. B. Harding, J. Chem. Phys. 119 (2003) 3063.

[16] S. Zhou, D. Xie, S. Y. Lin and H. Guo, J. Chem. Phys. 128 (2008) 224316.

[17] L. Pederson, G. Schatz, T. Hollebeek, T.-S. Ho, H. Rabitz, L. B. Harding and L. B. Harding, J. Phys. Chem. A 104 (2000) 2301.

[18] R. J. Buenker, M. Perić, S. D. Peyerimhoff and R. Marian, Mol. Phys. 43 (1981) 987.

[19] P. Jensen, T. E. Odaka, W. P. Kraemer, T. Hirano and P. R. Bunker, Spectrochimica Acta A 58 (2002) 763.

[20] Z.-W. Qu, H. Zhu, R. Schinke, L. Adam and W. Hack, J. Chem. Phys. 122 (2005) 204313.

[21] F. Santoro, C. Petrongolo and G. C. Schatz, J. Phys. Chem. A 106 (2002) 8276.

[22] L. Adam, W. Hack, G. C. McBane, H. Zhu, Z. Qu and R. Schinke, J. Chem. Phys. 126 (2007) 034304.

[23] P. Gamallo, P. Defazio, M. González and C. Petrongolo, J. Chem. Phys. 129 (2008) 244307.

[24] S. Y. Lin, L. Bañares and H. Guo, J. Phys. Chem. A 111 (2007) 2376.

[25] A. J. C. Varandas and S. P. J. Rodrigues, Spectrochimica Acta A 58 (2002) 629.

[26] A. J. C. Varandas and S. P. J. Rodrigues, J. Phys. Chem. A 424 (2006) 485.

[27] A. J. C. Varandas, S. P. J. Rodrigues and V. M. O. Batista, Chem. Phys. Lett. 424 (2006) 425.

[28] E. Martínez-Núñez and A. J. C. Varandas, J. Phys. Chem. A 105 (2001) 5923.

[29] A. J. C. Varandas and J. N. Murrell, Faraday Discuss. Chem. Soc. 62 (1977) 92.

[30] A. J. C. Varandas and J. N. Murrell, Chem. Phys. Lett. 88 (1981) 440.

[31] M. R. Pastrana, L. A. M. Quintales, J. Brandão and A. J. C. Varandas, J. Phys. Chem. 94 (1990) 8073.

[32] J. J. Moré, B. S. Garbow, and K. E. Hillstrom, Argonne National Laboratory, 1980; MINPACK package can be obtained from `http://www.netlib.org/minpack/`.

[33] J. J. Moré, in: Numerical Analysis, Lecture Notes in Mathematics, vol. 630, ed. G. A. Watson (Springer-Verlag, Berlin, 1977) p. 105.

[34] J. Tennyson, M. A. Kostin, P. Barletta, G. J. Harris, O. L. Polyansky, J. Ramanlal and N. F. Zobov, Comput. Phys. Commun. 163 (2004) 85.

[35] J. Tennyson and B. T. Sutcliffe, Int. J. Quant. Chem. 42 (1992) 941.

[36] J. Tennyson, J. R. Henderson and N. G. Fulton, Comput. Phys. Commun. 86 (1995) 175.

[37] C. D. Paulse and J. Tennyson, Mol. Phys. 168 (1994) 313.

[38] M. Menou and C. Leforestier, Chem. Phys. Lett. 210 (1994) 294.

[39] D. E. Milligan and M. E. Jacox, J. Chem. Phys. 43 (1965) 4487.

[40] A. J. C. Varandas, Physica Scripta; Comm. At. Opt. Mol. Phys. 76 (2007) C28.

[41] J. Demaison, L. Margulès and J. E. Boggs, Phys. Chem. Chem. Phys. 5 (2003) 3359.

[42] G. W. Hills and A. R. W. McKellar, J. Chem. Phys. 71 (1979) 3330.

Chem. Phys. Lett. **516**, 17-22 (2011).

Refining to near spectroscopic accuracy the double many-body expansion potential energy surface for ground-state NH_2

S.P.J. Rodrigues, A.C.G. Fontes, Y.Q. Li and A.J.C. Varandas

Departamento de Química, Universidade de Coimbra
3004-535 Coimbra Codex, Portugal.

(Received: August 1, 2011; In final form: September 21, 2011)

1 Suplementary material

Tables with the parameters of the EHF term of the DMBE II potentials and mean term rotational-vibrational energies up to $N = 3$.

Table 1. Fixed EHF parameters of the DMBE PES for NH_2 (in atomic units).

$C_1^{(1)}$= 0.28972574E+00	$C_2^{(1)}$= -0.55810849E+00	$C_3^{(1)}$= 0.35597867E+00
$C_4^{(1)}$= 0.30113790E-01	$C_5^{(1)}$= 0.25264641E+00	$C_6^{(1)}$= 0.71505040E-01
$C_7^{(1)}$= -0.25255300E-02	$C_8^{(1)}$= -0.21020530E+00	$C_9^{(1)}$= -0.10344050E-01
$C_{10}^{(1)}$= -0.56372700E-02	$C_{11}^{(1)}$= -0.40826443E+00	$C_{12}^{(1)}$= 0.43715500E-02
$C_{13}^{(1)}$= 0.24320295E+00	$C_{14}^{(1)}$= 0.58137000E-02	$C_{15}^{(1)}$= 0.52888720E-01
$C_{16}^{(1)}$= 0.75320790E-01	$C_{17}^{(1)}$= -0.32346470E-01	$C_{18}^{(1)}$= -0.10993160E-01
$C_{19}^{(1)}$= 0.36429000E-01	$C_{20}^{(1)}$= 0.15570612E+00	$C_{21}^{(1)}$= -0.39944820E-01
$C_{22}^{(1)}$= -0.59561850E-01	$C_{23}^{(1)}$= -0.62179700E-02	$C_{24}^{(1)}$= -0.27642050E-01
$C_{25}^{(1)}$= 0.15146780E-01	$C_{26}^{(1)}$= -0.28543790E-01	$C_{27}^{(1)}$= -0.10637500E-01
$C_{28}^{(1)}$= -0.28623610E-01	$C_{29}^{(1)}$= 0.24583000E-01	$C_{30}^{(1)}$= -0.21405070E-01
$C_{31}^{(1)}$= -0.57777600E-01	$C_{32}^{(1)}$= -0.16651480E-01	$C_{33}^{(1)}$= 0.21228470E-01
$C_{34}^{(1)}$= 0.19141940E-01	$C_{35}^{(1)}$= 0.24721800E-02	$C_{36}^{(1)}$= -0.12110480E-01
$C_{37}^{(1)}$= -0.71149700E-02	$C_{38}^{(1)}$= -0.18725770E-01	$C_{39}^{(1)}$= -0.12053570E-01
$C_{40}^{(1)}$= 0.41321600E-02	$C_{41}^{(1)}$= -0.41404200E-02	$C_{42}^{(1)}$= 0.12606300E-02
$C_{43}^{(1)}$= 0.13323720E-01	$C_{44}^{(1)}$= -0.37877710E-01	$C_{45}^{(1)}$= -0.26001130E-01
$C_{46}^{(1)}$= 0.11814540E-01	$C_{47}^{(1)}$= 0.95198500E-02	$C_{48}^{(1)}$= 0.12782030E-01
$C_{49}^{(1)}$= -0.48639300E-02	$C_{50}^{(1)}$= -0.14241900E-02	$C_1^{(1)}$= -0.22388382E+01
$C_2^{(2)}$= 0.13479885E+01	$C_3^{(2)}$= 0.25147920E+01	$C_4^{(2)}$= 0.46600400E-01
$C_5^{(2)}$= 0.32033747E+00	$C_6^{(2)}$= 0.79618730E-01	$C_7^{(2)}$= -0.21360102E+00
$C_8^{(2)}$= 0.33599947E+00	$C_9^{(2)}$= -0.29850390E-01	$C_{10}^{(2)}$= -0.15730581E+00
$C_{11}^{(2)}$= 0.23927521E+00	$C_{12}^{(2)}$= 0.33805178E+00	$C_{13}^{(2)}$= 0.52130976E+00
$C_{14}^{(2)}$= 0.10163321E+00	$C_{15}^{(2)}$= 0.14376423E+00	$C_{16}^{(2)}$= 0.15183690E-01
$C_{17}^{(2)}$= 0.23345430E-01	$C_{18}^{(2)}$= -0.21441955E+00	$C_{19}^{(2)}$= 0.32734850E-01
$C_{20}^{(2)}$= -0.59012730E-01	$C_{21}^{(2)}$= -0.23208490E-01	$C_{22}^{(2)}$= 0.73405890E-01
$C_{23}^{(2)}$= -0.84108000E-03	$C_{24}^{(2)}$= -0.53669660E-01	$C_{25}^{(2)}$= -0.24028500E-01
$C_{26}^{(2)}$= -0.18439500E-01	$C_{27}^{(2)}$= -0.33668800E-02	$C_{28}^{(2)}$= 0.27675990E-01
$C_{29}^{(2)}$= -0.76473400E-02	$C_{30}^{(2)}$= 0.84816490E-01	$C_{31}^{(2)}$= -0.11279160E-01
$C_{32}^{(2)}$= 0.53856740E-01	$C_{33}^{(2)}$= 0.17304480E-01	$C_{34}^{(2)}$= -0.17636770E-01
$C_{35}^{(2)}$= 0.52889500E-02	$C_{36}^{(2)}$= 0.38549900E-02	$C_{37}^{(2)}$= -0.79568300E-02
$C_{38}^{(2)}$= -0.71293000E-03	$C_{39}^{(2)}$= -0.40159900E-02	$C_{40}^{(2)}$= -0.77721000E-03
$C_{41}^{(2)}$= -0.42295000E-03	$C_{42}^{(2)}$= -0.16425190E-01	$C_{43}^{(2)}$= -0.90664500E-02
$C_{44}^{(2)}$= 0.11780700E-02	$C_{45}^{(2)}$= 0.82075200E-02	$C_{46}^{(2)}$= 0.82103600E-02
$C_{47}^{(2)}$= 0.11906000E-01	$C_{48}^{(2)}$= 0.15973000E-02	$C_{49}^{(2)}$= 0.64467000E-02
$C_{50}^{(2)}$= -0.27149000E-03		

(Table 5: cont.)

$C_1^{(4)}$= -0.10345479E+02	$C_2^{(4)}$= 0.68214645E+01	$C_3^{(4)}$= -0.16511647E+02
$C_4^{(4)}$= 0.41925703E+01	$C_5^{(4)}$= -0.31531844E+01	$C_6^{(4)}$= -0.16437615E+02
$C_7^{(4)}$= -0.36136157E+01	$C_8^{(4)}$= 0.25696468E+01	$C_9^{(4)}$= -0.30955447E+01
$C_{10}^{(4)}$= 0.11729748E+01	$C_{11}^{(4)}$= -0.12795762E+01	$C_{12}^{(4)}$= 0.42694465E+01
$C_{13}^{(4)}$= -0.49508061E+00	$C_{14}^{(4)}$= 0.89781794E+00	$C_{15}^{(4)}$= 0.10335586E+01
$C_{16}^{(4)}$= 0.32623867E+00	$C_{17}^{(4)}$= -0.10641794E+01	$C_{18}^{(4)}$= -0.26394441E+01
$C_{19}^{(4)}$= -0.11869115E+01	$C_{20}^{(4)}$= -0.47108207E+01	$C_{21}^{(4)}$= 0.10004673E+01
$C_{22}^{(4)}$= -0.67036214E+00	$C_{23}^{(4)}$= 0.14299508E+00	$C_{24}^{(4)}$= -0.99916190E+00
$C_{25}^{(4)}$= -0.82278451E+00	$C_{26}^{(4)}$= 0.22691603E+00	$C_{27}^{(4)}$= 0.40056270E+00
$C_{28}^{(4)}$= 0.75973486E+00	$C_{29}^{(4)}$= 0.95557878E+00	$C_{30}^{(4)}$= 0.12347535E+01
$C_{31}^{(4)}$= -0.18269793E+00	$C_{32}^{(4)}$= 0.97068822E+00	$C_{33}^{(4)}$= 0.49320770E+00
$C_{34}^{(4)}$= -0.22657901E+00	$C_{35}^{(4)}$= 0.19971700E-01	$C_{36}^{(4)}$= 0.39887510E-01
$C_{37}^{(4)}$= 0.19528166E+00	$C_{38}^{(4)}$= -0.78854540E-01	$C_{39}^{(4)}$= -0.91683830E-01
$C_{40}^{(4)}$= 0.23456180E-01	$C_{41}^{(4)}$= 0.27109770E-01	$C_{42}^{(4)}$= -0.36761250E-01
$C_{43}^{(4)}$= -0.59784200E-02	$C_{44}^{(4)}$= -0.28878921E+00	$C_{45}^{(4)}$= 0.70887480E-01
$C_{46}^{(4)}$= -0.24948561E+00	$C_{47}^{(4)}$= -0.23974016E+00	$C_{48}^{(4)}$= 0.15995300E-01
$C_{49}^{(4)}$= 0.10016699E+00	$C_{50}^{(4)}$= -0.20059570E-01	$C_1^{(5)}$= 0.33641700E-02
$C_2^{(5)}$= 0.40245800E-02	$C_3^{(5)}$= 0.77129200E-02	$C_4^{(5)}$= 0.12681360E-01
$C_5^{(5)}$= 0.12746660E-01	$C_6^{(5)}$= 0.36319290E-01	$C_{207}^{(5)}$= -0.15018760E-01
$C_8^{(5)}$= 0.51759200E-02	$C_9^{(5)}$= 0.24179860E-01	$C_{10}^{(5)}$= 0.68263600E-02
$C_{11}^{(5)}$= 0.28040540E-01	$C_{12}^{(5)}$= -0.24833530E-01	$C_{13}^{(5)}$= 0.21434040E-01
$C_{14}^{(5)}$= -0.16475900E-02	$C_{15}^{(5)}$= -0.19509600E-02	$C_{16}^{(5)}$= 0.31957500E-02
$C_{17}^{(5)}$= 0.34903100E-02	$C_{18}^{(5)}$= -0.60489600E-02	$C_{19}^{(5)}$= 0.62813000E-03
$C_{20}^{(5)}$= 0.66813300E-02	$C_{21}^{(5)}$= 0.31855000E-02	$C_{22}^{(5)}$= -0.25594300E-02
$\gamma_1^{(1)} = 1.45$	$\gamma_2^{(1)} = 0.50$	$\gamma_3^{(1)} = 0.50$
$R_1^{(1)} = 1.50$	$R_1^{(1)} = 4.00$	$R_1^{(1)} = 4.00$
$\gamma_1^{(2)} = 0.40$	$\gamma_2^{(2)} = 0.80$	$\gamma_3^{(2)} = 0.80$
$R_1^{(2)} = 2.50$	$R_1^{(2)} = 3.00$	$R_1^{(2)} = 3.00$
$\gamma_1^{(3)} = 0.35$	$\gamma_2^{(3)} = 0.85$	$\gamma_3^{(3)} = 0.85$
$R_1^{(3)} = 3.50$	$R_1^{(3)} = 2.00$	$R_1^{(3)} = 2.00$
$\gamma_1^{(4)} = 0.75$	$\gamma_2^{(4)} = 0.75$	$\gamma_3^{(4)} = 0.75$
$R_1^{(4)} = 3.70$	$R_1^{(4)} = 1.85$	$R_1^{(4)} = 1.85$
$\gamma_1^{(5)} = 3.95$	$\gamma_2^{(5)} = 0.65$	$\gamma_3^{(5)} = 0.65$
$R_1^{(5)} = 1.40$	$R_1^{(5)} = 6.55$	$R_1^{(5)} = 6.55$

Table 2. Optimized EHF parameters of the DMBE IIa PES for NH_2.

	$C_1^{(3)}$= -0.48203078E+01	$C_2^{(3)}$= -0.13329298E+02
$C_3^{(3)}$= 0.52041025E+01	$C_4^{(3)}$= -0.69816801E+01	$C_5^{(3)}$= -0.17607826E+01
$C_6^{(3)}$= 0.13151386E+02	$C_7^{(3)}$= 0.24085599E+01	$C_8^{(3)}$= -0.25155174E+01
$C_9^{(3)}$= -0.21823116E+01	$C_{10}^{(3)}$= -0.58689163E+00	$C_{11}^{(3)}$= 0.31513323E+01
$C_{12}^{(3)}$= -0.15130667E+01	$C_{13}^{(3)}$= -0.83764108E+00	$C_{14}^{(3)}$= -0.71413742E+00
$C_{15}^{(3)}$= -0.28996558E+01	$C_{16}^{(3)}$= -0.17437195E+00	$C_{17}^{(3)}$= 0.17845144E+00
$C_{18}^{(3)}$= 0.34796140E+01	$C_{19}^{(3)}$= 0.17393282E+01	$C_{20}^{(3)}$= 0.21861265E+01
$C_{21}^{(3)}$= -0.18640300E+00	$C_{22}^{(3)}$= 0.14717610E+00	$C_{23}^{(3)}$= -0.63846874E-01
$C_{24}^{(3)}$= 0.53214683E+00	$C_{25}^{(3)}$= 0.43115839E+00	$C_{26}^{(3)}$= -0.36436894E+00
$C_{27}^{(3)}$= -0.17123014E+00	$C_{28}^{(3)}$= -0.27535826E+00	$C_{29}^{(3)}$= -0.34060901E+00
$C_{30}^{(3)}$= -0.10005288E+01	$C_{31}^{(3)}$= 0.37409799E+00	$C_{32}^{(3)}$= -0.57363272E+00
$C_{33}^{(3)}$= -0.33902819E+00	$C_{34}^{(3)}$= 0.61214764E-01	$C_{35}^{(3)}$= -0.26699900E-01
$C_{36}^{(3)}$= -0.14925237E+00	$C_{37}^{(3)}$= -0.18427256E+00	$C_{38}^{(3)}$= 0.16204782E+00
$C_{39}^{(3)}$= 0.12556026E+00	$C_{40}^{(3)}$= -0.25671036E-01	$C_{41}^{(3)}$= -0.14045982E-01
$C_{42}^{(3)}$= 0.17900758E+00	$C_{43}^{(3)}$= 0.21452652E+00	$C_{44}^{(3)}$= 0.31183332E+00
$C_{45}^{(3)}$= -0.19080734E+00	$C_{46}^{(3)}$= 0.15583102E+00	$C_{47}^{(3)}$= 0.15156462E+00
$C_{48}^{(3)}$= -0.65763320E-01	$C_{49}^{(3)}$= -0.85906260E-01	$C_{50}^{(3)}$= 0.16555895E-01

Table 3. Optimized EHF parameters of the DMBE IIb PES for NH_2.

	$C_1^{(3)}$ = -0.48210758E+01	$C_2^{(3)}$= -0.13330577E+02
$C_3^{(3)}$ = 0.52043457E+01	$C_4^{(3)}$ = -0.69823709E+01	$C_5^{(3)}$= -0.17549151E+01
$C_6^{(3)}$ = 0.13148683E+02	$C_7^{(3)}$ = 0.24036659E+01	$C_8^{(3)}$= -0.25165102E+01
$C_9^{(3)}$ = -0.21832814E+01	$C_{10}^{(3)}$= -0.58086123E+00	$C_{11}^{(3)}$= 0.31521206E+01
$C_{12}^{(3)}$= -0.15098241E+01	$C_{13}^{(3)}$= -0.82473243E+00	$C_{14}^{(3)}$= -0.71450485E+00
$C_{15}^{(3)}$= -0.28962821E+01	$C_{16}^{(3)}$= -0.17167209E+00	$C_{17}^{(3)}$= 0.17824894E+00
$C_{18}^{(3)}$= 0.34777029E+01	$C_{19}^{(3)}$= 0.17384331E+01	$C_{20}^{(3)}$= 0.21833641E+01
$C_{21}^{(3)}$= -0.18094833E+00	$C_{22}^{(3)}$= 0.14279528E+00	$C_{23}^{(3)}$= -0.63798886E-01
$C_{24}^{(3)}$= 0.53197726E+00	$C_{25}^{(3)}$= 0.43031300E+00	$C_{26}^{(3)}$= -0.36376018E+00
$C_{27}^{(3)}$= -0.17007103E+00	$C_{28}^{(3)}$= -0.27561598E+00	$C_{29}^{(3)}$= -0.34006259E+00
$C_{30}^{(3)}$= -0.99835797E+00	$C_{31}^{(3)}$= 0.37388637E+00	$C_{32}^{(3)}$= -0.57381863E+00
$C_{33}^{(3)}$= -0.33800720E+00	$C_{34}^{(3)}$= 0.59817067E-01	$C_{35}^{(3)}$= -0.26684387E-01
$C_{36}^{(3)}$= -0.14925546E+00	$C_{37}^{(3)}$= -0.18429293E+00	$C_{38}^{(3)}$= 0.16213791E+00
$C_{39}^{(3)}$= 0.12538273E+00	$C_{40}^{(3)}$= -0.25425766E-01	$C_{41}^{(3)}$= -0.13882590E-01
$C_{42}^{(3)}$= 0.17910962E+00	$C_{43}^{(3)}$= 0.21473718E+00	$C_{44}^{(3)}$= 0.31178970E+00
$C_{45}^{(3)}$= -0.19090918E+00	$C_{46}^{(3)}$= 0.15520449E+00	$C_{47}^{(3)}$= 0.15155897E+00
$C_{48}^{(3)}$= -0.65839284E-01	$C_{49}^{(3)}$= -0.85643197E-01	$C_{50}^{(3)}$= 0.16855327E-01

Table 4. Mean term rotational-vibrational energies (in cm^{-1}) with $N = K_a$.

	K_a	exp.[a]	calc.[b]	calc.[c]	calc.[d]
(0 0 0)	1	34.28	34.3	34.11	34.04
(0 0 0)	2	116.29	116.5	115.72	115.46
(0 0 0)	3	244.36	244.4	243.12	242.56
(0 1 0)	1	1533.85	1533.9	1533.18	1533.38
(0 1 0)	2	1622.50	1623.3	1621.44	1621.05
(0 1 0)	3	1761.22	1761.2	1759.45	1758.07
(0 2 0)	1	3000.64	3001.6	3000.57	3000.24
(0 2 0)	2	3097.43	3097.4	3097.34	3095.48
(0 2 0)	3	3248.86	3248.3	3248.75	3244.26
(1 0 0)	1	3252.9	3249.6		3252.67
(1 0 0)	2	3332.2	3330.1		3332.23
(1 0 0)	3	3457.7	3455.9		3456.31
(0 0 1)	1	3334.3	3333.0		3334.10
(0 0 1)	2	3412.2	3412.1		3412.71
(0 0 1)	3	3535.5	3535.5		3535.20

[a] Compiled in Refs. 3,4.[b] Ref. 3.[c] Ref. 4.[d] This work.

Chapter 7

Conclusions

In the present thesis we reported a series of published results, mainly focused on the calculation and modeling of double many-body expansion potential energy surface for NH_x (x=2, 3) systems. It can therefore be recommended both for dynamics studies and as a building block for construction of DMBE forms for lager N_xH_y species. The DMBE-PES for the first excited state of NH_2 molecule and the ground state of the ammonia molecule were constructed by fitting extensive *ab initio* data at the MRCI level of theory.

For $NH_2(1\,^2A')$, a single-sheeted DMBE/SEC PES has been reported based on a realistic representation of the long-range forces and a fit to accurate *ab initio* energies calculated at the MRCI level with the AVQZ basis set, after slightly correcting semiempirically the dynamical correlation by the DMBE-SEC method. The resulting function has been compared in detail with the DMBE/CBS PES obtained by extrapolating the calculated raw energies to the CBS limit. The various topographical features of both DMBE/SEC and DMBE/CBS PESs have been carefully examined, and compared with previous results for the title system. Regarding accuracy attributes, the two forms can hardly be discriminated since they have rather similar rmsd. Of course, the DMBE/CBS PES has been constructed in a purely *ab initio* fashion, whereas the DMBE/SEC one here reported entails a small degree of empiricism via scaling of the external (or dynamical) correlation. The fact that they are so similar in topography and accuracy can therefore be regarded as an asset on the consistency of both schemes. The novel function has been built such as to become degenerate at linear geometries with the ground-state potential energy surface of A'' symmetry reported by our group,

where both form a Renner-Teller pair.

For the ground state of the ammonia molecule, a full six-dimensional configuration space global DMBE PES has been reported, proper dissociation at all asymptotes is warranted by employing a generalization of the Varandas-Poveda switching function approach originally reported for triatomic species. It can then be recommended both as a reliable functional form on which dynamics calculations can be performed and as a model for improvement that is open to refinement through further accurate *ab initio* calculations, vibrational calculations, or both.

For the ground-state of NH_2, a single-sheeted DMBE PES has been refined, the main goal of this work is to improve the spectroscopic properties of the single-sheeted DMBE PES of Varandas and Poveda for the ground-state of NH_2 by employing a multiproperty fit to both the DMBE/SEC energies and experimental vibrational levels. Quasiclassical trajectory calculations on both the original and newly reported potential energy surfaces suggest that the dynamical properties of the original form remain essentially unaltered as aimed.

Summarizing we can concludes that the DMBE PESs reported in the present thesis, are expected to mimic the correct behavior at all dissociation channels while providing a realistic representation at all interatomic separations. they can therefore be recommended both for dynamics studies and as a building block for construction of DMBE forms for larger N_xH_y species. The main achievements of the reported DMBE PESs are its smoothness and its accuracy. In turn, special care was devoted during the fitting procedure to avoid the appearance of sprious stationary points and/or unphysical behaviors in the potential.